Optimized And Sub-Metric Indoor Localization System Based On Uhf Rfid Technology

Elias Hatem

UNIVERSITÉ PARIS-EST

Université Libanaise
Ecole Doctorale
Sciences et Technologie

Thèse de doctorat de l'Université Paris-Est

Electronique, Optronique et Systèmes

Elias HATEM

Système de Localisation Indoor Optimisé et Sub-Métrique basé sur la Technologie RFID UHF

Thèse dirigée par Jean-Marc LAHEURTE et Bachar El HASSAN

Soutenue le 10 décembre 2021

Jury :

Mme. Fouzia Boukour, Directrice de Recherche, Université Gustave Eiffel	Présidente
M. Yvan Duroc, Professeur, Université Claude Bernard Lyon 1	Rapporteur
M. Antoine Diet, Maître de Conférences, Université Paris Saclay	Examinateur
M. Youmni Ziadeh, Maître de Conférences, Beirut Arab University	Examinateur
M. Jean-Marc Laheurte, Professeur, Université Gustave Eiffel	Directeur de thèse
M. Bachar El Hassan, Professeur, Université Libanaise	Directeur de thèse
Mme. Elizabeth Colin, Enseignant-chercheur, Efrei Paris	Co-Directrice
Mme. Sara Abou Chakra, Maître de Conférences, Université Libanaise	Co-Directrice
M. Eddy Jehamy, Ingénieur d'application, Altair Engineering France	Invité

Acknowledgments

This work was carried out jointly at the University Paris Est, in the laboratory of Electronique, Systèmes de Communication et Microsystèmes (ESYCOM), directed by Prof. Jean-Marc Laheurte, and the Lebanese University, in the laboratory of Systèmes Electroniques, Télécommunications et Réseaux (LaSTRe), directed by Prof. Bachar El Hassan. It was funded by l'Ecole d'Ingénieurs Généraliste du Numérique - EFREI Paris.

This study would not have been possible without the guide, supervision and support of several people who believed in me and encourage me to conduct this work and reach the end of this thesis.

First, I would like to address a special acknowledgment to Prof. Fouzia Boukour and Prof. Yvan Duroc for accepting to evaluate and report my research work.

I would like to thank Dr. Antoine Diet and Dr. Youmni Ziadeh for accepting to examine my manuscript.

Foremost, I would like to thank Prof. Jean-Marc Laheurte and Prof. Bachar El Hassan for their support.

My sincere gratitude goes to my sisters' advisors Dr. Sara Abou Chakra and Dr. Elizabeth Colin, for their continuous support, patience, motivation and immense knowledge. Their guidance and dedication to research have been a real inspiration for me all along. I could not hope better advisors and mentors for my PhD.

Dr. Sara Abou Chakra, thanks for all the support, scientific knowledge and advice you provided me and all what you have taught me during my thesis. Thank you for the trust you gave me during the four years. Thanks for learning me to do everything in a perfect and right way. I will keep following your advice in my life.

Dr. Elizabeth Colin, thanks for your trust in me, the scientific discussions and remarks all over the years of my thesis. I will never forget your advices and the great interactions by treating me like your son. You inspired me the passion in research and patience in learning.

My sincere thanks go also to Altair Company and specially to Dr. Eddy Jehamy for the stimulating discussions and the sleepless nights. He has guided me to get impressive simulation results. Without his precious support, it would not have been possible to conduct this research.

A special thanks to my fellow AlliansTic Lab Mates at EFREI-Paris for all the fun we have had since October 2017.

I can’t forget Prof. Katarzyna Wegrzyn for encouraging me to work hard and making our research work much more comfortable.

Last but not least, I present this dissertation to my brother Noel Hatem and to all my friends who gave me the challenge to keep forward till the end. They had a significant influence on my career path, academic motivation and pursuits.

Finally, I dedicate all my hard work to get the PhD degree to the soul of my parents, my father Moufid Hatem and my mother Alice Thouma Hatem, and to Marie-Thérèse Baddour “TiTo”.

Abstract

Performance of outdoor localization systems has become excellent since the emergence of GPS. Indoors, the need for positioning services in all environments is highly recommended.

Up to date, there is no standard solution equivalent to indoor GPS. Several technologies and different techniques are used for indoor localization. Radio Frequency Identification (RFID) has received great attention, thanks to its low cost, high accuracy and Non-Line-of-Sight (NLoS) detection. RFID positioning systems can use either active or passive tags. Our work proposes a simple and effective active UHF RFID-based indoor localization system featuring sub-metric accuracy.

First of all, two environments are modeled via WinProp tool, in order to reduce manpower and time needed for measurements.

Most RFID indoor localization systems, found in the literature, use Received Signal Strength (RSS) based techniques for distances estimation. They mainly consist of two stages: offline and online. Within our offline stage, RSS values are collected to build a radio map and extract the attenuation parameters of the considered environment. Online, the RFID reader position is estimated by multilateration.

Moreover, present systems suffer from low accuracy and limited stability. The proposed system's parameters are improved through different approaches. First, the RSSs fluctuations are minimized by using the Maximum Likelihood Estimator (MLE) as combining technique. Second, two new generic and configurable empirical signal propagation models: the Dual One Slope Model (DOSM) and the Dual One Slope with Second Order Model (DOSSOM) are defined to better characterize signals propagation in a classroom at EFREI Paris. Associated with a new calibration procedure based on Weighted Average Attenuation Factors (WAAF), these two models extract accurately the environmental parameters offline and improve the localization accuracy, reaching 90 centimeters using only four active RFID tags.

In addition, the concept of "constellation of tags" is introduced to even more enhance the system's performance. The constellation is a group of tags that operate together at the same frequency creating signals' diversity. The complete proposed localization system features an optimal location accuracy of 60 centimeters, with only 0.25 RFID tags per square meter. This reduced number of tags deployed confirms the system cost effectiveness.

Résumé général

1. Introduction

De plus en plus de services nécessitent des informations de localisation pour satisfaire aux besoins des utilisateurs. Le système de positionnement global par satellite (*Global Positioning System* GPS) qui apporte ces données dans les environnements extérieurs (*Outdoor*) est désormais généralisé. Les performances de ce système sont devenues excellentes et permettent d'atteindre des précisions de l'ordre de quelques mètres.

Le besoin de se localiser dans tous types d'environnements est devenu essentiel dans diverses applications, par exemple pour trouver des objets perdus ou pour aider les personnes âgées dans le cadre de leurs activités quotidiennes. On peut aussi utiliser ces systèmes dans le domaine médical pour détecter la position des patients dans les hôpitaux, ou celle des véhicules dans les parcs de stationnement.

Cependant, la détection des positions des personnes et des objets dans les environnements intérieurs (*Indoor*) présente une problématique toujours d'actualité vu que le système GPS fonctionne en mode dégradé, ou ne fonctionne pas en *indoor*. En effet, la localisation *indoor* est particulièrement difficile pour plusieurs raisons : la présence de multi-trajets, l'importance de la visibilité indirecte (*None Line-of-Sight* NLoS), l'atténuation et les évanouissements des signaux à cause de la présence d'obstacles.

Des travaux de recherche sont menés aujourd'hui pour concevoir des systèmes de positionnement *indoor* (*Indoor Positioning System*, IPS) avec une grande précision, un coût raisonnable et une adaptation à des environnements et des scénarios multiples. Souvent, un certain compromis entre la précision, la couverture, le temps de latence, le coût et la robustesse, s'impose.

Les systèmes de localisation *indoor* peuvent être classés en systèmes exogènes ou endogènes. Cette classification est principalement basée sur l'infrastructure disponible qui peut être utilisée pour fournir des informations servant à la localisation. Cependant, dans des environnements complexes, l'infrastructure déjà existante ne peut pas être efficace pour des précisions élevées. D'où la nécessité de développer des systèmes de positionnement dédiés ou endogènes.

Au prix d'une main d'œuvre et de temps de déploiement importants, les solutions endogènes sont plus précises. Pour cette raison, nous nous intéressons au développement d'une solution de type endogène, afin d'améliorer la précision de localisation dans différents scénarios indoor.

Le reste de ce résumé sera élaboré comme suit : la section 2 présente les différentes métriques et techniques utilisées dans les systèmes de localisation indoor. Les différentes technologies seront détaillées dans la section 3. La section 4 définit les limitations des systèmes de localisation existants et les objectifs de notre thèse. Les systèmes de localisation conventionnels et le système que nous utilisons comme base seront décrits dans la section 5. La section 6 détaille la modélisation de l'environnement de test et du matériel RFID. Le système complet proposé, ainsi que toutes les améliorations apportées sont détaillés et évalués dans la section 7. Le concept de constellation de balises, appliqué dans notre système de localisation, est ensuite introduit dans la section 8. Les résultats obtenus sont synthétisés en conclusion, section 9.

2. Métriques et techniques de localisation *indoor*

Il existe plusieurs métriques et techniques appliquées pour la localisation et le suivi des personnes et des objets à l'intérieur des bâtiments. Elles doivent tenir compte de la complexité de l'environnement afin d'atteindre un niveau de précision acceptable pour l'application.

Parmi ces métriques, le temps d'arrivée (*Time of Arrival,* ToA), la différence du temps d'arrivée (*Time Difference of Arrival,* TDoA), l'angle d'arrivée (*Angle of Arrival,* AoA) et la puissance du signal reçu (*Received Signal Strength,* RSS) sont les plus fréquentes. ToA et TDoA nécessitent une synchronisation. La mesure de AoA nécessite des dispositifs complexes et un calibrage précis afin d'estimer la position de la cible. La phase (*Phase of Arrival* PoA) et la différence de phase (*Phase Difference of Arrival* PDoA) sont deux métriques précises, mais moins utilisées.

La puissance du signal reçu (RSS) présente une grande simplicité et une large utilisation en localisation *indoor*, grâce à son accessibilité dans la plupart des dispositifs de communication. En revanche, la majorité des systèmes de localisation *indoor,* utilisant des techniques basées sur le RSS, restent de faible précision et de stabilité limitée à cause de la présence de multi-trajets et de la visibilité directe réduite.

Les systèmes de localisation *indoor* utilisent différentes techniques pour déterminer la position de la cible, telles que : la proximité, la triangulation, la multi/trilatération et le *fingerprinting*. La technique de proximité présente une grande simplicité d'implémentation et dépend de la densité de balises déployées dans l'environnement considéré. Elle consiste à signaler que la cible est dans la zone de couverture d'au moins une balise. La technique de triangulation utilise des propriétés géométriques pour déterminer la position de la cible, en se servant de plusieurs antennes de référence. Cette approche utilise généralement différentes métriques telles que RSS, ToA, TDoA et AoA.

La multi/trilatération quant à elle, est basée sur l'estimation de distances balises-cible ; la position de la cible étant le point d'intersection des cercles/sphères de rayons correspondants aux distances estimées. La trilatération utilise trois balises fixes de position connue pour la détection de la position de la cible et permet une localisation en deux dimensions (2D). En revanche, la multilatération nécessite plus de trois balises fixes, pour localiser un objet et peut permettre une localisation en trois dimensions (3D).

La technique de *fingerprinting* est une méthode très employée. Elle est composée de deux étapes : hors ligne (*offline*) et en ligne (*online*). Pendant la phase hors ligne ou phase de calibrage, les puissances reçues sont enregistrées pour créer une carte radio (*radio map*) de l'environnement. La fiabilité de cette phase exige des ressources humaines et du temps pour récupérer les informations de puissance. Durant la phase en ligne, la position de la cible est estimée en faisant correspondre la puissance reçue avec la base de données de la carte radio à l'aide de méthodes probabilistes ou d'apprentissage.

Ces quatre techniques sont appliquées dans différents scénarios de localisation *indoor* et présentent l'avantage d'être simples à mettre en œuvre pour une précision de localisation variable. En revanche, ces techniques ont des limitations dues entre autres à l'influence des obstacles ou les effets des multi-trajets.

3. Technologies de localisation

Plusieurs technologies sont employées par les systèmes de localisation *indoor*. Ces technologies sont divisées en plusieurs catégories : la vision, la navigation inertielle, les ondes acoustiques et les ondes électromagnétiques. Dans le cadre de cette thèse, nous nous concentrerons essentiellement sur les technologies Radiofréquence (RF) omniprésentes et peu coûteuses. Contrairement aux systèmes de localisation basés sur la vision, les ondes électromagnétiques se propagent dans l'environnement permettant la localisation dans des

scénarios sans visibilité directe (NLoS). Grâce à cette caractéristique, les systèmes de positionnement RF présentent une large zone de couverture et nécessitent moins de matériel que les autres systèmes.

Les technologies hertziennes telles que ZigBee, Bluetooth, WiFi, Ultra-Wide Band ou RFID, sont couramment implémentées dans la plupart des objets connectés. Les trois premières technologies fonctionnent dans la bande de 2,4 GHz et leur précision de positionnement est affectée par les effets des multi-trajets dominants dans les environnements *indoor*.

ZigBee est une technologie de communication sans fil. Elle présente un faible coût et une consommation d'énergie réduite. La portée du signal peut atteindre 100 mètres en espace libre. Alors que dans les environnements *indoor*, la couverture est généralement comprise entre 20 et 30 mètres.

Comme Zigbee, Bluetooth est un système de communication personnel (*Wireless Personal Area Network*, WPAN). Il partage les informations avec un haut niveau de sécurité, un coût et une consommation d'énergie réduits. La portée de communication en *indoor* est comprise entre 10 centimètres et 15 mètres, suivant la visibilité directe ou non. Bluetooth est intégré dans la plupart des téléphones portables, montres intelligentes et ordinateurs portables. Cette technologie peut ainsi être utilisée dans les systèmes de localisation. La dernière version de Bluetooth (*Bluetooth Low Energie*, BLE) présente une amélioration de la plage de couverture pour atteindre 100 mètres en *outdoor*. Elle permet d'utiliser différentes métriques de positionnement telles que RSS, ToA, TDoA et AoA.

Wireless Fidelity (WiFi) offre un faible coût et une faible consommation d'énergie. Récemment, la plage de couverture du WiFi (*version 802.11ax*) a été augmentée de 100 mètres à 1 kilomètre *en indoor*, notamment dans les applications IoT (*Internet of Things*). Vu que le réseau WiFi est couramment déployé dans les bâtiments, il peut également être utilisé dans des applications de localisation, en utilisant différentes métriques de positionnement.

Ultra-Wide Band (UWB) est une technologie radio pour les communications à courte portée (moins de 100 mètres) et large bande passante. Cette technologie fonctionne dans la gamme de fréquence comprise entre 3.1 et 10.6 GHz, avec une faible consommation d'énergie. En localisation *indoor*, UWB présente une forte résistance contre les multi-trajets due à sa large bande passante. La position de la cible peut être estimée en utilisant ToA, TDoA et AoA. Ainsi, le système de localisation avec UWB a besoin de synchronisation entre les émetteurs et les

récepteurs. Ce système de localisation présente également un coût élevé dû au besoin d'équipements spécifiques pour l'utilisateur.

Les technologies d'identification par radiofréquence (*Radio Frequency IDentification, RFID*) sont devenues très courantes, notamment en logistique grâce à leur capacité d'identification en visibilité indirecte (NLoS) et leur faible coût. Les technologies RFID peuvent opérer dans plusieurs bandes de fréquence (Basse Fréquence de 125 kHz - 134 kHz, Haute Fréquence à 13,56 MHz, Ultra Haute Fréquence à 433 MHz et de 850 à 960 MHz et Super Haute Fréquence à 2.45 GHz et à 5.8 GHz). La position de la cible peut être estimée en utilisant RSS, ToA, TDoA et AoA. La précision de la localisation augmente avec le nombre de balises/tags RFID déployées dans l'environnement. Ces balises peuvent être classées en actives et passives. La balise active dispose d'un émetteur et est alimentée par batterie, ce qui la rend plus lourde et coûteuse. Elle permet une plage de couverture de 200 mètres. La balise passive fonctionne sans émetteur et avec ou sans batterie, elle est beaucoup moins chère et plus petite que la balise active. Le lecteur RFID est responsable de l'alimentation et la communication avec la balise passive. L'antenne de la balise capte l'énergie et transmet son identifiant. Sa plage de couverture est très variable selon la bande de fréquence utilisée, typiquement de quelques dizaines de centimètres à plusieurs centaines de mètres dans certains cas. La distance est de 1 à 3 mètres en moyenne pour les systèmes fonctionnant à 860 MHz.

Vu que la technologie RFID active apporte des avantages pertinents, plus précisément le coût et la grande zone de couverture, nous avons choisi de l'utiliser pour notre système de localisation. Les problématique et les objectifs de notre travail seront détaillés dans la section suivante.

4. Problématiques et Objectifs

Plusieurs inconvénients entravent le développement des systèmes de localisation RFID. Ces systèmes, implémentés souvent avec des techniques de proximité, deviennent coûteux lorsqu'un grand nombre de balises et de lecteurs RFID sont déployés dans l'environnement. De plus, le déploiement d'un grand nombre de balises augmente les interférences. Par ailleurs, la variabilité dans la propagation des signaux est un problème courant dans la plupart des systèmes de localisation RFID basés sur le RSS. Cette instabilité est due à la non-stationnarité du canal, ce qui affecte la précision de la localisation.

Les recherches pour proposer des solutions de localisation abondent, mais les implémentations de ces solutions, à coût réduit, se font rares. Dans ce contexte, l'objectif de cette thèse est d'introduire un nouveau système de localisation avec la technologie RFID, offrant un coût bas, ainsi qu'une fiabilité, stabilité et précision élevées. Par conséquent, trois objectifs principaux sont définis : améliorer le calibrage, optimiser la densité des balises et augmenter la précision de la localisation (Figure R.1).

Pour ce faire, cinq axes de recherche principaux sont menés. La première contribution est de modéliser de manière fiable deux environnements intérieurs, ce qui permet de remplacer de longues compagnes de mesure. De plus, l'estimateur de maximum de vraisemblance (*Maximum Likelihood Estimator,* MLE) est appliqué en tant que technique de combinaison RSS, dans le but d'atténuer les fluctuations des signaux. Le troisième axe se concentre sur la présentation de nouveaux modèles de propagation empiriques *indoor* associés à une nouvelle approche de calibrage déterminant les facteurs d'atténuation pondérés (*Weighted Average Attenuation Factor*, WAAF). Afin d'améliorer davantage la précision, en s'inspirant de l'approche MISO (*Multiple Inputs Single Output*), nous introduisons le concept de constellation de balises RFID. Cette constellation est constituée d'un groupe de balises actives, opérant ensemble à la même fréquence et profitant de la diversité des signaux. La taille, la forme et le nombre de balises de la constellation sont les principales clés pour améliorer la précision de la localisation (Figure R.1).

A travers ce travail de thèse, nous proposons un système endogène de localisation RFID *indoor* qui garantit un faible coût en termes de nombre de dispositifs déployés et une précision de localisation d'ordre sub-métrique. Cet ordre de précision est nécessaire pour des applications personnelles, car c'est équivalent au pas d'un individu (moins de 1 mètre).

Dans le but de couvrir une large zone, les balises doivent avoir une longue portée. Notre choix s'est porté sur un système actif fonctionnant à 433 MHz. De plus, cela permet de réduire la densité de balises déployées.

Les objectifs et contributions réalisés dans ce travail de thèse sont présentés ci-dessous :

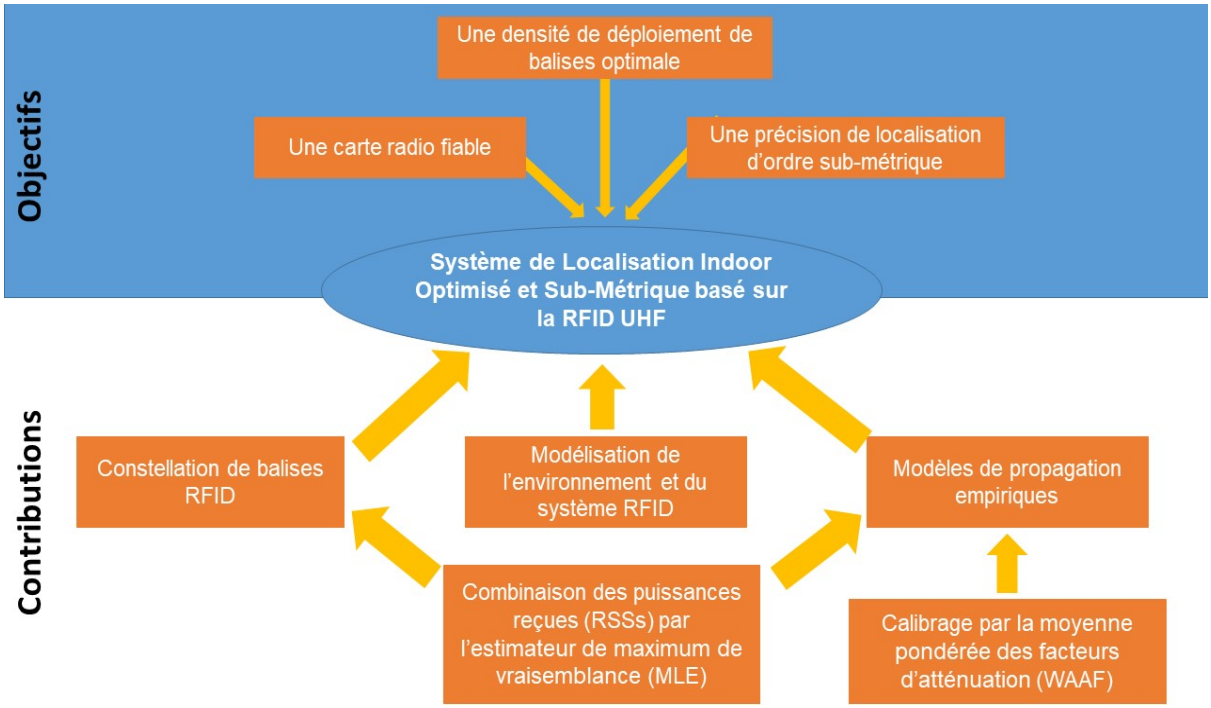

Figure R.1 Objectifs et contributions

5. Système de localisation de base

Notre système de localisation RFID se compose d'un lecteur monté sur un robot à deux roues et de balises RFID UHF actives fixes qui fonctionnent à la fréquence de 433 MHz. L'équipement RFID d'Ela-Innovation est un système propriétaire. Les tags peuvent être détectés jusqu'à 20 mètres en intérieur. De plus, la transmission du signal est discontinue, le temps d'émission est environ 1 milliseconde. La différence de temps entre deux émissions est 200 millisecondes. Du fait de l'intermittence de la transmission et de la durée d'acquisition, le canal de propagation, entre tag et lecteur, peut être considéré comme non stationnaire.

Ce système a été déployé dans une salle de classe de 63,75 mètres carrés à EFREI Paris. Il est basé sur l'acquisition des puissances du signal reçu (RSS) par le lecteur RFID.

Le processus de localisation est divisé en deux étapes : hors ligne (*offline*) et en ligne (*online*). L'étape hors ligne représente la phase de calibrage de l'environnement et celle en ligne est la phase de positionnement (Figure R.2).

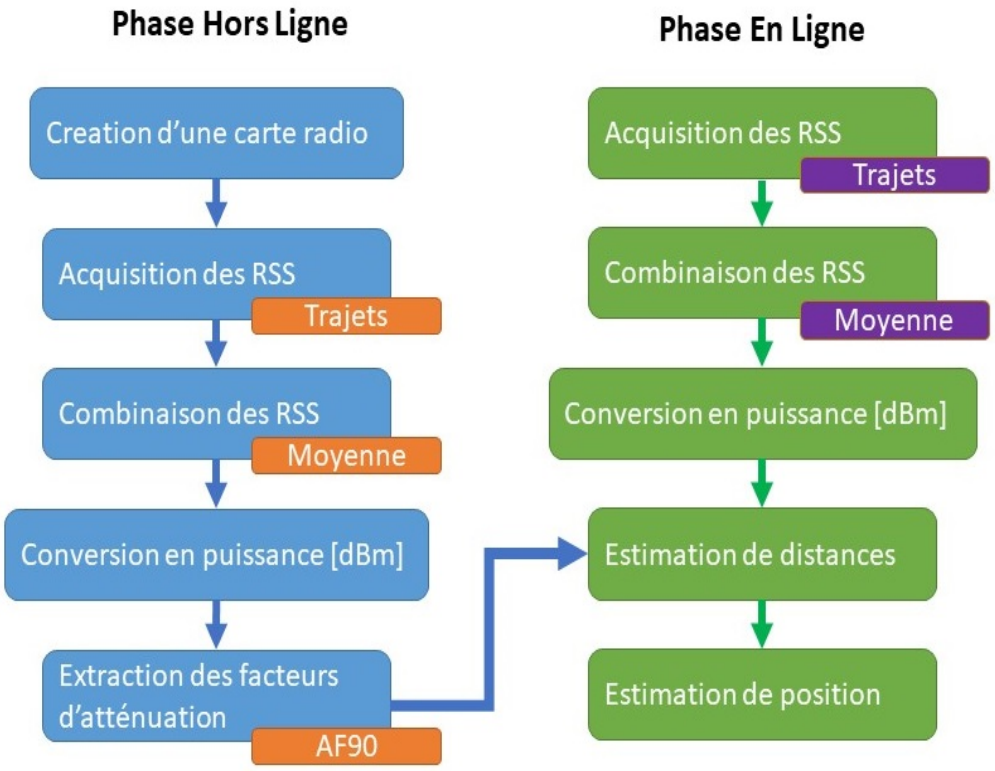

Figure R.2 Schéma fonctionnel du système de localisation RFID de base

La phase hors ligne consiste à établir une carte radio sous la forme d'une base de données reflétant l'atténuation du signal dans l'environnement considéré. Cette phase est réalisée à l'aide d'une seule balise RFID fixée au centre du mur principal de la salle de classe, suivant des trajectoires radiales (Figure R.3 a). Cette forme de trajectoires est introduite afin de réduire le nombre de positions de mesure tout en assurant une carte radio fiable de l'environnement.

Lors de cette phase, les puissances émises par la balise RFID et reçues par le lecteur (RSS), sont récupérées sur 64 positions de référence espacées de 50 centimètres, sur les sept trajets de A30 à A150 (Figure R.3 a). A chaque position, 200 acquisitions de puissance sont enregistrées et combinées avec la technique de moyenne classique.

Pour extraire les facteurs d'atténuation correspondant à l'environnement, un modèle de propagation est appliqué sur les valeurs RSS du trajet A90 ; ce trajet possède le plus grand nombre de positions. Ces coefficients sont symbolisés par AF90.

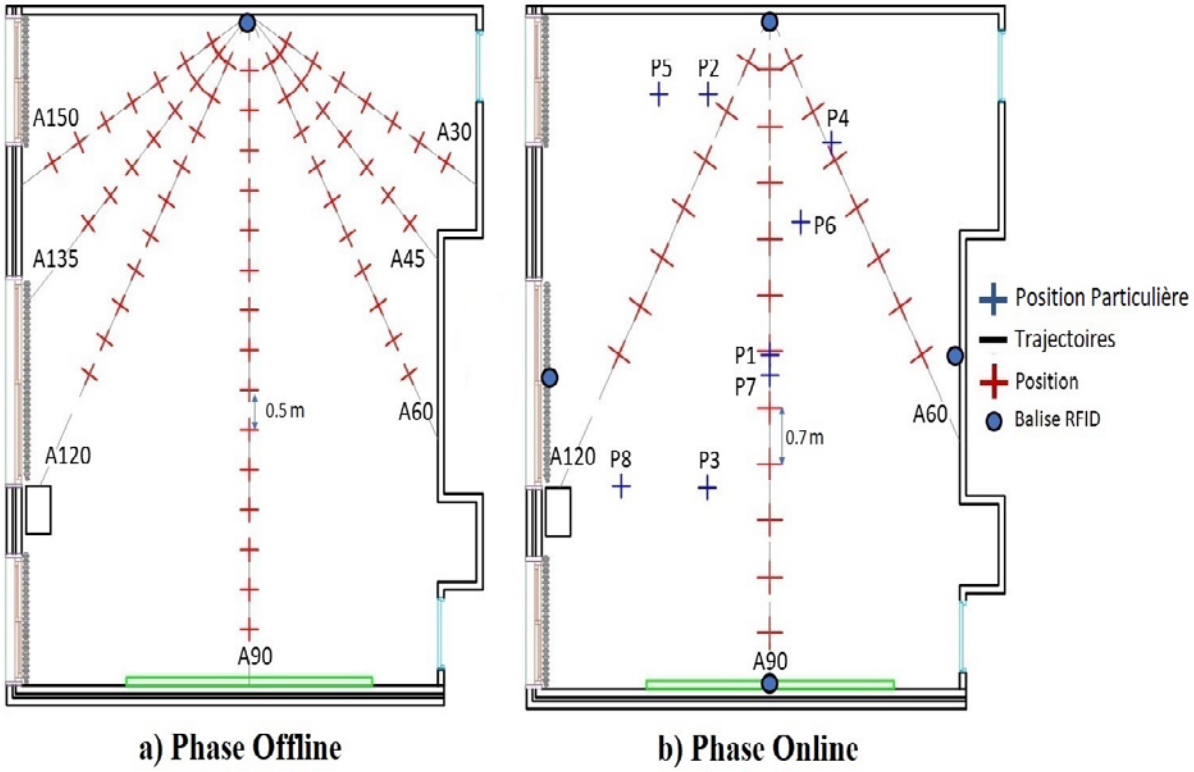

Figure R.3 Plan d'expérimentation des phases hors et en ligne (Offline and Online phase)

Durant la phase en ligne (Figure R.3 b), 20 acquisitions de puissance sont collectées tous les $\lambda \cong 70$ centimètres et combinées avec la même technique déjà utilisée durant la phase de calibrage, c.à.d. elles sont moyennées.

L'estimation de distance est obtenue en appliquant le modèle de propagation avec les paramètres correspondant à l'environnement. Enfin, la position du lecteur RFID est estimée en appliquant la technique de multilatération.

6. Modélisation de l'environnement et du système RFID

Afin de raccourcir le temps nécessaire pour les mesures, nous avons opté pour la validation de nos propositions d'abord par simulation. Nous avons donc modélisé l'environnement de test. Parmi les nombreux logiciels existants, nous avons choisi Winprop, qui permet de configurer des environnements et de modéliser des antennes avec une grande précision. Winprop contient plusieurs outils (WallMan, AMan, ProMan) (Figure R.4). WallMan est utilisé pour construire la structure de l'environnement indoor. AMan permet la configuration des antennes. ProMan, qui comprend des modèles empiriques et semi-empiriques, étudie la propagation des signaux dans l'environnement.

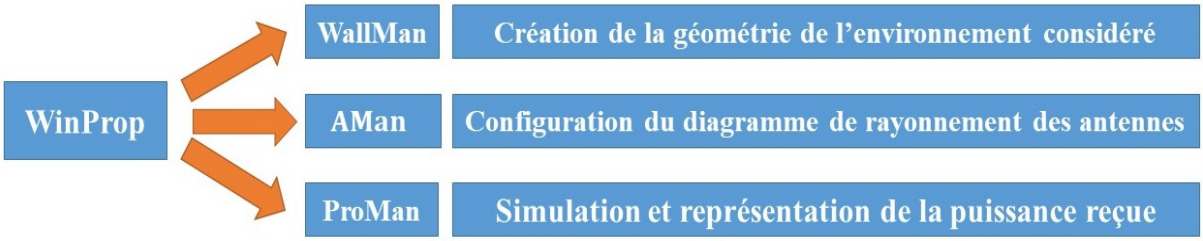

Figure R.4 Outils de simulation

La configuration de l'environnement est divisée en deux parties : la première consiste à le modéliser avec tous les détails et les dimensions des matériaux qui le constituent. La deuxième partie consiste à définir les pertes empiriques (Transmission, Réflexion et Réfraction) et les coefficients de Fresnel (perméabilité, permittivité et conductivité) correspondants aux matériaux.

Deux environnements ont été modélisés pour valider notre configuration : la salle de classe au quatrième étage de 63,75 mètres carrés et un hall au rez-de-chaussée de 205 mètres carrés, à l'école d'ingénieurs EFREI Paris.

Bien que non meublée, la salle de classe peut être considérée comme complexe en raison de la dissymétrique des murs. Plus précisément, un des murs présente des renforcements et l'autre est entièrement vitré (Figure R.5). Cet environnement inclut aussi des objets métalliques, un grand radiateur (de 8 mètres de longueur et 1 mètre de hauteur), un tableau métallique, un projecteur LCD, un détecteur de feu, et des haut-parleurs fixés au plafond et sur le mur du fond.

Figure R.5 Disposition 3D des environnements réels et simulés

Après avoir examiné les différents modèles de propagation des signaux présents dans Winprop, nous avons choisi 3D Ray-Tracing (RT). Dans les deux environnements, la comparaison des puissances reçues par simulation et par mesure a amené à une différence maximale de 0.5 dB. Ainsi, la simulation a remplacé les mesures réelles dans plusieurs tests.

7. Système de localisation RFID proposé

Dans cette section, une meilleure technique de combinaison des signaux acquis, deux modèles de propagation et une nouvelle méthode de calibrage seront introduits.

7.1 Combinaison des RSS

Les acquisitions de RSS, récupérées durant la phase hors ligne (offline) et en ligne (online), sont combinées par le biais de l'estimateur de maximum de vraisemblance (MLE).

Considérant K acquisitions à chaque position, le MLE détermine la valeur RSS qui maximise la vraisemblance avec la puissance réelle mesurée par le lecteur RFID; cette valeur est celle avec la probabilité d'occurrence la plus élevée.

$$RSS = [RSS_1, RSS_2, \ldots . RSS_K] \quad \text{(R.1)}$$

Avec *K* est le nombre d'acquisitions par position.

Le MLE des puissances mesurées est défini par

$$RSS_{MLE} = arg\ max\ p(RSS_K) \tag{R.2}$$

Avec, argmax est l'opérateur qui donne la valeur de RSS la plus probable.

7.2 Modèles de propagation

De nombreux modèles de propagation indoor empiriques, présents dans la littérature, ont été dédiés à améliorer la précision des systèmes de localisation. Parmi ces modèles, on peut citer COST 231 ou modèle à pente unique (*One Slope Model*, OSM), modèle de propagation de second ordre (*Second order Propagation Propagation Model*, SOPPM).

Dans nos travaux, les modèles de propagation proposés sont empiriques. Nous les avons appelés : le modèle à double pente (*Double One Slope Model* DOSM) et le modèle à double pente et de second ordre (*Double One Slope Second Order Model* DOSSOM).

Le modèle DOSM est alors représenté par :

$$P_r(d) = \begin{cases} P_0 - 10.n_{1T_i}.log_{10}(d) + X_{1T_i} & d \leq 3\lambda \\ P_0{}' - 10.n_{2T_i}.log_{10}(d) + X_{2T_i} & d > 3\lambda \end{cases} \tag{R.3}$$

Et, le modèle DOSSOM est défini par :

$$P_r(d) = \begin{cases} P_0 - 10.n_{T_i}.log_{10}(d) + X_{T_i} & d \leq 3\lambda \\ P_0{}' - a_{T_i}.log_{10}(d)^2 - b_{T_i}.log_{10}(d) - c_{T_i} & d > 3\lambda \end{cases} \tag{R.4}$$

$P_r(d)$ est la puissance reçue en dBm à une distance (d) en mètres, P_0 est la puissance reçue à la distance de 1 mètre. $P_0{}'$ est la puissance reçue à 3λ en dBm. *i* représente l'indice du trajet correspondant parmi les sept trajets utilisés lors de la phase de calibrage.

Pour le modèle DOSM, n_{1Ti} et n_{2Ti} représentent les coefficients d'atténuation du trajet T_i. Les termes X_{1T_i} et X_{2T_i}décrivent une variable log-normale pour l'erreur de la puissance reçue tout au long de la première partie de chaque trajet modélisé par la variation de la pente (premier ordre).

Pour le modèle DOSSOM, n_{Ti} est le coefficient d'atténuation du trajet qui correspond à la première partie de chaque trajet. X_{T_i} présente la variation log-normale de la puissance reçue modélisée par la variation de la pente. a_{T_i}, b_{T_i} et c_{T_i} sont les paramètres du polynôme du second ordre qui correspond à la seconde partie de chaque trajet.

En effet, notre système de localisation RFID de base utilise les paramètres d'atténuation du trajet A90 abrégés par n_{T90}, $a_{T_{90}}$, $b_{T_{90}}$ et $c_{T_{90}}$.

Les deux modèles que nous avons proposés ont été comparés aux modèles de propagation empiriques déjà présents dans la littérature. Les résultats obtenus montrent que DOSSOM présente une amélioration de l'erreur d'au moins un mètre.

7.3 Méthode de calibrage

Après l'introduction des deux modèles de propagation indoor, l'optimisation de notre système de localisation consiste à améliorer la fiabilité du calibrage et la précision de la localisation.

Nous proposons un facteur d'atténuation global pour l'environnement via la moyenne pondérée des facteurs d'atténuation (WAAF). WAAF correspond aux facteurs d'atténuation de la salle de classe en prenant en couvrant tout l'environnement.

Dans ce contexte, les coefficients d'atténuation $n_{T_i}, a_{T_i}, b_{T_i}\ et\ c_{T_i}$ correspondants au modèle DOSSOM de l'équation (R.4) et associés aux sept trajets A30 à A150 (Figure R.3 a), sont pondérés afin de déterminer les coefficients WAAF définis par les équations suivantes :

Pour d ≤ 3

$$n_{w1} = \sum_{i=1}^{7} n_{T_i} \frac{N'_{Pos/T_i}}{N'_{Total}} \tag{R.5}$$

Pour d > 3

$$\begin{cases} A_{w2} = \sum_{i=1}^{7} a_{T_i} \frac{N''_{Pos/T_i}}{N''_{Total}} \\ B_{w2} = \sum_{i=1}^{7} b_{T_i} \frac{N''_{Pos/T_i}}{N''_{Total}} \\ C_{w2} = \sum_{i=1}^{7} c_{T_i} \frac{N''_{Pos/T_i}}{N''_{Total}} \end{cases} \tag{R.6}$$

n_{w1} est le facteur d'atténuation moyen pondéré correspondant à la première partie du trajet. n_{T_i} est le facteur d'atténuation associé à chaque trajet. A_{w2}, B_{w2} et C_{w2} représentent les paramètres de la moyenne pondérée correspondants au modèle de propagation du second ordre (DOSSOM). a_{T_i}, b_{T_i} et c_{T_i} sont les paramètres associés à chaque trajet. N'_{Total} et N''_{Total} représentent le nombre total de positions de chacune des deux parties. N'_{Pos/T_i} et N''_{Pos/T_i} sont les nombres de positions sur chaque partie de chaque trajet.

Les coefficients WAAF sont directement proportionnels au nombre de points considérés dans le calibrage. Ils prennent en compte toutes les positions afin de couvrir tout l'environnement.

Avec le modèle de propagation DOSSOM associé aux facteurs d'atténuation (WAAF), la puissance reçue par le lecteur RFID est exprimée par l'équation suivante :

$$P_r(d) = \begin{cases} P_0 - 10.n_{w_1}.\log_{10}(d) + X_{w_1} & d \leq 3\lambda \\ P_0' - A_{w_2}.\log_{10}(d)^2 - B_{w_2}.\log_{10}(d) - C_{w_2} & d > 3\lambda \end{cases} \quad (R.7)$$

$P_r(d)$ est la puissance reçue en dBm à la distance d en mètres, P_0 est la puissance reçue à 1 mètre en dBm. P_0' est la puissance reçue à 3λ en dBm. X_{w_1} représente variation log-normale de la puissance reçue sur la première partie de tous les trajets. A_{w2}, B_{w2} et C_{w2} représentent les paramètres de la moyenne pondérée correspondant au modèle de propagation du second ordre.

Dans la phase en ligne (online), 20 valeurs de RSS sont acquises à chaque position, et combinées via la même technique (MLE). La position du lecteur RFID est ainsi estimée en appliquant la technique de multilatération.

Pour évaluer le système proposé, la localisation est réalisée avec quatre balises RFID fixées au centre de chaque mur de la classe. Trente-deux positions sont estimées. Parmi ces positions, vingt-quatre sont uniformément réparties dans l'environnement, tous les 70 centimètres sur les trois trajets A60, A90 et A120. Huit autres positions particulières sont choisies dans la salle de classe afin d'évaluer la performance du notre système (Figure R.3 b).

Les erreurs de position obtenues avec MLE, ont été déterminées et comparées à celles obtenues avec la technique de la moyenne.

Les figures suivantes présentent la fonction de distribution cumulative (Cumulative Distribution Function, CDF) des erreurs de position obtenues en utilisant les paramètres de calibrage WAAF avec le modèle de propagation DOSSOM.

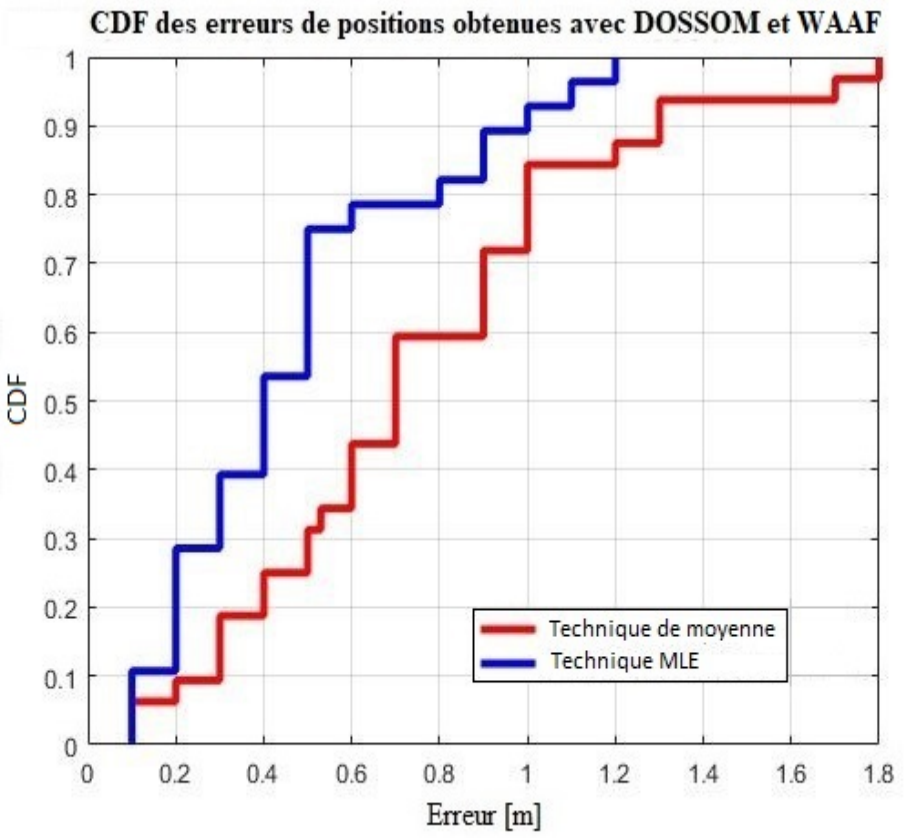

Figure R.6 CDF des erreurs de position avec la moyenne et MLE

La précision de localisation obtenue à 90% CDF est égale à 1,3 mètres avec la moyenne et 90 centimètres avec MLE. Ainsi, l'efficacité du MLE est bien validée. Le système de localisation *indoor* proposé, a amélioré la précision (moins du mètre), tout en déployant, seulement, 0,062 balises RFID par mètre carré.

8. Constellation de balises RFID

Grâce à la technologie MISO (Multiple Input Single Output), les performances des systèmes de communication sans fil peuvent être améliorées en adoptant plusieurs antennes émettrices. Pour l'estimation de distance, nous avons remplacé de manière analogue, la balise RFID unitaire par un groupe de balises qui fonctionnent à la même fréquence et appelé "constellation".

Cette approche de constellation conduit à plusieurs études. Définir la dimension, la forme et le nombre de balises qui la constituent sont une étape essentielle permettant de déterminer la constellation optimale offrant la meilleure précision.

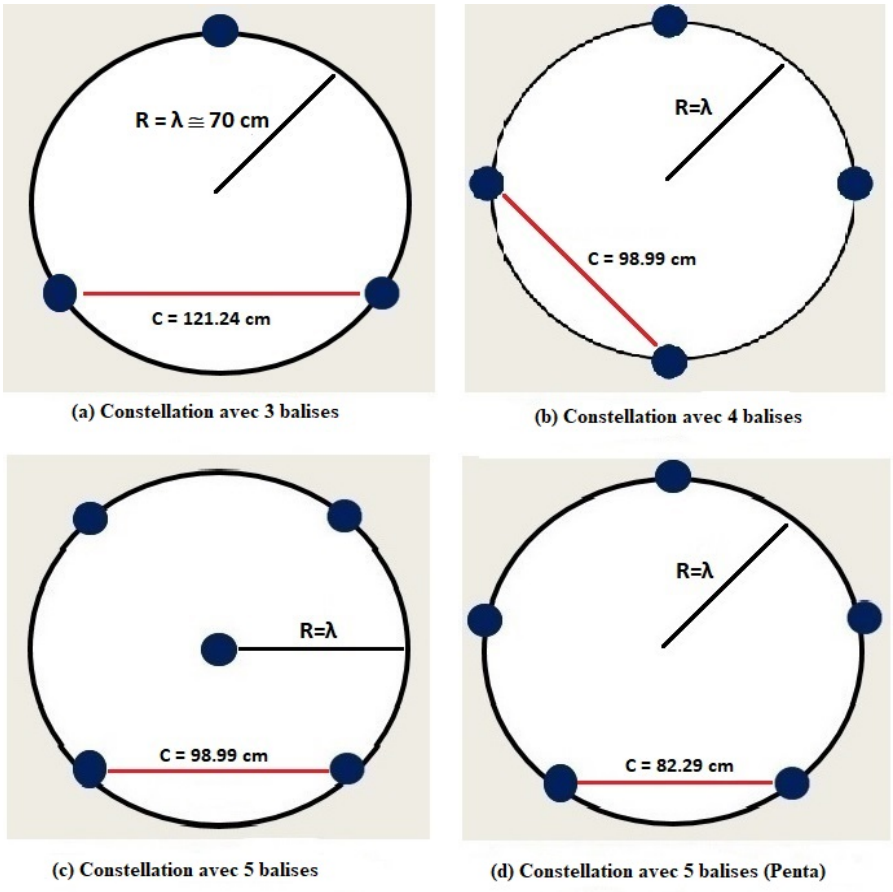

Figure R.7 Constellation avec différentes formes et nombres de balises RFID

Cette étude a été validée par simulation et par mesure. Elle nous a amené à constater que la constellation constituée de 4 balises et de rayon égal à la longueur d'onde λ présente moins d'erreurs.

Le modèle de propagation DOSSOM est toujours appliqué pour extraire les coefficients d'atténuation de l'environnement en utilisant la méthode de la moyenne pondérée (WAAF).

La localisation est réalisée avec quatre constellations de quatre balises RFID chacune. Le centre de chaque constellation est situé au centre de chaque mur de la classe (Figure R.3 b). Dans cette phase, 20 acquisitions des puissances reçues sont acquises et combinées via l'estimateur de maximum de vraisemblance (MLE) à chacune des positions des trois trajets A60, A90 et A120. Les distances entre les balises et le lecteur RFID ont été estimées en appliquant le modèle de propagation DOSSOM. La position du lecteur RFID est déterminée par multilatération.

Les résultats obtenus avec les constellations ont été analysés et comparés à ceux obtenus avec le scénario de balise unitaire. La Figure R.8 présente la fonction de distribution cumulative des erreurs de position obtenues, en utilisant les paramètres de calibrage WAAF avec le modèle de propagation DOSSOM, dans les deux cas : constellation de balises et balise unitaire.

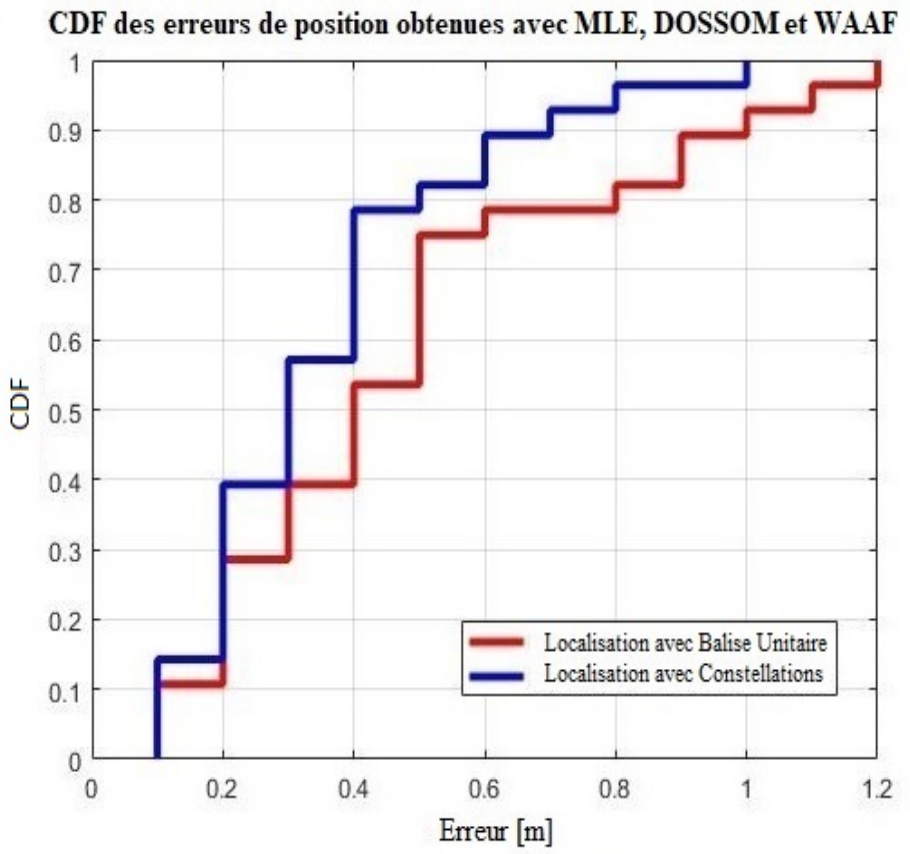

Figure R.8 CDF des erreurs de position avec constellations ou balise unitaire

Les erreurs de position obtenues à 90% CDF sont de 90 et 60 centimètres avec une seule balise et la constellation de balises, respectivement. Ainsi, l'utilisation de la constellation de balises améliore la précision de localisation de 33.3%, tout en déployant, seulement, 0,25 balises RFID par mètre carré.

9. Conclusion

La modélisation de l'environnement et des équipements RFID qui s'y trouvent, est essentielle pour la fiabilité de la simulation. Les résultats de simulation présentés, ont un écart maximal de 0,5 dB avec les mesures réelles. Cette compatibilité a été obtenue à l'aide du modèle 3D Ray-Tracing. La simulation peut ainsi remplacer les mesures dans différents scénarios.

La modélisation du canal de propagation par DOSSOM - WAAF présente une meilleure fiabilité dans l'extraction des paramètres d'atténuation, en couvrant tout l'environnement.

La localisation a été étudiée premièrement avec une balise unitaire, puis par quatre constellations de balises RFID actives fixées respectivement au centre de chaque mur de la salle de classe. L'expérience a montré que combiner les RSSs par MLE aussi bien dans la phase de calibrage que dans la phase de localisation proprement dite, présente une amélioration dans la précision de localisation.

Ainsi, la précision du système proposé atteint une erreur de position de 60 centimètres (dans 90% des cas) avec 0,25 balise RFID déployées par mètre carré contre 2.5 mètres (dans 90% des cas) avec 0,063 balise par mètre carré dans le système de base (modèle *One Slope* avec le coefficient d'atténuation AF90, moyenne des RSS, balise unitaire).

Contents

List of Tables

List of Figures

Nomenclature and Abbreviations

AoA	Angle of Arrival
AFC	Attenuation Factor Classic Model
AMan	Antenna Manager
AM	Arithmetic Mean
BLE	Bluetooth Low Energy
BI	Bilinear Interpolation
CDF	Cumulative Distribution Function
DOSM	Dual One Slope Model
DOSSOM	Dual One Slope with Second Order polynomial Model
DBN	Deep Belief Network
DPM	Dominant Path Model
DR	Dielectric Resonator
EXP	Exponential Interpolation
GPS	Global Positioning System
GTD	Geometric Theory of Diffraction
HF	High Frequency
HPI	Horizontal Projection Interpolation (HPI)
ILS	Indoor Localization System
IPS	Indoor Positioning System
IR	InfraRed
IRT	Intelligent Ray Tracing
ISM	Industrial, Scientific and Medical
IoT	Internet of Things
KNN	K-nearest-neighbor

LED	Light Emitting Diode
LF	Low Frequency
LiFi	Light Fidelity
LoS	Line-of-Sight
KNN	K-Nearest-Neighbor
MDE	Mean Distance Error
MFSM	Modified Free Space Model
MISO	Multiple Input Single Output
MIMO	Multiple Input Multiple Output
MLE	Maximum Likelihood Estimator
MCL	Monte Carlo localization (MCL)
MoM	Method of Moment
MWMF	Multi-Wall Multi-Floor Model
NLoS	Non-Line-of-Sight
NLLS	Non-Linear Least Square
NMDS	Nonmetric Multi-Dimensional Scaling
OSM	One Slope Model
PDR	Pedestrian Dead Reckoning
PDoA	Phase Difference of Arrival
PoA	Phase of Arrival
ProMan	Propagation Manager
PSO	Particle Swarm Optimization
RF	Radio Frequency
RFID	Radio Frequency Identification
RPD	Received Power Difference
RSS	Received Signal Strength

RSSI	Received Signal Strength Indicator
RTLS	Real-Time Location System
Rx	Receiving Antenna
SCCL	Self-Calibrating Centroid Localization
SHF	Super High Frequency
SIMO	Single Input Multiple Output
SNR	Signal-to-Noise Ratio
SMP	Smallest M-vertex Polygon
SOPPM	Second Order Polynomial Propagation Model
SRT	Standard Ray Tracing
Std	Standard Deviation
SVM	Support Vector Machine
ToA	Time of Arrival
TDoA	Time Difference of Arrival
ToF	Time of Flight
Tx	Transmitting Antenna
UHF	Ultra-High Frequency
UTD	Uniform Theory of Diffraction
UWB	Ultra-Wide Band
WAAF	Weighted Average Attenuation Factor
WallMan	Wall Manager
WBI	Weighted Bilinear Interpolation
WLAN	Wireless Local Area Network
WLLS	Weighted Linear Least-Squares
WLS-RW	Weighted Least Squares combined with Residual Weighted
WIFI	Wireless Fidelity

WPAN	Wireless Personal Area Networks
WSN	Wireless Sensor Network
2D	Two-dimensional
3D	Three-dimensional

Introduction

The Global Positioning System (GPS) already provides a satisfactory solution for outdoor localization. Extending that service to indoor environments is still limited due to many substantial challenges. Thus, an accurate indoor localization approach is important and needed for different applications. Among these applications, we can mention public safety, commercial and security domains. For instance, indoor localization solutions can assist the elderly in their homes as part of their daily activities. They can play a significant role in the medical field and are recommended for police and firefighters. However, none of the existing localization services have yet accurately localized people in indoor environments with low cost and complexity solutions.

Intense research works are carried today to design Indoor Localization Systems (ILS). Many technologies have been considered, e.g. ultrasonic, InfraRed (IR), vision, and Radio Frequency (RF). RF standards such as Wireless Fidelity (WiFi), Zigbee, Bluetooth, Ultra-Wide Band (UWB), and Radio Frequency IDentification (RFID) predominate today to develop accurate ILS. Despite the RF Non-Line-of-Sight (NLoS) detection capabilities, these can have an adverse impact on the overall ILS accuracy.

Recently, RFID promoted the potential of the RF technology for indoor localization in many scenes. Multiple RFID readers and tags are used to form the RFID based localization system. The placement and density of RFID readers, tags or both, in a given layout, are key parameters to provide satisfactory localization accuracy. Estimated locations are usually more accurate with a higher density of components. However, this will increase the system's cost substantially.

This Ph.D. thesis seeks to present a new ILS based on the RFID technology. The proposed system's must be reliable, accurate and characterized by an effective low cost. Hence, three main objectives are defined: improve the calibration, optimize the tags density, and enhance the location accuracy (Figure I.1)

To this end, five main research lines are conducted. The first contribution is to accurately model two indoor environments; this accelerates the analysis by avoiding long durations needed for real measurements. In addition, the Maximum Likelihood Estimator (MLE) is applied as an RSS combining technique, in the aim to mitigate signals fluctuations.

The third axis is focused on introducing new empirical indoor propagation models associated with a new calibration approach determining Weighted Average Attenuation Factors (WAAF). Finally, referring to the Multiple Inputs Single Output (MISO) approach, the concept of using a group of active RFID tags instead of a single one is analyzed to enhance the location accuracy thanks to signals' diversity. We have named this group of tags as a "Constellation". The size, shape, and the number of tags in the constellation are main keys for improving the location accuracy.

Work is summarized as follows:

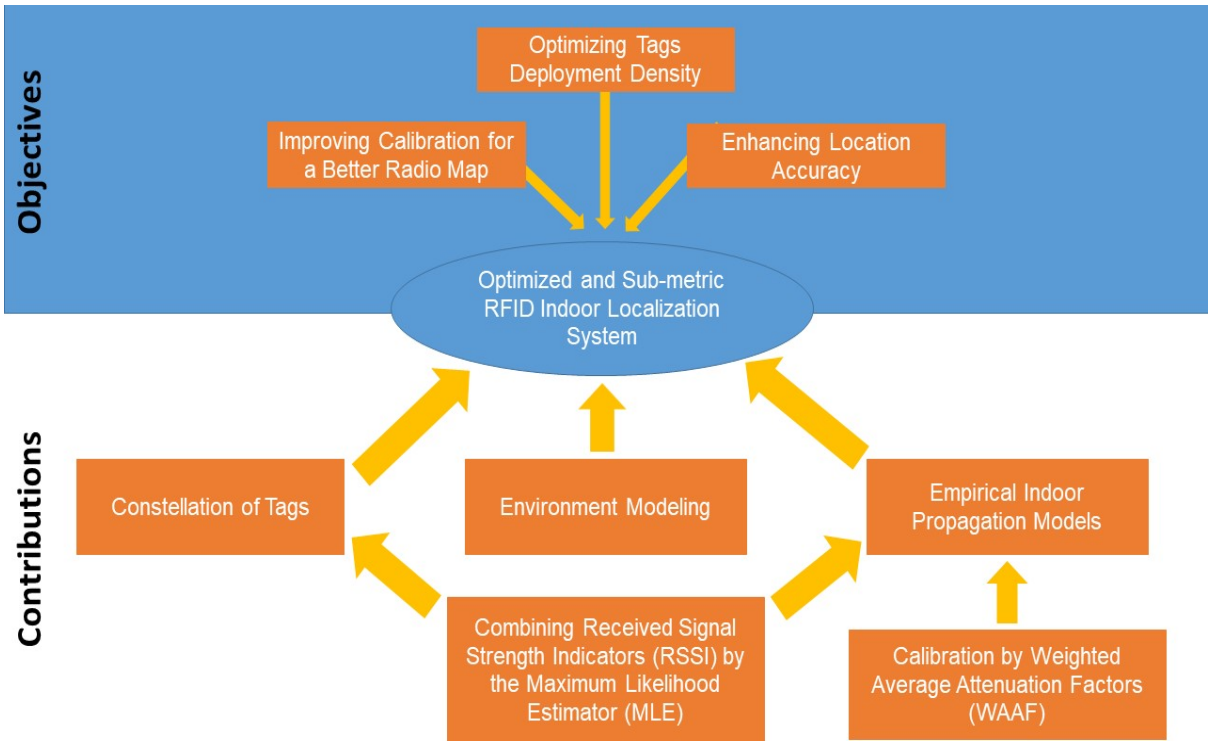

Figure I.1 Research lines

The thesis is derived as follows:

Chapter 1 consists of a literature review about indoor localization systems with their respective performances. The main positioning metrics, techniques, technologies and their limitations, are presented. The main characteristics of indoor positioning systems in terms of their availability, cost, range, latency, scalability, variability and location accuracy are assessed. In particular, active and passive RFID-based indoor localization systems are described to give a detailed insight about their operational capabilities and limitations in such environments.

Chapter 2 presents our conventional RFID positioning system, using the Received Signal Strength (RSS) with the average combining technique. The One Slope propagation Model (OSM), that is the most commonly one used indoor, followed by the multilateration technique, are shown. Finally, the experimental arrangement is set.

Chapter 3 shows the indoor environment where all experiments are conducted. Then, the WinProp tool, used for simulations, is introduced. Besides, all modeling steps are detailed by defining all Fresnel parameters of the materials constituting the environment, as well as their empirical losses in order to get an accurate simulated environment. The RFID reader antenna and the tag emitting antenna are also described and modeled to get accurate signals propagation.

Chapter 4 introduces the location improvements by signal processing. The RSSIs variability and reliability are examined using two different combining techniques i.e. the conventional average and the Maximum Likelihood Estimator (MLE). Moreover, in order to improve the environment calibration, the Weighted Average Attenuation Factor (WAAF) procedure is established. After introducing existing ones, two new empirical indoor propagation models are proposed to improve the location accuracy using the multilateration technique.

Chapter 5 suggests a Multiple Inputs Single Output system (MISO) approach to define the concept of constellation of RFID tags used for indoor positioning. The best shape, radius, and the optimal number of tags in the constellation are studied. Then, the position errors obtained with the proposed localization system, performing with the optimal constellation of tags, are analyzed and compared with those obtained with the single tag architecture.

After a comparative analysis regarding the density of tags deployed, the last part is dedicated to summarize all gathered results and give conclusions. Recommendations are elaborated to open perspectives for future work.

Chapter 1 State of the Art

1.1 Introduction

Locating people or devices in a given area appeared a few years ago and has become an essential element of the contextual information [1]. Due to the excellent performance of the Global Positioning System (GPS) in outdoor environments, determining positions of people indoors such as buildings, houses, warehouses, airports and industries has also become highly needed. Moreover, this aim has been largely boosted by the widespread use of wireless communications.

Recently, indoor localization has witnessed large interest due to the wide range of potential services provided by the Internet of Things (IoT) and ubiquitous connectivity. Different technologies and techniques are introduced to provide indoor localization services to the end-users; they will be expanded in detail in this chapter.

In addition, each Indoor Positioning System (IPS) performs some specific characteristics such availability, cost, range, latency, scalability and location accuracy, depending on the application and the considered indoor environment [2]. Systems found in the literature will be highlighted and assessed upon their performance and limitations.

In this context, Radio Frequency (RF) based localization techniques become increasingly popular as they offer pervasive and low-cost solutions, as discussed in [3]. In contrary to localization systems based on vision, electromagnetic waves propagate through the environment allowing localization in Non-Line-of-Sight (NLoS) scenarios. Thanks to this characteristic, RF-based positioning systems have a larger coverage area and need less hardware compared to other systems.

This chapter begins with presenting the radio frequency positioning metrics in section 1.2. The different techniques used in IPS are discussed in section 1.3. Section 1.4 is dedicated to provide an overview of existing localization technologies and their limitations. Then, major characteristics of an Indoor Localization System (ILS) followed by existing ILS as well as their efficiency and drawbacks are defined and discussed in section 1.5. Finally, the chapter ends by a detailed conclusion and motivations in section 1.6.

1.2 Overview of Positioning Metrics

Despite a large number of different RF positioning systems and solutions, there are very few forms of metrics used to detect the user's location. such as: These metrics can be broadly classified into: time as Time of Arrival (ToA) or Time Difference of Arrival (TDoA), angle such as Angle of Arrival (AoA), Phase of Arrival (PoA) or Phase Difference of Arrival (PDoA) and power measurements or Received Signal Strength (RSS).

This section presents the most popular positioning metrics used to locate a person or object in an indoor environment i.e. ToA, TDoA, AoA and RSS.

1.2.1 Time of Arrival

The Time of Arrival (ToA) or Time of Flight (ToF) method is based on a theoretical propagation model of a radio frequency signal. The distance between the transmitting antenna (Tx) and the receiving antenna (Rx) can be determined by measuring the travel time of the signal between them. This distance is estimated by multiplying the ToA by the light celerity. The location of the receiving antenna (Rx) can be deduced using ToA estimations from various reference transmitting antennas (Tx). The intersection of three signals and nonlinear least-squares approaches are applied to get optimal errors, as shown in Figure 1.1.

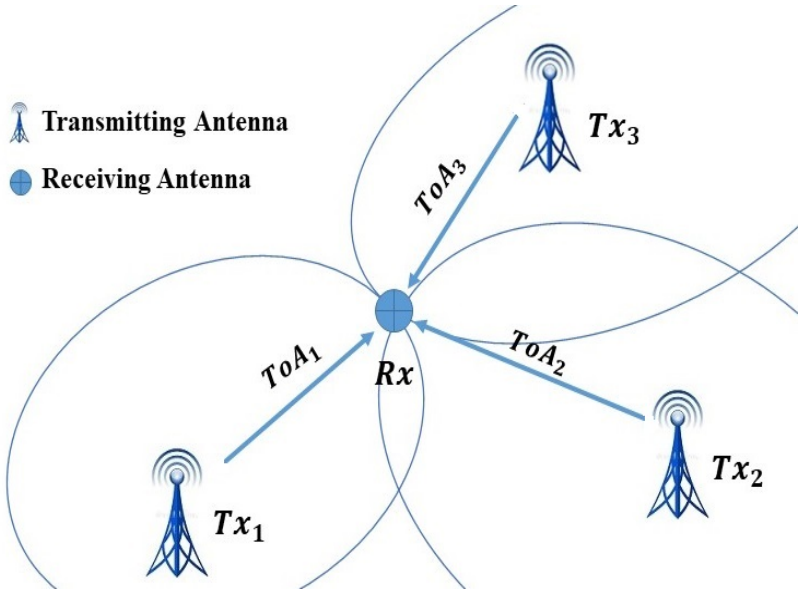

Figure 1.1 ToA-based localization

The typical signals' propagation time from the transmitting to the receiving antennas is about tens of nanoseconds in an indoor environment. Therefore, the ToA approach requires strict synchronization between Tx and Rx [4].

1.2.2 Time Difference of Arrival

The Time Difference of Arrival (TDoA) principle is focused on estimating the receiving antenna's location by determining the difference in time at which the signal is received from different transmitting antennas [5]. Thus, time difference is, in this case, sufficient to estimate the distance between the transmitter and receiver, instead of knowing the time of transmission. This method requires at least three transmitting antennas for each TDoA measurement to detect the receiver's position as the intersection of three (or more) hyperboloids.

The 2D model, illustrated in Figure 1.2 presents the intersection of the hyperboloids generated by all transmitting antennas to determine the receiver's location.

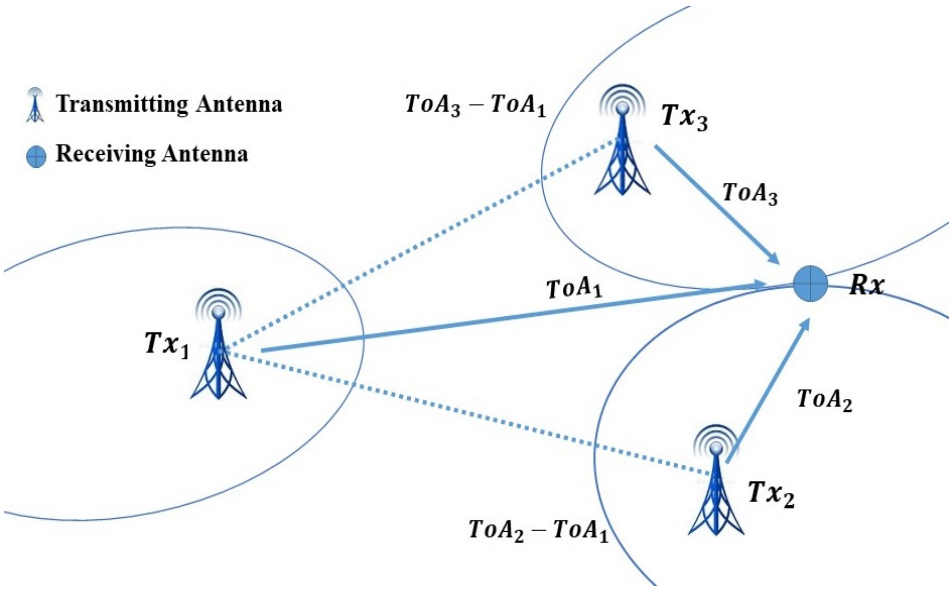

Figure 1.2 TDoA-based localization

Like the ToA, TDoA requires LoS to mitigate multipath that affect the location accuracy. Furthermore, synchronization is also mandatory in order to estimate the receiver's location accurately. But unlike the ToA technique, synchronization in TDoA is only required between the transmitting antennas (Tx), since the receiver's location is determined based on time or distance difference between them. The TDoA technique presents higher location accuracy compared to the ToA [6].

1.2.3 Angle of Arrival

Angle of Arrival (AoA) uses the angle at which the signal is received from a transmitting antenna. In the case of Angle of Departure (AoD), the transmitting antenna needs to send its absolute coordinates to the receiving antenna. With AoA, the transmitting antenna determines a directional line from its location to estimate different positions of the receiving antenna. The location of the receiver is then the intersection of several lines from several transmitting antennas (Figure 1.3).

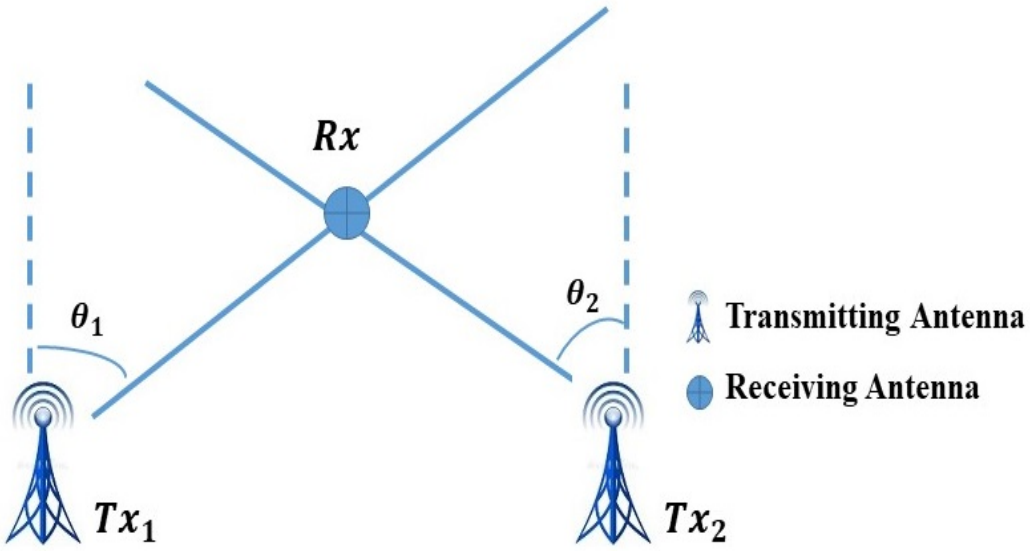

Figure 1.3 Positioning based on AoA measurement

At least two fixed transmitting antennas (Tx_1, Tx_2) with the two corresponding angles are used to determine the receiver's location (Rx) in the two dimensions space (2D). This method can also be extended into 3D, using at least three transmitting antennas.

AoA doesn't need time synchronization between transmitting (Tx) and receiving (Rx) antennas. However, although the need of complex hardware, the receiving antenna's location accuracy reduces with the increase of the transmitter-receiver distance.

Finally, the transmitter-receiver distance can also be estimated through PoA and PDoA. These two metrics are based on the phase or phase difference. It requires the pure emission of sinusoidal signals from transmitting antennas [1].

1.2.4 Received Signal Strength

The Received Signal Strength Indicator (RSSI) or the Received Signal Strength (RSS) is the simplest and the widely used approach for indoor localization due to the availability of the RSS data in most end-user devices [1]. RSS is used for distances estimation. The distance between the transmitting and receiving antennas is estimated based on RSS by converting the received power into distance. Then, a classical technique like the trilateration can be applied to detect the receiver's location (Rx) position, as illustrated in Figure 1.4.

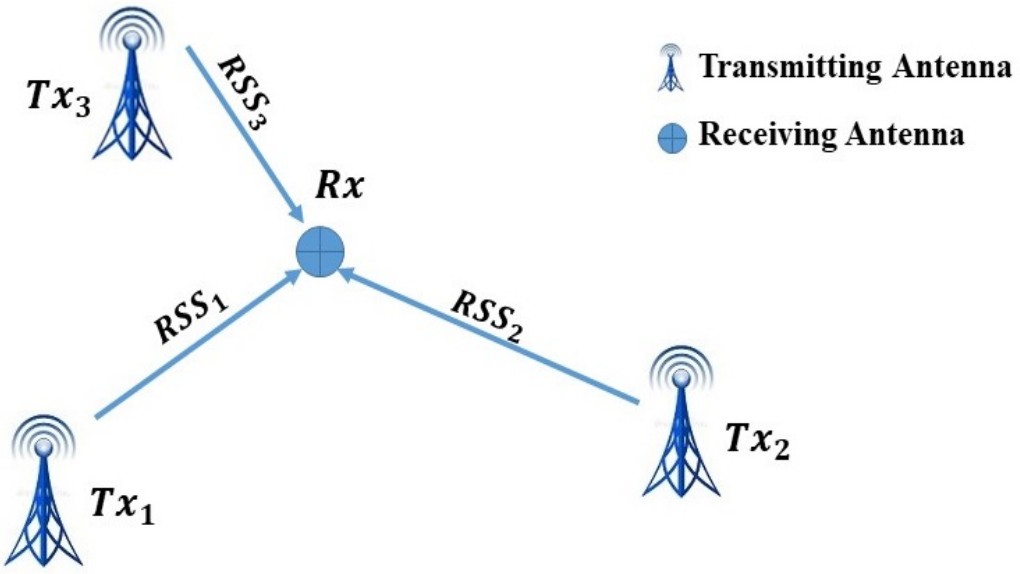

Figure 1.4 RSSI-based localization

The improvement of the location accuracy depends on the density of antennas deployed in the considered environment. Unlike ToA and TDoA, this method does not need time synchronization between the transmitting and receiving antennas.

In outdoor scenarios, RSS values are conversely proportional to the square of the transmitter-receiver distance. The RSS metric provides high location accuracy thanks to the dominance of LoS signal propagation. However, the propagated signals are affected and obstructed indoors due to shadowing and several multipath fading, making this positioning metric less accurate for distances estimation, compared to other metrics presented previously [8]. Moreover, there is no unique solution based on theoretical and empirical propagation models that could be used to avoid multipath effects. Hence, the fingerprinting method is introduced to build a radio map reflecting the real environmental impacts and investigating signals' uncertainties.

1.2.5 Summary for Positioning Metrics

Advantages and defaults of the different metrics used for localization purposes are summarized in the Table 1.1.

Table 1.1 Comparison of positioning Metrics

Metric	Advantages	Disadvantages
ToA	High localization accuracy	Time synchronization (Rx and Tx) LoS measurement Complex end-user hardware High cost
TDoA	Very High localization accuracy	Time synchronization (only Tx) LoS measurement High cost Complex end-user hardware
AoA	High localization accuracy No need for time synchronization	Calibration phase for the environment LoS measurement High cost Complex end-user hardware
RSS	Affordable cost Availability in most end-user devices Easy to implement	Dense deployment of transmitting antennas Low accuracy Radio map of the environment

Overall, the RSS positioning metric is mostly effective for ILS thanks to the availability of RSS data in most end-user devises such as smart phones. However, its high sensitivity to multipath affects the accuracy significantly.

1.3 Overview of Positioning Techniques

This section gives an overview of fundamental principles for positions determination, from various basic datasets, such as proximity, triangulation, multi/trilateration and fingerprinting observations.

1.3.1 Proximity

The proximity technique can be categorized as of three types [9]. The first one is detecting physical contact. The second one is monitoring antennas to locate the target if it is in the range of one or more antennas. The third one is observing the identification of the labeled target such as public transport cards. Labels are usually a tag, button or barcode attached on the target.

The proximity technique needs a dense number of deployed antennas in the desired field to provide the location information. This approach is relatively simple to be implemented. If only one antenna detects the target, it must be collocated with it. However, when more than one antenna detect the target, the antenna that receives the strongest signal, must be collocated with the target [10].

As in Figure 1.5, more than one reader are used, in this case the target receiving the antenna's location is defined by the intersection of these readers' coverage areas. Hence, a smaller range of the central node is recommended to improve the location accuracy.

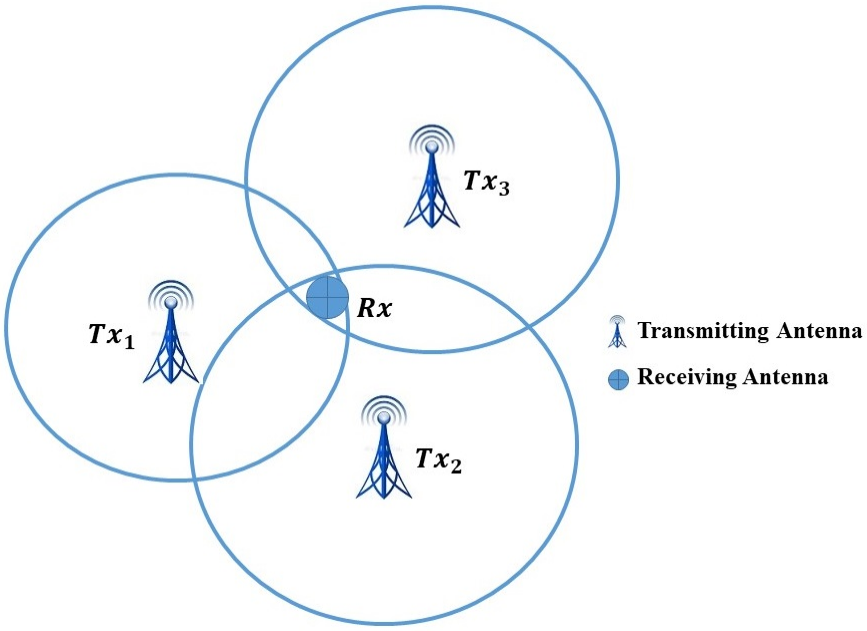

Figure 1.5 Localization by Proximity

1.3.2 Triangulation

The triangulation approach uses the triangular geometric properties to determine the target position [11]. It is estimated by determining its distance from multiple reference antennas. This approach usually uses different positioning metrics to measure the distance between the transmitting antennas and the target object such as RSS, ToA, TDoA, AoA and AoD. The advantage of AoA and AoD approaches, compared to other metrics, is that the location estimation can be made only with two transmitters in 2D.

Figure 1.6 illustrates the localization by triangulation with the AoA method. The receiving antenna indicates the target object or person to be located, and the transmitting antennas represent the location reference devices. The target location is estimated by the intersection point of the directional lines.

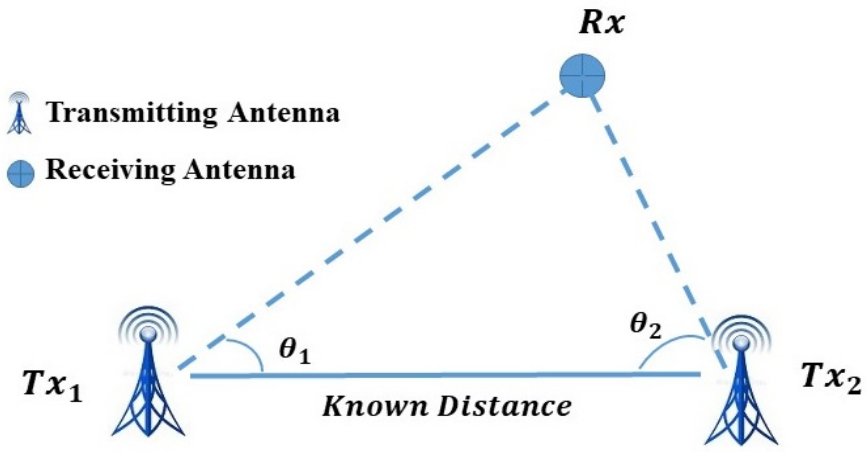

Figure 1.6 The Triangulation Technique

1.3.3 Multi/Trilateration

The term trilateration refers to the process that estimates the target position based on the distance from three known antennas [12]. After converting the RSS value to a length, each transmitter-receiver distance is represented by a circle with a radius around the fixed antenna (Tx_i) in 2D. The intersection of the three circles provides a common point or coverage area of received signals, as shown in Figure 1.7.

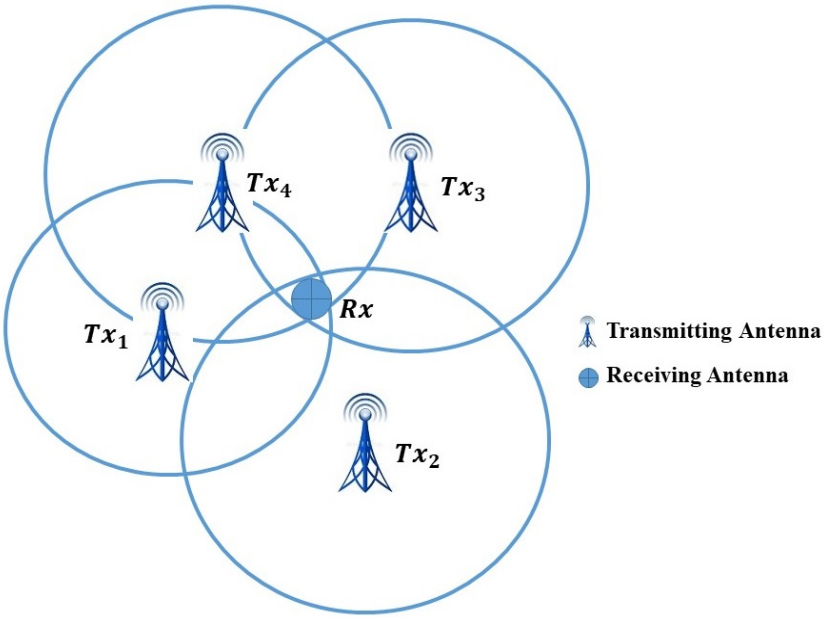

Figure 1.7 The Multi/Trilateration Technique

The multilateration technique has the same concept as trilateration, but it requires more than three fixed known antennas to locate an object [13]. Using the Euclidean distance formula, the (Rx) position is estimated.

1.3.4 Fingerprinting

Researchers have focused on applying fingerprinting within indoor localization systems [14]. It is a popular method to estimate a target location. This technique involves two stages: offline and online (Figure 1.8). During the offline stage, the collected RSSs are stored in order to build a radio map. The reliability of this stage requires more effort in terms of time and labor for the collection of fingerprints. Within the online stage, the target's location is estimated by matching the collected RSSs with the built database.

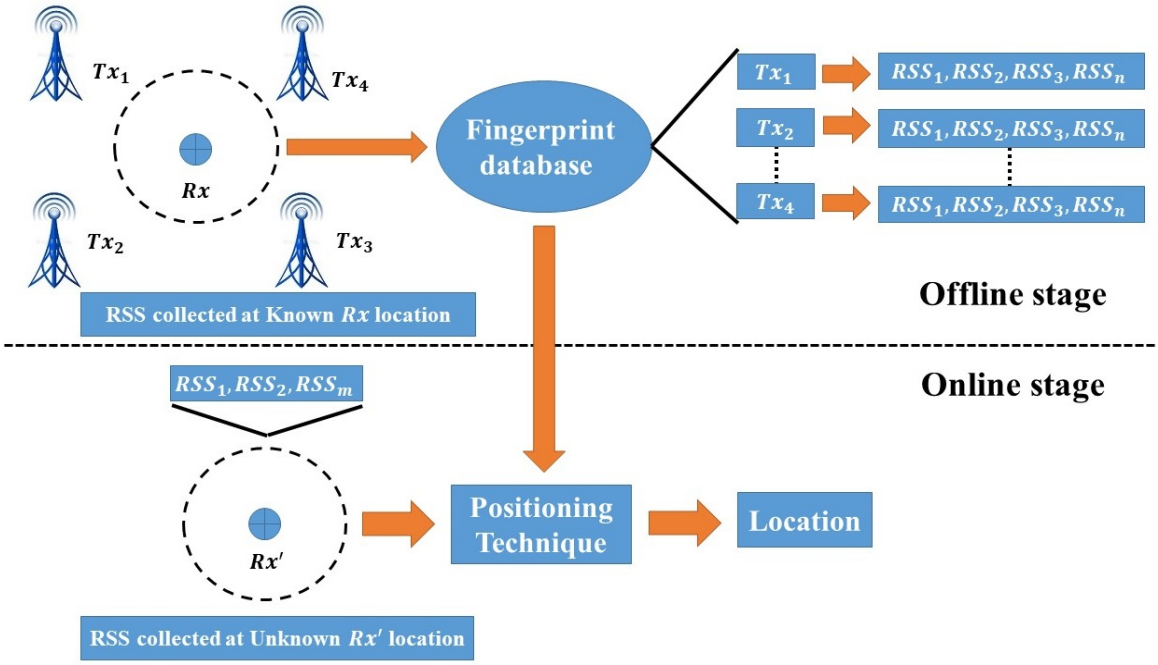

Figure 1.8 Fingerprinting

Fingerprinting can be based on either probabilistic or machine learning methods such as the K-nearest-neighbor (KNN), neural networks, Support Vector Machine (SVM), and Smallest M-vertex Polygon (SMP) [15].

The probabilistic approach stores the RSS measurements at every known position to build the probabilistic model, during the offline stage. Then, the online RSS observations are matched with the optimal RSS calculated during the offline process, to identify the target location [16].

KNN is one of the learning algorithms used by several IPSs. The target position is estimated according to the greatest similarity between the measured RSS and its k-nearest neighbors. The SVM algorithm is a more advanced learning algorithm that shows better localization accuracy with a higher computational cost. It is extensively used in medicine, engineering and science.

The SMP algorithm uses the online RSS values to detect the target's location by taking the location unit in which the RSS value is the closest to the observations. Then, it founds the nearest point within the closest boundary using the smallest distance function [17].

Any changes in the considered environment geometry or structure (walls and ceilings) as well as in furniture, modify the diffraction, reflection, and scattering; this leads to variations in the RSS spatial distribution, that doesn't correspond to the database build initially and increases the target location uncertainty. Hence, the need to update the radio map.

1.4 Overview of Positioning Technologies

In this section, technologies that have been used to provide indoor localization services will be presented and discussed. There is a wide variety of localization technologies such as vision, acoustic, ultrasound, light and Infrared (IR).

The camera or vision technology is performed in different way with fixed camera systems and mobile camera systems. The success of ILS based on optical methods comes from the improvement and miniaturization of devices and the advancement of smartphones [19]. Therefore, the location accuracy of the camera-based localization system is affected by the camera pose errors [20].

The acoustic technology shares many characteristics with Radio Frequency (RF). Three mutual challenges are faced in all acoustic-based localization systems: low Signal-to-Noise Ratio (SNR), multipath effects and the selection of speakers and microphones already embedded in smart devices [21].

The Ultrasound-based ILSs use quality control in manual assembly processes to detect the object's location [22]. This technology needs synchronization between the ultrasound emitters and receivers because the travelled distance is determined via the ToA method [23].

Concerning the light-based ILSs, they are cost-effective solutions with the popularity of Light Emitting Diode (LED). Most of the existing systems perform in 2D and fail to reach the target location in 3D [24]. This technology presents a fundamental limitation due to the NLoS between the LED and the target. It can provide a localization error less than 8 centimeters in a 25 square meters' room [25]. In the same context, Light Fidelity (LiFi) is a new wireless technology to provide the connectivity within network environments. It sends the data through LED lights with a high speed and low-cost. It also provides high security communications with large bandwidth [26].

In addition, [27] mentions that IR positioning system based on AoA present an accurate target's location. IR signals do not penetrate through walls, therefore IR ILS require a LoS communication between transmitter and receiver to perform properly.

These systems are beyond the scope of our research work. It is worth recalling that RF technology offers pervasive and low-cost solutions. We focus on radio communication technologies such as ZigBee, Bluetooth, Wireless Fidelity (WIFI), Ultra-Wideband (UWB) and Radio Frequency Identification (RFID) that will be adopted for our activity.

The following subsections present the characteristics such as cost, reliability, performance, confidentiality, coverage and the location accuracy for these radio communication technologies used within localization applications.

1.4.1 ZigBee

Referring to IEEE 802.15.4 standard, Zigbee provides low cost, low data rate and low power consumption [1]. But, it presents high maintenance cost. ZigBee usually uses the RSS values to estimate the target's position [28]. The signal coverage of a ZigBee node is up to 100 meters in free space, whereas it is typically between 20 and 30 meters indoors [29]. As this technology operates at 2.4 GHz in an Industrial, Scientific and Medical (ISM) radio frequency band, it may suffer from unintentional interference from coexisting radio devices [30].

Concerning ZigBee-based localization systems, [31] proposes an algorithm named Self-Calibrating Centroid Localization (SCCL) based on ZigBee. The optimal estimated position error achieved is less than 1 meter in an L-shaped 168 square meters' corridor. In the same context, [32] introduces a ZigBee-based ILS; in order to improve the location accuracy and mitigate the RSS fluctuations and the number of samples, a ZigBee Wireless Sensor Network (WSN) of regular variance and gradient data particle filter is used. The proposed system performs with low power consumption to achieve an average accuracy of approximately 1.5 to 2 meters in a laboratory. Recently, [33] suggests a deep learning-based device-free localization system using ZigBee. The target location is estimated via RSS. The mean error achieved is 53 centimeters in an office room with dimensions of 51.84 square meters.

1.4.2 Bluetooth

Similar to ZigBee, Bluetooth is a Wireless Personal Area Network (WPAN) standard. Yet, the Bluetooth Special Interest Group guides the proprietary specification of Bluetooth. This technology shares information between devices with high security, low cost, low power consumption, and small size [34]. It uses Frequency Hopping to protect signals against other systems that operate within the same 2.4 GHz ISM band. The communication range is about 10 centimeters to 15 meters, depending on the propagation factors such as LoS, material coverage, and antennas configuration [29]. This technology is embedded in most devices such as smartphones, smartwatches and laptops. Hence, Bluetooth can be reused by localization architectures instead of installing additional hardware. In fact, the Bluetooth-based ILSs can

use the RSS technique to estimate the target's location. However, they suffer from the instability of the RSS values due to multipath in indoor environments; this increases the positioning latency by around 10 to 30 seconds, the power consumption, and localization uncertainty between 2 and 3 meters as well [27].

With the emergence of the Bluetooth Low Energy (BLE) as the latest version of Bluetooth, data rate is improved to 24 Mega bit per second (Mbps) and the outdoor coverage to 70 to 100 meters with high energy efficiency [35]. Compared to the conventional Bluetooth, the BLE can perform with different positioning metrics such ToA, TDoA, AoA and RSS. Although, most of the existing BLE-based ILS rely on the RSS positioning metric [1]. The target location is usually determined with the proximity method when the distance between the BLE and the user is less than 1 meter.

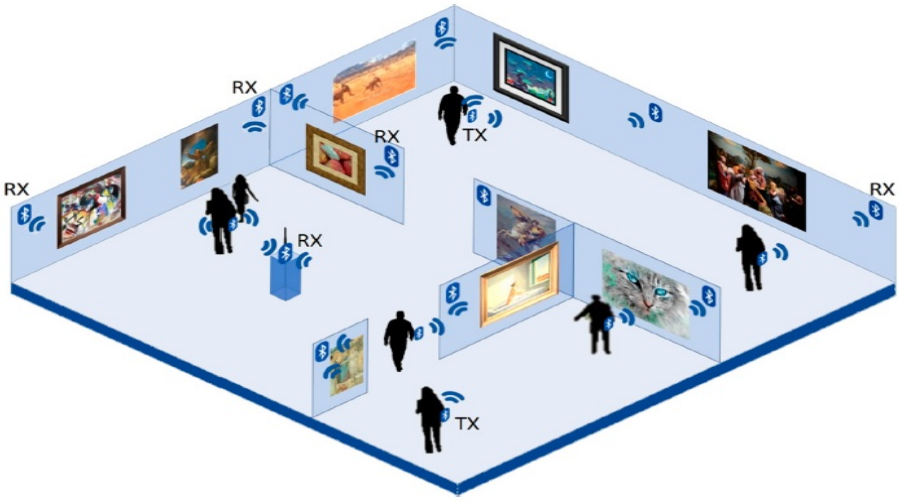

Figure 1.9 Typical architecture for BLE-based localization system [39]

According to the indoor localization literature, [2] investigates the use of Bluetooth wireless technology for positioning in different applications. [36] proposes a technique that uses the Monte Carlo localization (MCL) algorithm that exploits two sensors: accelerometer and compass, with commonly deployed BLE beacons. The average position accuracy achieved in a laboratory and an office space is less than 1 meter in LoS scenario, and 3 meters in NLoS environment. Besides, [37] intends to evaluate the accuracy of a BLE positioning system especially when multiple devices are used. That accuracy is improved by using the average or median of a certain number of RSS measurements instead of a single RSS value collected at the same spot. Furthermore, [38] studies the optimal number of BLEs to enhance the localization accuracy, using ten beacons as transmitting devices. Two algorithms and two types of filtering are used to develop an accurate ILS. By placing six beacons in a 78.84 square

meters' research lab, the optimal error achieved is 1.15 meters. Recently, [39] develops a BLE-based ILS that allows to determine the target's location accurately in a museum. The positioning scenario considers that visitors are equipped with BLE equipment. People location is estimated by applying a Non-Linear Least Square (NLLS) algorithm in the considered environment. Results, obtained by measurements, show a position accuracy in the order of 2 meters.

1.4.3 Wireless Fidelity

Wireless Fidelity (WiFi) is supported by the IEEE 802.11 standard, it operates in the 2.4 GHz ISM band. Similar to other RF technologies, WiFi provides also an effective cost and low power consumption solution. It has a communication range about 100 meters in outdoor environments. In addition, WiFi (IEEE 802.11a,h operating at 900 MHz) range is increased to cover 1 kilometer for IoT applications outdoors [1]. WiFi becomes an increasingly common infrastructure in many buildings and can be an ideal candidate for ILSs because most of current smart devices such as watches, phones and laptops are WiFi enabled. In the same context, RSS, ToA, AoA positioning metrics can be used for WiFi-based localization system.

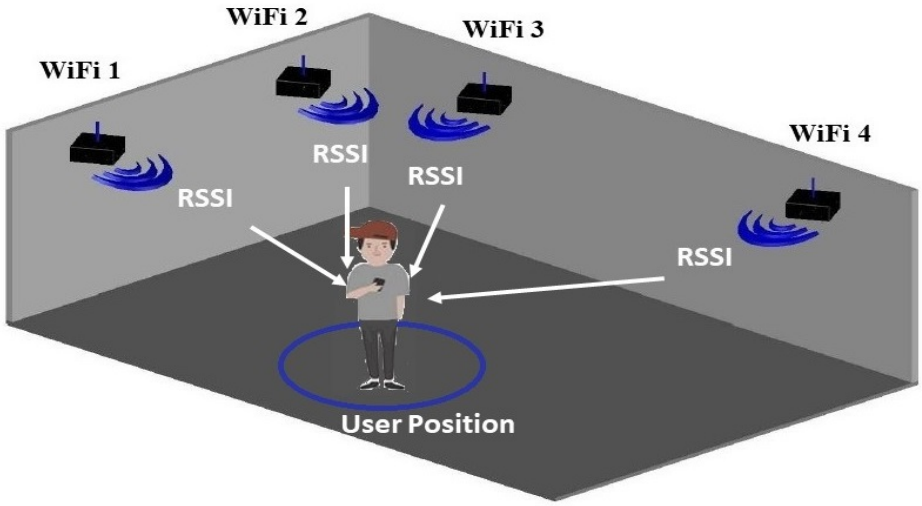

Figure 1.10 Typical architecture for WIFI-based localization system

Wireless Sensors Network (WSN) is a developed technique that can be used for indoor localization. The concept of WSN is to limit the computational power and the signal bandwidth of a WSN node to a low level. Therefore, the overall performance is well enough for monitoring environmental applications. According to some relevant researches, [40] integrates a typical WiFi-based ILS, with Pedestrian Dead Reckoning (PDR) systems using Maximum Likelihood

based fusion algorithm, to eliminate the cumulative tracking error. Corresponding results show an accuracy of about 3 to 5 meters in a 4212 square meters' area of the Nangang exhibition hall. In order to enhance performance, [41] proposes a synchronization algorithm for a WiFi-based localization system while collecting and locating. Experimental results show a maximal accuracy of 2 meters. In addition, [42] presents a real-time ILS-based on WiFi technology. The target's location is estimated using AoA method. The experiment achieves an accuracy of 1.2 meters for a Cumulative Distribution Function (CDF) of 67%. Lately, [43] proposes a High-Adaptability Indoor Localization (HAIL) approach using WiFi technology. The proposed ILS performed with the RSS positioning metric and machine learning. The achieved average localization error is of 87 centimeters in a 37.2 square meters' corridor and a 128 square meters hall.

1.4.4 Ultra-Wide Band

Ultra-Wide Band (UWB) is a radio technology for short-range and large-bandwidth communications. In UWB, a sequence of ultra-short-pulses with a low duty cycle (1 nanosecond) is transmitted through a large bandwidth (greater than 500 MHz). This technology operates in the frequency range between 3.1 to 10.6 GHz, with low power consumption [1]. UWB is widely used for short-range communications, such as PC peripherals and other indoor applications [29]. For indoor positioning, UWB can be used because it presents a strong multipath immunity. To determine the target's location, the three different positioning metrics ToA, TDoA and AoA can be used [2]. Thus, UWB-based localization systems exploit the feature of time synchronization with both ToA and TDoA metrics. However, by applying the AoA method, UWB-based ILSs perform at the expense of a high cost due to the need for end-user's hardware.

To date, several UWB localization systems have been listed. [44] proposes an ILS-based on UWB channel sounding. By combining the triangulation and the trilateration methods for ToA, AoD and AoA positioning metrics, the optimal location accuracy is 42 centimeters with LoS. Furthermore, [45] presents a fast ILS at a theoretically upper bound of 2.3 kHz. The proposed system uses the TDoA for distance estimation between anchors. It is implemented and evaluated experimentally on a low-cost platform based on the Decawave (DW1000) UWB radio. The positioning accuracy reached at 90% CDF is of 33.4 centimeters. Recently, [46] shows an UWB-based ILS using a particle filter that mitigates the ranging error of human body shadowing. ToF metric is used to determine the location of the user. Based on simulations and

measurements, performances of the proposed system are assessed in a laboratory of 78 square meters. Results show a reduction in the median position error of up to 69 and 77 centimeters, through simulations and experiments, respectively.

1.4.5 Radio Frequency IDentification

Radio Frequency IDentification (RFID) technology has received great attention in the last decade. Typical applications include baggage handling, supply chain, or fixed assets tracking [7]. It can operate at different frequency bands such as Low Frequency (LF) from 30 to 150 kHz, High Frequency (HF) from 3 to 30 MHz, Ultra-High Frequency (UHF) at 433 MHz and from 868 to 915 MHz, and Super High Frequency (SHF) from 2.4 to 2.5 GHz and 5.8 GHz [29].

RFID systems consist of readers and tags that communicate via an electromagnetic wave. Systems that operate from 30 kHz to 150 kHz and at 13.56 MHz, work in the near-field region where the distance traveled by the propagating signal is much less than its wavelength. RFID systems operating in typical UHF and SHF frequency bands, perform in the far-field region where the distance traveled by the RF propagating signal is much greater than its wavelength [47]. Tag-reader coupling is inductive in near-field region (mainly at LF and HF) while it is radiative in the far-field region (UHF and SHF).

The RFID range is wide and varies in terms of the frequency, from few centimeters up to 200 meters, whether the deployed RFID tags are passive or active [48].

1.4.5.1 Passive RFID

Passive RFID tags usually operate without battery, but an internal battery can be added to improve the system range. The passive tag consists of three parts: an antenna, a semi-conductor chip attached to the antenna, and some form of encapsulation. The RFID reader is responsible for powering and communicating with the tag. The RFID tag antenna captures the energy. Then, load modulation allows to transfer the tag's ID to the reader. Passive RFID tags are much cheaper and smaller than the active ones [29]. However, in UHF and SHF bands, due to multipath fading or absorption by objects in the range of the reader, the readability of passive tags is severely affected [49].

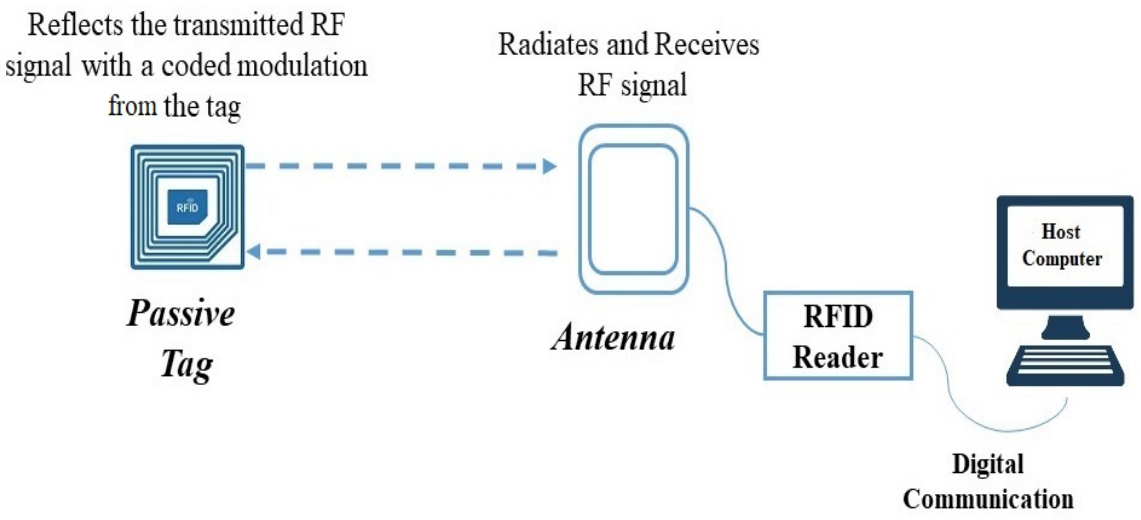

Figure 1.11 Typical architecture of Passive RFID systems

Advantages of passive RFID tags-based localization systems are their small size, strong ruggedness, relatively inexpensive installation, and maintenance specifications. They can operate at different LF, HF, UHF and microwave frequency bands. Table 1.2 lists the frequency categories and most common passive RFID system frequencies along with its communication range [48].

Table 1.2 Passive RFID Frequency Bands

Frequency Bands	Common Frequency	Communication Range
LF	30 - 150 kHz	20 centimeters
HF	3-30 MHz	10 centimeters
UHF	433 MHz	10 meters
	868 - 915 MHz	Up to 10 meters
Microwave	2.4 - 2.5 GHz	3 meters
	5.8 GHz	3 meters

Dense RFID tags or readers need to be deployed to improve the location accuracy in indoor environments. For instance, [50] applies WallSence algorithm to detect directly the target's location by applying Particle Swarm Optimization (PSO) with a novel weighted function. In fact, the localization algorithm is associated with two orthogonal tag arrays. The RFID reader operates at 920 MHz to 926 MHz band and provide the phase acquisitions for each successful identification, and reach an optimal location accuracy of 24 centimeters using 50 passive RFID tags in a large empty room of 102.3 square meters.

1.4.5.2 Active RFID Tags

An active RFID tag is equipped with a transceiver and an internal battery. This active tag provides an autonomous signals transmission to the RFID reader antenna. The embedded battery makes active transmitters heavier and costlier but allows for long detection range up to 200 meters outdoors [1].

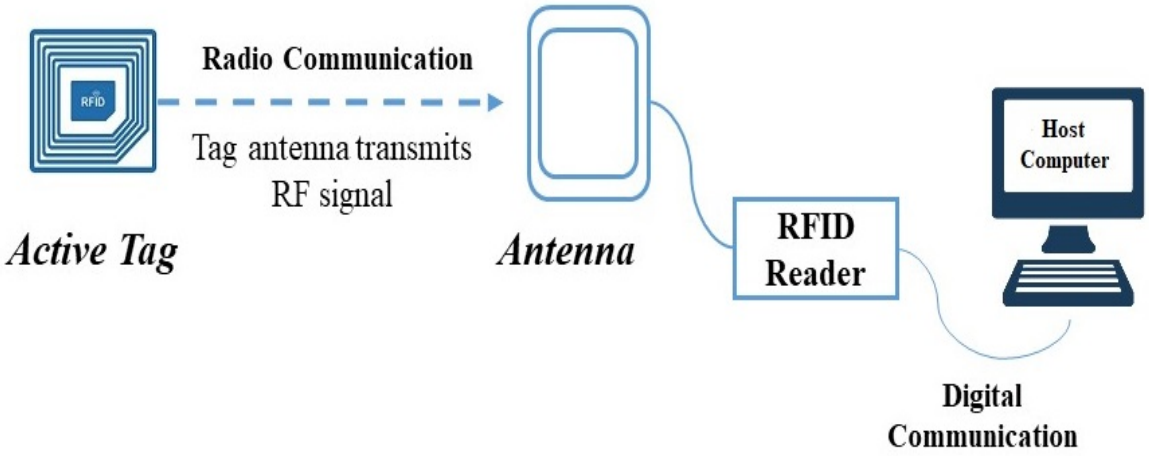

Figure 1.12 Typical architecture of Active RFID systems

The active RFID technology can be used in localization thanks to its long range detection. For instance, [51] demonstrates an auto-calibration method using 64 active RFID tags operating at 433 MHz, in a 1600 square meters indoor environment; The RFID tag detection range can reach 20 meters. The detected position accuracy is 4.9 meters using the RSS metric and 3.4 meters while applying a particle filter.

Based on the associated high coverage, we are interested to implement a new ILS using active UHF RFID tags. The proposed system will be described in the following chapter.

1.4.6 Summary for Optimal ILSs Performance

Several recently implemented ILSs were studied along with their advantages and limitations. Some of these ILSs meet high reliability, strict energy efficiency and robustness indoors. The choice of technology is a key criterion to achieve the most suitable indoor localization solution. Table 1.3 summarizes the optimal ILSs' performance for each technology, based on the associated algorithms and accuracy.

Table 1.3 Summary of the optimal ILS performance for each technology

Technology		Covered Area [m^2]	Accuracy [m]
ZigBee [33]		51.84	0.53
Bluetooth [38]		78.87	1.15
WiFi [43]		128	0.87
UWB [45]		60.5	0.33
RFID	**Passive [50]**	102.3	0.24
	Active [51]	1600	3.4

In short, the RF technology is a critical factor affecting the ILS accuracy and performance in complex indoor environments. Among these technologies, ZigBee, Bluetooth and WiFi present limited communication ranges and low locations accuracy. The UWB technology presents high location accuracy with expensive cost. However, RFID-based localization systems offer affordable cost, high-range communication, fast readability and accurate localization solutions [7].

In fact, the localization accuracy is an essential criterion. However, other ILS characteristics should be taken into consideration. They will be presented in the following section.

1.5 Indoor Localization Systems Characteristics

First of all, IPSs are generally classified into exogenous or endogenous [52], [53]. This classification is mainly based on the available infrastructure that can be used to establish locations information. For instance, WiFi infrastructures are available in the majority of indoor scenarios, and the cost of WiFi-based localization is low because no specific infrastructure is required. These exogenous IPSs were extensively studied in the past years. However, in the case of harsh indoor conditions, the already implemented infrastructure may not be efficient for high precisions. Hence, the need for developing tailored positioning systems.

Whereas, endogenous IPSs are made up of infrastructure not been installed in advanced. This kind of solutions usually requires a comprehensive site survey, a significant manpower and time for deployment, as well as more hardware. However, it provides optimal positioning

systems. In our activity, we are interested in the endogenous solution in the aim to enhance the localization accuracy in different indoor scenarios.

It is worth recalling that characteristics and performance of ILSs are application dependent. Hence, the main challenge is to define the ILS features that correspond to the application needs. Many aspects characterize each ILS and its performance [1]. Table 1.4 defines the main IPSs characteristics.

Table 1.4 Indoor Positioning Systems Characteristics

Characteristics	Definition
Availability	The technology is readily available and no need for any end-user hardware.
Cost	The system should not incur any additional infrastructure (Exogenous solution) and does not require any complex end-user hardware.
Reception Range	An accurate location recommends a reasonable communication range that depends on the application and the environment.
Accuracy	The positioning system should limit the impact of multipath effects.
Latency	The Real Time Localization System (RTLS) requires the user location without any noticeable delay.
Scalability	The system should be able to simultaneously locate or provide services to a large number of users in a large space.

These aforementioned characteristics are significant in all localization systems evaluation. Each system depends on the corresponding application and the scale of deployment. An ideal localization system should gratify all indoor applications. Yet, there is no such proposed system that satisfies all of these requirements. However, some systems, that have been proposed recently, insure most of these factors.

Finally, Table 1.5 summarizes all characteristics for each technology.

Table 1.5 Comparative Table for the different Radio Frequency Based-ILSs

Technology	Metrics	Indoor Maximum Range	Accuracy	Advantages	Disadvantages
ZigBee	RSS	30 meters	2 meters	Low cost Wide range Low power consumption	High maintenance costs Not Secure
Bluetooth	RSS; ToA; TDoA; AoA	15 meters	2 to 3 meters	Low cost Low power consumption	Limited range
Wi-Fi	RSS; ToA; TDoA; AoA	100 meters	2 meters	Low cost Large range	High variance signal High power consumption
UWB	ToA; TDoA; AoA	< 100 meters	< 1 meter	High accuracy High resistance against interference	Very expensive for end user
RFID	RSS; ToA; TDoA; AoA	< 100 meters with active tag; 2 meters with passive tag	< 1 meter with active tag; 2 to 5 meters with passive tag	Low cost with passive tags High accuracy and wide range with active tags	Limited accuracy and range with passive tags; Reasonable cost with active tags

1.6 Summary

In this chapter, we have detailed the most used positioning metrics (ToA, TDoA, AoA and RSS) followed by the different localization techniques (proximity, triangulation, trilateration and fingerprinting). In addition, different technologies, especially those based on the radio frequency, (ZigBee, Bluetooth, WiFi, UWB and RFID) are defined taking into account their features and limitations in indoor localization such as availability, cost, reception range, latency, location accuracy and scalability. The choice of the suitable technology depends on the user's application and its requirements. Based on the literature reviews, with particular emphasis on some of the IPSs performances', these competitive RF technologies are then evaluated and compared.

Based on its features, a special focus was given to the RFID technology. It will be implemented within our system. More details will be presented in the following chapters.

Bibliography

[1] F. Zafari, A. Gkelias, and K. K. Leung, “A survey of indoor localization systems and technologies,” IEEE Communications Surveys & Tutorials, vol. 21, no. 3, pp. 2568-2599, 2019.

[2] H. Liu, H. Darabi, P. Banerjee, and J. Liu, “Survey of wireless indoor positioning techniques and systems,” IEEE Trans. Syst., Man, Cybern., vol. 37, no. 6, pp. 1067-1080, Nov. 2007.

[3] C. Xu, B. Firner, Y. Zhang, and R. E. Howard, ‘‘The case for efficient and robust RF-based device-free localization,’’ IEEE Trans. Mobile Comput., vol. 15, no. 9, pp. 2362-2375, 2016.

[4] Y. T. Ma, K. Pahlavan, and Y. S. Geng, “Comparative Behavioral Modeling of POA and TOA Ranging for Location-Awareness Using RFID,” International Journal of Wireless Information Networks, vol. 23, no. 3, pp. 187-198, 2016.

[5] B. O’Keefe, “Finding Location with Time of Arrival and Time Difference of Arrival Techniques,” ECE Senior Capstone Project, 2017.

[6] R. Kaune, “Accuracy studies for TDOA and TOA localization,” in Proc. IEEE 15th International Conference on Information Fusion, Singapore, pp. 408-415, 2012.

[7] C. Li, L. Mo, and D. Zhang, “Review on UHF RFID localization methods,” IEEE Journal of Radio Frequency Identification, vol. 3, no. 4, pp. 205-215, 2019.

[8] Z. Yang, Z. Zhou, and Y. Liu, “From RSSI to CSI: Indoor localization via channel response,” ACM Computing Surveys (CSUR), vol. 46, no. 2, pp. 1-32, 2013.

[9] F. Gu, X. Hu, M. Ramezani, and D. Acharya, “Indoor localization improved by spatial context-A survey,” ACM Computing Surveys (CSUR), vol. 52, no. 3, pp. 1-35, 2019.

[10] D. Plets, N. Podevijn, J. Trogh, and L. Martens, “Experimental performance evaluation of outdoor TDoA and RSS positioning in a public lora network,” in Proc. IEEE International Conference on Indoor Positioning and Indoor Navigation (IPIN), Nantes, France, pp. 1-8, 2018.

[11] O. Tekdas and V. Isler, “Sensor placement for triangulation-based localization,” IEEE transactions on Automation Science and Engineering, vol. 7, no. 3, pp. 681-685, 2010.

[12] S. Sadowski and P. Spachos, “RSSI-Based Indoor Localization With the Internet of Things,” IEEE Access, vol. 6, pp. 30149-30161, 2018.

[13] G. Guo, R. Chen, F. Ye, X. Peng, Z. Liu, and Y. Pan, “Indoor Smartphone Localization: A Hybrid WiFi RTT-RSS Ranging Approach,” IEEE Access, vol. 7, pp. 176767-176781, 2019.

[14] C. Basri, A. El. Khadimi, “Survey on indoor localization system and recent advances of WIFI fingerprinting technique,” in Proc. 5th International Conference on Multimedia Computing and Systems (ICMCS), Marrakech, Morocco, pp. 253-259, 2016.

[15] D. Fahed and R. Liu, “Wi-Fi-based localization in dynamic indoor environment using a dynamic neural network,” International Journal of Machine Learning and Computing, vol. 3, no. 1, p. 127, 2013.

[16] Y. Li, S. Williams, B. Moran, and A. Kealy, “A probabilistic indoor localization system for heterogeneous devices,” IEEE Sensors Journal, vol. 19, no. 16, p. 6822-6832, 2019.

[17] M. D. Messaoudi, B. A. J. Menelas, and H. Mcheick, “Autonomous Smart White Cane Navigation System for Indoor Usage,” Technologies, vol. 8, no. 3, p. 37, 2020.

[18] P. Roy, and C. Chowdhury, “A Survey of Machine Learning Techniques for Indoor Localization and Navigation Systems,” *Journal of Intelligent & Robotic Systems*, 2021, vol. 101, no. 3, p. 1-34.

[19] Y. Zhao, J. Xu, J. Wu, J. Hao, and H. Qian, “Enhancing Camera-Based Multimodal Indoor Localization With Device-Free Movement Measurement Using WiFi,” IEEE Internet of Things Journal, vol. 7, no. 2, pp. 1024-1038, 2019.

[20] S. Xu, W. Chou, H. Dong, “A robust indoor localization system integrating visual localization aided by CNN-based image retrieval with Monte Carlo localization,” Sensors, vol. 19, no. 2, p. 249, 2019.

[21] M. Liu, L. Cheng, K. Qian, J. Wang, J. Wang and Y. Liu, “Indoor acoustic localization: a survey,” Human-centric Computing and Information Sciences, vol. 10, no. 1, pp. 1-24, 2020.

[22] D. Esslinger, M. Oberdorfer, M. Zeitz, and C. Tarín, “Improving ultrasound-based indoor localization systems for quality assurance in manual assembly,” In Proc. IEEE International Conference on Industrial Technology (ICIT), Buenos Aires, Argentina, pp. 563-570, 2020.

[23] R. Carotenuto, M. Merenda, D. Iero, and F. G. Della Corte, “Mobile Synchronization Recovery for Ultrasonic Indoor Positioning,” Sensors, vol. 20, no. 3, p. 702, 2020.

[24] Y. Wu, X. Liu, W. Guan, B. Chen, X. Chen, and C. Xie, “High-speed 3D indoor localization system based on visible light communication using differential evolution algorithm,” Optics Communications, vol. 424, pp. 177-189, 2018.

[25] G. Shi, Y. Li, W. Cheng, L. Dong, J. Yang, and W. Zhang, “Accuracy analysis of indoor visible light communication localization system based on received signal strength in non-line-of-sight environments by using least squares method,” Optical Engineering, vol. 58, no. 5, p. 056102, 2019.

[26] I.A. Mariya, A. G. Ettiyil, A. George, S. Nisha, and I. T. Joseph, “Li-Fi based blind indoor navigation system,” In Proc. 5th IEEE International Conference on Advanced Computing & Communication Systems (ICACCS), Coimbatore, India ,pp. 675-677, 2019.

[27] L. Mainetti, L. Patrono, and I. Sergi, “A survey on indoor positioning systems,” in Proc. IEEE International Conference on Software, Telecommunications and Computer Networks (SoftCOM), Split, Croatia, pp. 111-120, 2014.

[28] S. Lei, “Design of data acquisition system based on zigbee for wireless sensor networks,” in Proc. MATEC Web of Conferences 246, EDP Sciences, p. 3036, 2018.

[29] R. Mautz, “Indoor Positioning Technologies,” PhD thesis, ETH Zurich, 2012

[30] H. Pirayesh, P. K. Sangdeh, and H. Zeng, “Securing ZigBee Communications against Constant Jamming Attack Using Neural Network,” IEEE Internet of Things Journal, 2020.

[31] T. Ahmad, X. J. Li, and B. C Seet, “A self-calibrated centroid localization algorithm for indoor ZigBee WSNs,” in Proc. 8th IEEE International Conference on Communication Software and Networks (ICCSN), Beijing, China, pp. 455-461, 2016.

[32] M. Aykaç, E. Erçelebi, and N. B. Aldin, “ZigBee-based indoor localization system with the personal dynamic positioning method and modified particle filter estimation,” Analog Integrated Circuits and Signal Processing, vol. 92, no. 2, pp. 263-279, 2017.

[33] Y. Sun, X. Wang, and X. Zhang, “Deep Learning-Based Device-Free Localization Using ZigBee.” In Proc. International Conference in Communications, Signal Processing, and Systems. Springer, Singapore, pp. 2046-2049, 2019.

[34] R. Faragher and R. Harle, “Location Fingerprinting with Bluetooth Low Energy Beacons,” IEEE Journal on Selected Areas in Communications, vol. 33, no. 11, pp. 2418-2428, 2015.

[35] P. Octaviani and W. Ce, “Inventory Placement Mapping using Bluetooth Low Energy Beacon Technology for Warehouses,” in Proc. IEEE International Conference on Information Management and Technology (ICIMTech), Bandung , Indonesia, pp. 354-359, 2020.

[36] X. Hou and T. Arslan, “Monte Carlo localization algorithm for indoor positioning using Bluetooth Low Energy devices,” in Proc. IEEE International Conference on Localization and GNSS (ICL-GNSS), Nottingham, United Kingdom, pp. 1-6, 2017.

[37] M. Kaczmarek, J. Ruminski, and A. Bujnowski, “Accuracy analysis of the RSSI BLE Sensor Tag signal for indoor localization purposes,” in Proc. IEEE Federated Conference on Computer Science and Information Systems (FedCSIS), Gdańsk, Poland, pp. 1413-1416, 2016.

[38] S. Sadowski and P. Spachos, “Optimization of BLE beacon density for RSSI-based indoor localization,” in Proc. IEEE International Conference on Communications Workshops (ICC Workshops), Shanghai, China, pp. 1-6. 2019.

[39] R. Fazzolari, F. Mazzenga, M. Re, and A. Vizzarri, “Indoor localization system based on Bluetooth low energy for museum applications,’’ Electronics, vol. 9, no. 6, p. 1055, 2020.

[40] L. H. Chen, E. H. K. Wu, M. H. Jin, and G. H. Chen. “Intelligent Fusion of Wi-Fi and Inertial Sensor-Based Positioning Systems for Indoor Pedestrian Navigation,” IEEE Sensors Journal, vol. 14, no. 11, pp. 4034-4042, 2014.

[41] H. Yan, T. Peng, H. Liu, and Y. Ding, “Indoor Position Method of Industrial Robot Based on Wifi Fingerprint Position Technology,” in Proc. IEEE International Conference on Industrial Artificial Intelligence (IAI), Shenyang, China, pp. 1-6, 2019.

[42] Z. Tian, Z. Wang, Z. Li, and M. Zhou, “RTIL: A Real-Time Indoor Localization System by Using Angle of Arrival of Commodity WiFi Signal,” in Proc. IEEE 11th International Conference on Wireless Communications and Signal Processing (WCSP), Xi'an, China, pp. 1-6, 2019.

[43] J. Xue, J. Liu, M. Sheng, Y. Shi, and J. Li, “A WiFi fingerprint based high-adaptability indoor localization via machine learning,” China Communications, vol. 17, no. 7, pp. 247-259, 2020.

[44] B. Hanssens, D. Plents, E. Tanghe, C. Oestges, D. P. Gaillot, M. Liénard, and W. Joseph, “An indoor localization technique based on ultra-wideband AoD/AoA/ToA estimation,” in Proc. IEEE International Symposium on Antennas and Propagation (APSURSI), Fajardo, Puerto Rico, USA, pp. 1445-1446, 2016.

[45] B. Groβwindhager, M. Stocker, M. Rath, C. A. Boano, and K. Römer, “SnapLoc: An ultra-fast UWB-based indoor localization system for an unlimited number of tags,” in Proc. 18th ACM/IEEE International Conference on Information Processing in Sensor Networks (IPSN), Montreal, QC, Canada, pp. 61-72, 2019.

[46] T. Otim, TIM, A. Bahillio, L. E. DÍEZ, P. Lopez-Iturri, and F. Falcone, "Towards Sub-Meter Level UWB Indoor Localization Using Body Wearable Sensors," IEEE Access, vol. 8, pp. 178886-178899, 2020.

[47] D. Zhang, L. T. Yang, M. Chen, S. Zhao, M. Guo, and Y. Zhang, "Real-time locating systems using active RFID for Internet of Things," IEEE Systems Journal, vol. 10, no. 3, pp. 1226-1235, 2016.

[48] S. A. Ahson and M. Ilyas, "RFID handbook: applications, technology, security, and privacy," CRC press, 2017.

[49] S. Bhaskar and A. K. Singh, "A dual band dual antenna with read range enhancement for UHF RFID tags," International Journal of RF and Microwave Computer-Aided Engineering, vol. 29, no. 7, p. 21717, 2019.

[50] L. Ma, M. Liu, H. Wang, Y. Yang, N. Wang and Y. Zhang, "WallSense: Device-free indoor localization using wall-mounted UHF RFID tags," Sensors, vol. 19, no. 1, p. 68, 2019.

[51] F. Seco and A. R. Jiménez, "Autocalibration of a wireless positioning network with a FastSLAM algorithm," in Proc. IEEE International Conference on Indoor Positioning and Indoor Navigation (IPIN), Sapporo, Japan, pp. 1-8, 2017.

[52] G. Cullen, K. Curran, J. Santos, G. Maguire, and D. Bourne, "CAPTURE-Extending the scope of self-localization in Indoor Positioning Systems," In Proc. IEEE International Conference on Indoor Positioning and Indoor Navigation (IPIN), Banff, Alberta, Canada, pp. 1-10, 2015.

[53] G. Cullen, K. Curran, and J. Santos, "CAPTURE–Widening the Net–Indoor Positioning using Cooperative Techniques," In Proc. 12th International Conference on Wireless and Mobile Communications (ICWMC), Barcelona, Spain, p.81, 2016.

Chapter 2 RFID Based Localization System

2.1 Introduction

The RFID technology has shown an importance for indoor localization services, presenting a low cost, high coverage and fast readability. Several ILSs based on RFID have been proposed [1]-[3]. They can be categorized into two types: reader-based and tag-based localization.

In the case of reader-based localization, the RFID reader is usually attached to the tracked person or object while tags are installed in the environment at known locations [4]. The location of the reader is estimated through signals transmitted from tags. Accuracy and resolution of the position estimation are increased with a high density of tags deployed in the environment [5]. Hence, the system cost relatively increases with either active or passive RFID tags indoors.

Otherwise, tag-based localization systems allow to estimate positions of the RFID tags, that are placed on objects [6]. They are suitable for several applications, starting from locating goods in warehouses to tracking luggage in airports. They can provide the same location accuracy as that by reader-based localization structures.

Both architectures face several challenges. They will be described in the following section.

This chapter is organized as follows: Section 2.2 describes the major challenges facing most RFID-based localization systems along with solutions found in the literature. Section 2.3 presents the environment where our experiments will be conducted. The conventional architecture is presented in section 2.4. RFID equipment used are presented in section 2.5. Finally, the chapter is summarized in section 2.6.

2.2 Drawbacks and Existing Solutions of UHF RFID based ILSs

Several challenges hinder further development of existing RFID-based IPSs. Some of the drawbacks faced in the ILSs are the system's cost, signals' interference, signals' variability and the computation complexity.

The system's cost relies on the large number of tags and readers to be deployed [7]. Examined systems, in this subsection, are based either on passive or active RFID tags, and use

several localization techniques. [8] proposes passive RFID-based ILS. It deploys 50 passive RFID tags in a large empty room of 102.3 square meters. [9] uses 64 active RFID tags operating at 433 MHz, in a 1600 square meters indoor environment.

LANDMARC is the first feasible method that uses active RFID tags; they are usually placed in the form of a regular grid with a limited number of readers. Two different categories of tags are defined: reference and tracking tags. Reference tags are deployed and installed at known locations covering the environment. Tracking ones are attached to the moving objects. Readers receive RF signals from both tags categories. LANDMARC uses reference tags emitting the closest RSS values to those collected by the tracking tags. They are called candidate reference tags and are used to estimate the locations of the tracking tags. For instance, [10] introduces the LANDMARC concept as a solution; the RFID reader is operating at 308 MHz and the detection range of the used RFID active tags is 45.7 meters. The maximum error distance achieved is less than 2 meters, while 4 readers and 16 active reference tags are deployed to detect 8 active target tags in an indoor environment of 36 square meters. In the same context, [11] proposes an approach to improve the LANDMARC algorithm; this RFID-based ILS reaches an average estimated distance error of 75 centimeters in 50 square meters by deploying 4 RFID readers and 28 active RFID reference tags, operating at 433 MHz. Moreover, VIRE method is applied to improve the localization performance based on LANDMARC. [12] adapts the VIRE solution by adopting an array formed by 8 active reference tags. One RFID reader is used to determine the location of the target tag. This approach is validated in 9 square meters through a simulated environment. The achieved average location error is 37 centimeters.

On the same way, [13] shows a novel hybrid system for indoor localization; both SA-LANDMARC and COCKTAIL algorithms were introduced within a tested area of 36 square meters. These two algorithms run in two phases. The first phase is SA phase, which stands for Sensor Assisted. The second phase is the localization phase. It uses information of all reference tags and the Support Vector Regression (SVR) to localize the object. Accuracy reached 70 and 45 centimeters respectively, using 49 active RFID tags, operating at 303.825 MHz. Despite the SA-LANDMARC's implementation simplicity and COCKTAIL's efficiency, the achieved high precision, using both algorithms, refers to the dense deployment of active RFID tags which is around one tag per square meter. After stating these references [10]-[13], it is verified that major RFID localization systems count on the number of tags. To overcome this issue, our

proposed ILS presents an accurate and cost-efficient positioning solution by deploying a reduced number of active RFID tags.

Another drawback of existing RFID-based ILSs is the RF interference between reference tags. Moreover, the deployment of many reference tags indoors may interference between them [14]. To improve the detectability of the location target, while reducing the inter-tags interference, [15] proposes a passive RFID-based ILS with Dielectric Resonator (DR) tags with an operating bandwidth of 100 MHz. The proposed system uses the potential of the large-scale Multiple Input Multiple Output (MIMO) technology. The DR tag is composed of an array of DR elements with a unique resonance frequency. These passive tags are designed to work as reference tags. The target location is estimated by applying the Weighted Linear Least-Squares (WLLS) estimator combined with the optimal large scale MIMO-based ranging technique. This RFID localization architecture produces high location accuracy of around 75 centimeters in an office environment of 300 square meters. [16] presents an RFID localization method that uses the interference of 121 reference tags to detect the location of the passive target tag. The position information is captured by measuring the phase difference of reference tags. The frequency ranges from 920.625 MHz to 924.375 MHz. The location accuracy achieved is less than 6 centimeters in an experimental lab environment.

As additional default, large signals variability is a common anecdotal problem in most ILSs based on the RSS positioning metric [17]. This instability is due to the propagation channel non-stationarity and multipath. Therefore, the need for assuring signals stability is very essential to mitigate the location uncertainty. An available solution is presented by [18]; it implements and assesses the D-Watch device using both the direct path and multipath to improve the location accuracy to the decimeter level. Another solution is proposed by [19]. It presents an IPS-based on AoA and PDoA using Weighted Least Squares combined with Residual Weighted (WLS-RW) algorithm. This system performs with passive UHF-RFID tags in NLoS indoors. To distinguish multipath signals, an antenna array is used to find the strongest path based on RSS values. According to simulation results, this localization system can improve the location accuracy to reach 20 centimeters with a probability of 90%, in a 100 square meters' modeled room.

Looking at systems' complexity, [20] investigates the RFID localization systems based on fingerprinting. RSS data, collected by 6 readers, are from 619 passive UHF RFID reference tags, deployed in a square warehouse of 124 square meters. To know the RSS spatial distribution, during the offline stage, a deep learning algorithm called Deep Belief Network

(DBN) is designed. During the online or positioning stage, the target location is determined. The RFID localization system reaches high accuracy of 1 meter, in the considered indoor environment and outperforms several systems based on fingerprinting. Hence, the use of advanced algorithms will be recommended. However, this increases the system's cost and complexity. Table 2.1 recapitulates the main RFID-based ILSs' drawbacks and given solutions.

Table 2.1 Summary of RFID-based ILSs' Drawbacks and Solutions

Drawbacks	Proposed Solutions
High Cost	Introducing feasible algorithms to reduce the number of deployed RFID tags.
RF Interference	Integrating DR tags with the optimal large–scale MIMO technology. Measuring the phase difference of reference RFID tags.
Signals' Variability	Implementation of a D-Watch device that uses both the direct path and multipath. Use of an antenna array to find the strongest path.
Systems' complexity	Introducing a deep learning algorithm

Given the RFID-based ILSs' drawbacks aforementioned, solutions found in the literature are still laborious and complex. They differ whether the RFID system is active or passive. A brief comparison of UHF RFID localization schemes surveyed is presented in Table 2.2, showing the frequency, localization algorithm, tags density and accuracy.

Table 2.2 Comparison of UHF RFID Localization schemes

RFID-based ILS		Frequency Band	Range [m]	Tags Density/Square meters	Technique	Metric	Accuracy [m]
Passive RFID-based ILS	[8]	920-926 MHz	Not specified	0.48	WallSense	PoA	0.24
	[16]	920.25-924.37 MHz	Not specified	0.4	Landmark	PDoA	0.06
	[19]	UHF	Not specified	0.01	WLS-RW	AoA, PDoA	0.2
	[20]	UHF	Not specified	4.99	DBN	RSS	1
Active RFID-based ILS	[9]	433 MHz	20	0.04	Filter	RSS	3.4
	[10]	308 MHz	45.7	0.66	Landmark	RSS	2
	[11]	433 MHz	Not specified	0.56	Landmark	RSS	0.75
	[13]	303.72 MHz	Not specified	1.36	Cocktail	RSS	0.45
	[15]	100 MHz	Not specified	0.88	WLLS	RSS	0.75

Looking at passive UHF RFID-based ILSs providing good results, they usually performed using either the phase or deep learning algorithms. It is clear that methods using the metric of phase are more accurate but need specific hardware. In addition, deep learning approaches have a major shortcoming appearing in the computation complexity, hence increasing the computation time and the system complexity. So, the use of active RFID tags is more advantageous.

To overcome the aforementioned appearing drawbacks, we are focused on reducing the system's cost and complexity, by deploying a reduced number of UHF active RFID tags. Interference is mitigated by creating diversity of signals emitted by a group of tags. Stability is enhanced through the Maximum Likelihood Estimator (MLE) applied as RSSs combining technique.

Moreover, the system's accuracy is improved by proposing a reliable calibration approach associated with empirical indoor propagation models.

The proposed ILS is reader-based. It features locating people, with a positioning error equivalent to an individual step i.e. less than 1 meter. In the aim of covering a wide area, the tags need to have a long operation range. Hence, the proposed system operates at 433 MHz. In addition, this reduces the density of deployed tags.

2.3 Experimental Environment

Experiments were carried out in two different environments at the Engineering School EFREI-Paris: an unfurnished classroom on the fourth floor and a hall on the ground. However, the proposed localization system is assessed only in the classroom.

The environment has an area of approximately 63.75 square meters (8.5 x 7.5 square meters). Although unfurnished, this environment can still be considered complex for RF signals propagation due to its asymmetric geometry and specific structure. More precisely, the left wall presents some strengthening corners, and the right wall is full of glass. This classroom environment is also occupied by some unmovable metallic objects, including a very large heater (with 8 meters of length and 1 meter of height) with sharp blades, a metallic board on the back wall, an LCD projector on the ceiling, one fire detector fixed on the ceiling, and speakers fixed on the ceiling and also on the back wall. The four views of the classroom are shown in (Figure 2.1).

Figure 2.1 Indoor site of experiments in the classroom

The use of AutoCAD is helpful to design the indoor environment with small details. To get an accurate configuration, each object or material is drawn carefully and classified under different layers. For instance, fourteen different layers in the considered environment scenarios were introduced: concrete walls, plywood walls and ceiling, doors, LCD projector, six lamp boxes, three speakers, one fire detector, duct, big heater, pillar, windows and their frames and boards in aluminum, as illustrated in Figure 2.2. More studies on the environment structure that affects signals propagation will be elaborated in the following chapter.

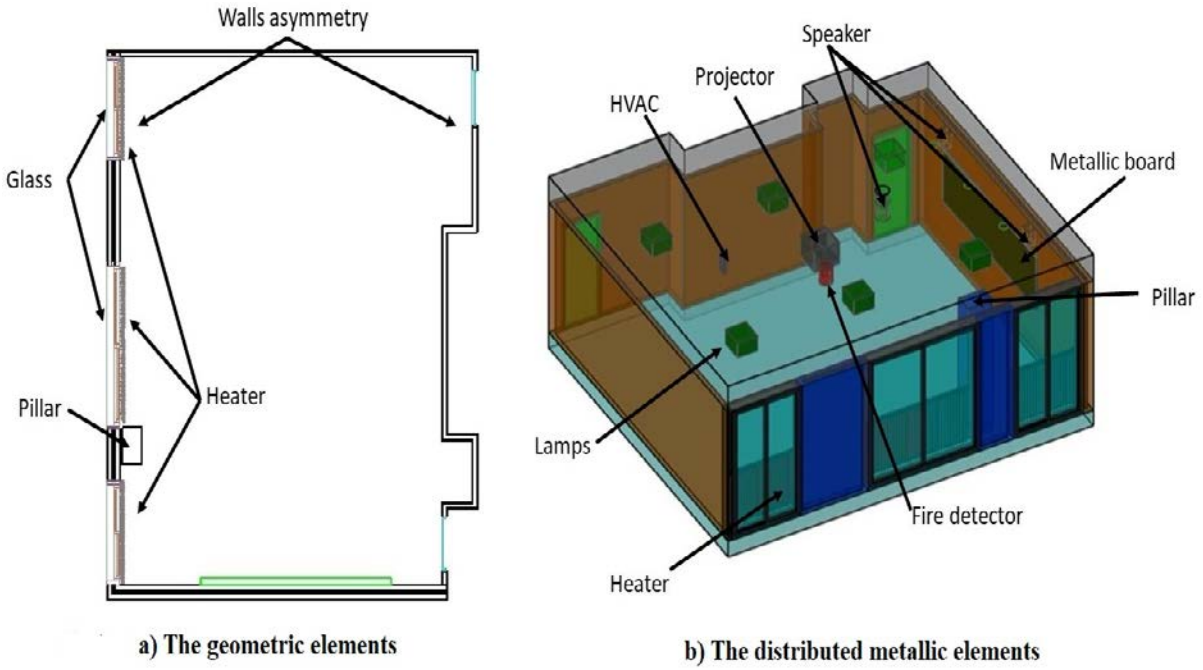

Figure 2.2 The geometric and the distributed metallic elements in the classroom environment

2.4 Conventional RFID based Localization System

It is worth recalling that our conventional localization system is reader-based with active UHF RFID tags (Figure 2.3). It applies the RSS metric for (tags-reader) distances estimation. The reader's position is then determined by applying the multilateration.

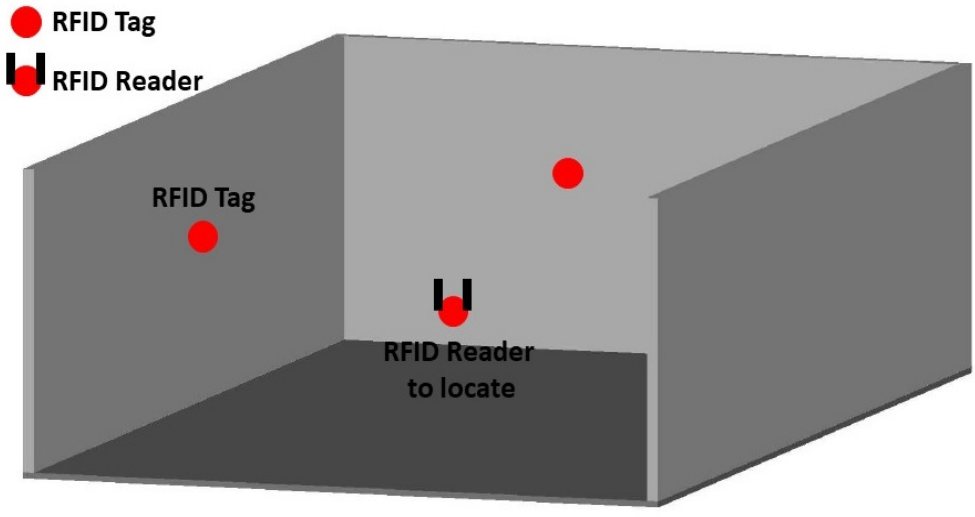

Figure 2.3 UHF RFID Based Localization Architecture

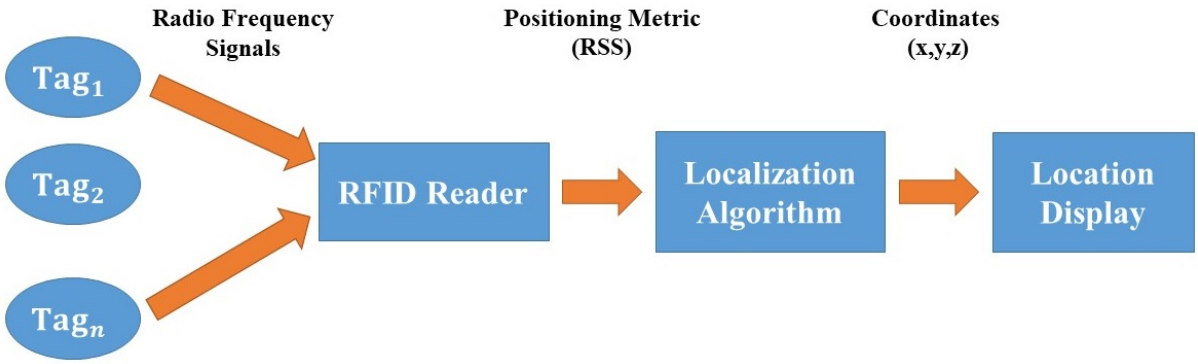

Figure 2.4 General Overview of the Conventional UHF RFID localization system

The system handles RSS values acquired in an indoor environment. It is based on auto-fingerprinting, where the RFID reader is mounted over a mobile robot.

The main principle of operation of our system is realized through two stages: offline and online stages, as illustrated in Figure 2.5. The offline stage represents an auto-calibration phase for the considered indoor environment and the online stage is the positioning phase.

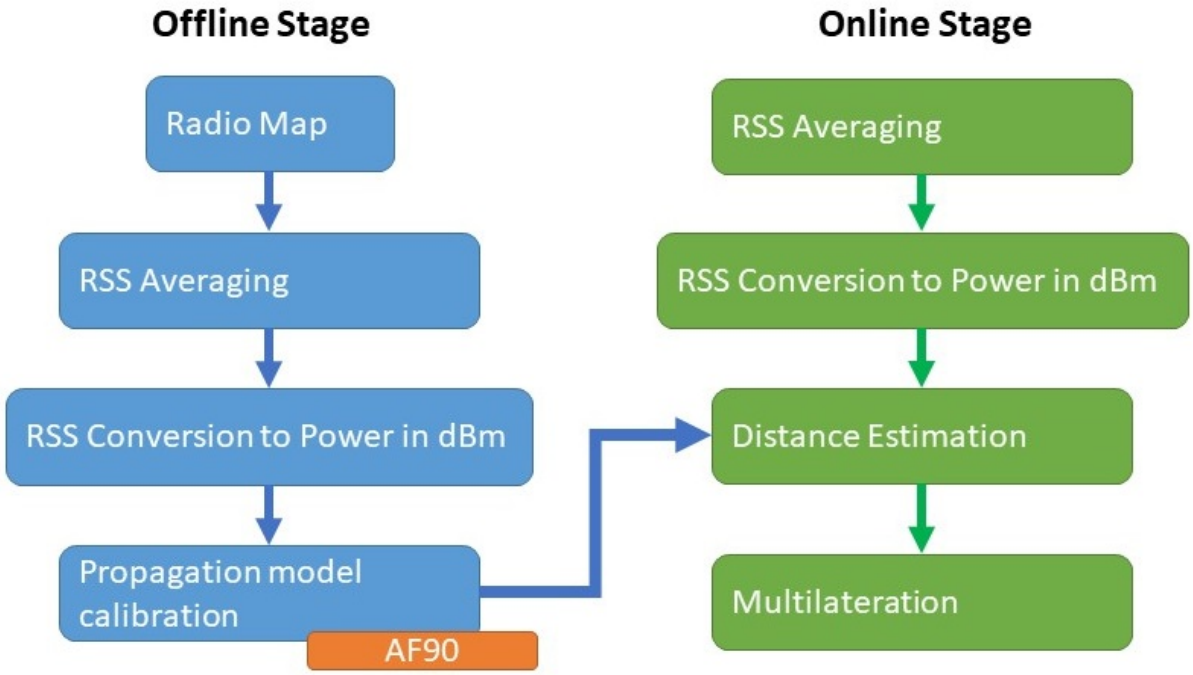

Figure 2.5 The Conventional RFID based localization system's Flowchart

Generally, the offline stage consists in establishing a radio map under the form of a training database reflecting how the signal propagates in the area of interest. This radio map is built by measuring the received power at reference positions covering this area.

Usually, advanced probabilistic or statistical algorithms are applied to match the online collected signals with the radio map, while deploying a defined number of reference tags. Thus, the computational complexity grows with the size of the database.

In our case, the training stage is performed following radial paths to limit the number of positions, which are symmetrically distributed in both sides of the classroom. Only one active RFID tag is used as a reference, to reduce the offline complexity. It is placed on the center of the front wall of the classroom as shown (Figure 2.11).

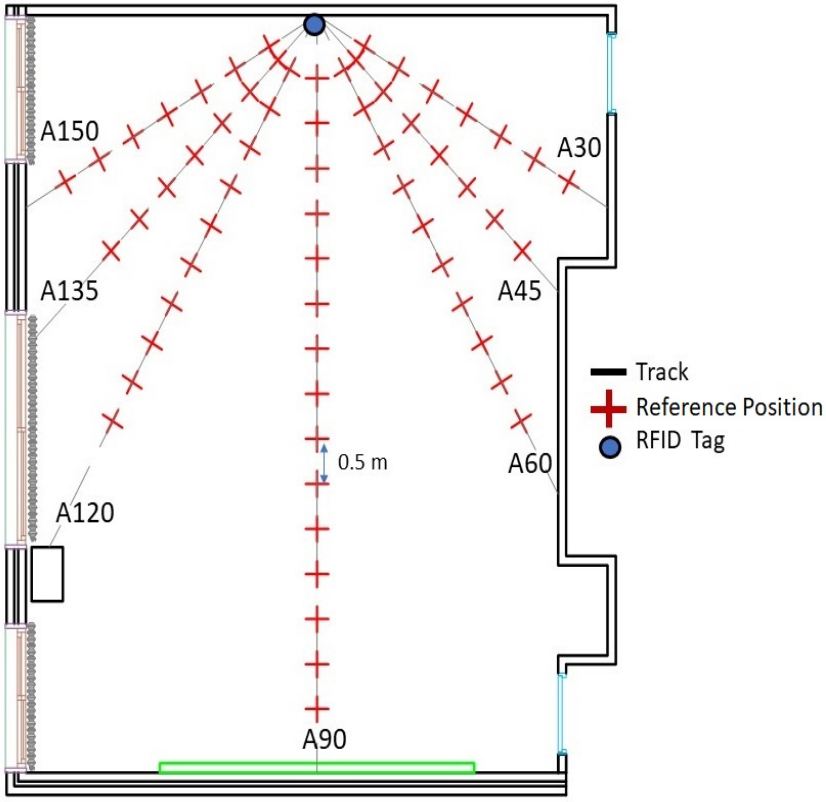

Figure 2.6 Two-dimensional floor map of the experiment site (Offline Stage)

RSSs emitted from the RFID tag are collected at reference positions, spaced by 50 centimeters over seven paths or tracks, from A30 until A150 (Figure 2.6). In fact, we would rather a half wavelength step (λ/2), in order to have a reliable calibration. However, we had to space positions by 50 centimeters to fit with the width of the isolated RFID reader mounted on the robot. At each position, 200 acquisitions of RSS are recorded and averaged. To represent propagation in the considered environment, a defined indoor propagation model is applied over the central track (A90) characterized by the highest number of positions compared to other tracks, as illustrated in Figure 2.6. These extracted attenuation parameters of the central line are symbolized by AF90.

During the online stage, RSS samples are collected. These RSSs are combined with the same technique used during the calibration stage i.e. they are averaged. The tag-reader distance is then estimated by applying the propagation model (with the parameters corresponding to our indoor environment) to the averaged values. Finally, the reader position is determined by Multilateration (Figure 2.5).

In the following subsections, our conventional RFID ILS will be introduced. The auto-radio map technique with the robot's calibration experiments are detailed in subsection 2.4.1. The RSS averaging combining technique, followed by the One Slope propagtion Model (OSM) and the multilateration, are described in subsections 2.4.2, 2.4.3 and 2.4.4, respectively.

2.4.1 Auto-Radio Map

In the aim of improving the calibration reliability as well as the localization accuracy, we investigate the robot's displacement issue. We start by an overview on the robot's systematic error and the way of calibration to typically keep it on the considered trajectory and collect the RSS acquisitions accurately, in both offline and online stages.

Most mobile robots induce systematic errors caused by imperfections in the design and mechanical implementation [21]. Therefore, robot's calibration is a key process to achieve proper results in the odometry-based navigation of any moving system.

Odometry is a fundamental robot's calibration technique. It is used in robotics to improve auto-fingerprinting and to typically keep the robot on track [22]; it handles data from motion to estimate changes in position over time; Moreover, well-calibrated odometry is an essential phase for a mobile robot to have an accurate displacement over a long path; this can be achieved through different test scenarios.

As robot platform, the model Pioneer 3-DX [23], shown in Figure 2.7, is used in the experiment. Pioneer 3-DX is a two-wheeled robot with dimensions 45.5 x 38.1 centimeters. The Software Development Kit (SDK) provided by the brand is used to control it combined with the Advanced Robot Interface for Applications (ARIA), which is a C++ library for all mobile robot platforms, allowing to access all parameters such as speed and heading.

For navigation, the two key factors are: the robot's deviation and stop estimation [24]. To guarantee accurate displacement, many experiments have been carried out by a master student on the robot odometry errors such as: the straight line, the wheels' velocity, the wheels' rotation, and the square path calibrations tests.

Figure 2.7 The Pioneer 3-DX Mobile Robot

2.4.1.1 Straight Line Test

The projection of the wheelbase center is considered as the robot's location, as shown in Figure 2.8. The robot moves along a straight line of length L until it reaches the end position.

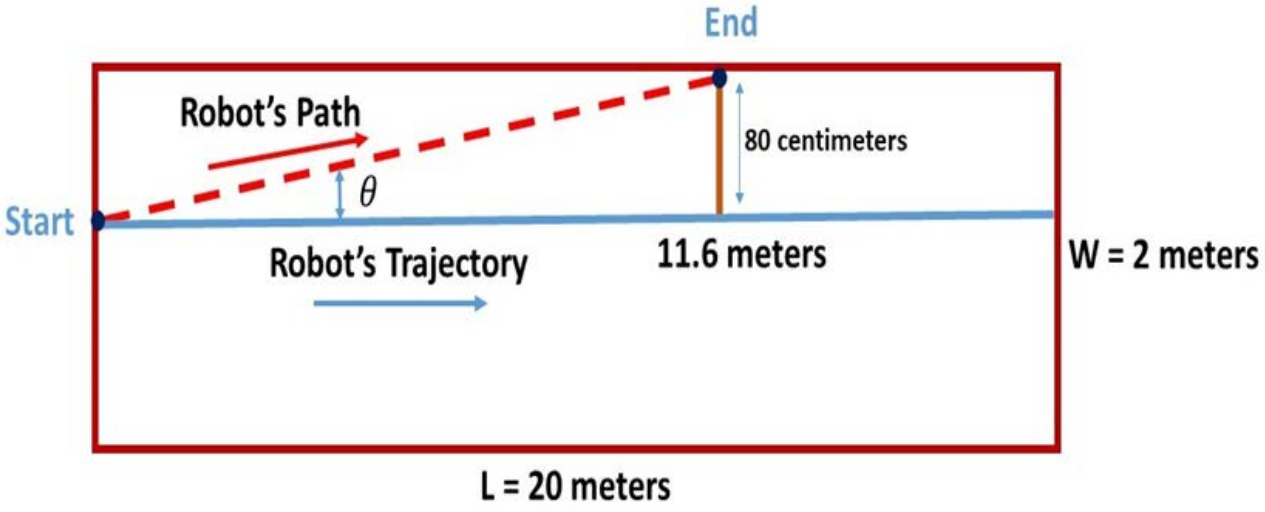

Figure 2.8 The diagram of Straight Line

This test was done in a corridor whose dimensions are: 22.5 x 2 meters. The robot was placed at a distance of 80 centimeters from the left wall instead of the midline as the right wall of the corridor isn't straight all long. The expected robot's trajectory is the straight line of 20 meters. As shown in Table 2.3, three tests were carried out and the deviation was calculated at each 1 meter.

Table 2.3 Wheels' Deviations over Straight Path

Number of Tests	Test 1	Test 2	Test 3	Mean Deviation [cm]
Deviation/1 m [cm]	6.78	6.75	6.72	6.75

It can be noticed that the robot deviates to the left and hits the wall at a distance of 11.6 meters. This deviation can be neglected at the beginning. But, correction is required as the robot moves forward. Before evaluating the localization system performance, further investigations about the robot's displacement are needed to correct its deflection. A straight trajectory may be obtained by changing the speed of the left wheel.

2.4.1.2 Wheels' Velocity Test

In this subsection, the wheels' speed test was applied in order to figure out the origin of the robot's drift away from the straight line. ARIA has some functions that make it possible to obtain the linear speed of each wheel. Test was done over a straight line of 5 meters by displaying the speed of each wheel every second. Experiment was repeated three times. Angular velocities (rad/s) are converted into linear speeds (mm/s) using the equations expressed below:

$$V_l = R.W_l \tag{2.1}$$

And

$$V_r = R.W_r \tag{2.2}$$

With V_l and V_r are the linear speed of the left and right wheel respectively. W_l and W_r are the angular velocity of the left and right wheels respectively. R is the wheels' radius.

Knowing that the wheels radius is of 92.5 mm [23], Table 2.4 represents the absolute difference between the speed of the right and left wheel.

Table 2.4 Difference between Wheels velocity

Number of Tests	Test 1	Test 2	Test 3
$\|V_l - V_r\|$ **[mm/s]**	0.04	0.01	0.03

Based on these tests, the difference between speeds is quiet small with a worst case of 0.04 mm/s. In short, the problem of the robot's deviation was not due to the difference in the wheels' velocity.

2.4.1.3 Wheels' Rotation Test

As the wheels speed is not behind the robot's drift, wheels rotation test is necessary to analyze the wheels' rotation stability. Thus, the robot was rotated about itself 360° at the same speed in two directions i.e. ClockWise (CW) and CounterClockWise (CCW). The difference in angular velocity between the two wheels was analyzed. Then, the angle deviations are measured in both directions. Figure 2.9 presents the rotation errors for the six trials.

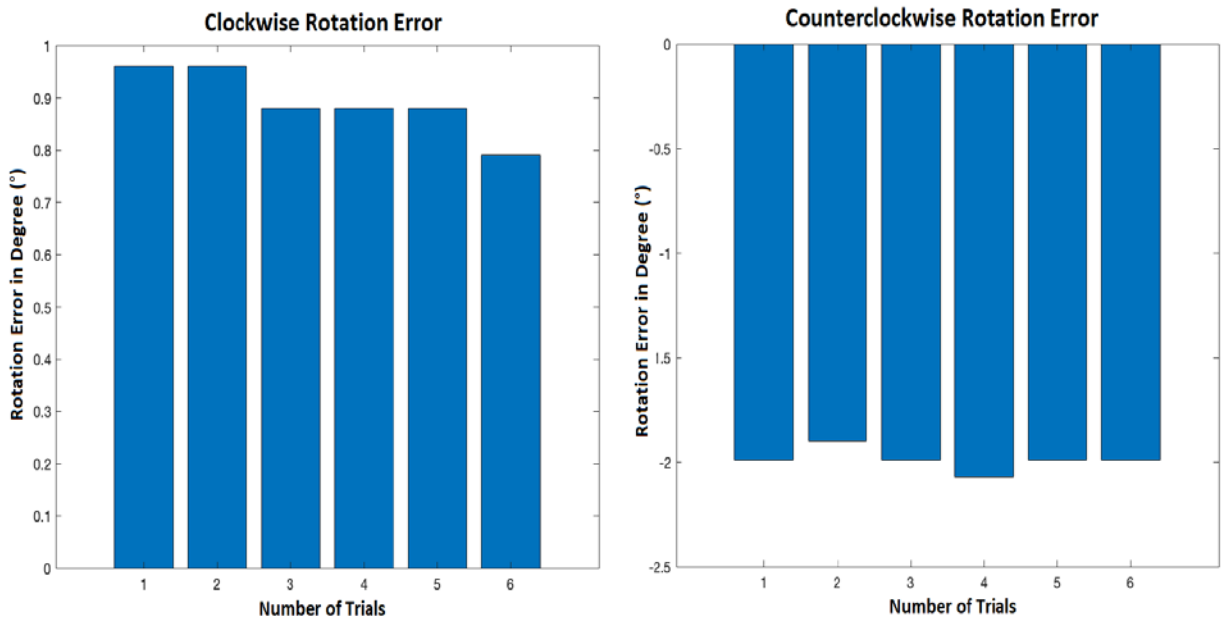

Figure 2.9 Clockwise and Counterclockwise rotation error

Figure 2.9 shows that when the robot turns clockwise, it can almost do 360° whereas it rotates 359.1° on average. However, counterclockwise, the robot tends to rotate more than 360° whereas it rotates around 362° on average. It can be noticed that the wheels' rotation is almost stable and cannot be considered as the cause of the robot's deviation. Hence, another test is finally elaborated to show the robot's performance in a complete cycle path.

2.4.1.4 Square Path Test

For this test, the procedure defined as the University of Michigan Benchmark test (UMBmark) [25] is adopted as it is especially designed to uncover certain systematic errors. This method is a set of test runs in which the robot is programmed to follow a 4×4 meters

square path, as shown in Figure 2.10. Due to systematic errors, after linear and turning movement, the robot had a position offset and could not get back to the initial point.

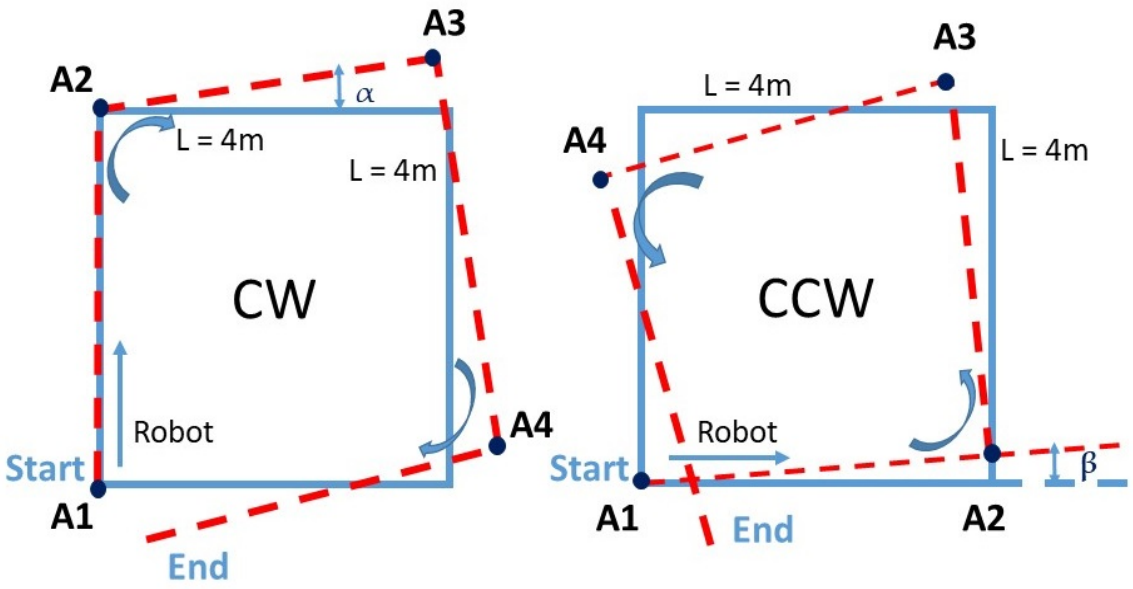

Figure 2.10 Diagram of a square path clockwise and counterclockwise

For both CW and CCW scenarios followed by the mobile robot, offsets were studied upon ten trials. The average of each angle was calculated as shown in Table 2.5.

Table 2.5 Robot Angles' deviation

Angle	**A1**	**A2**	**A3**	**A4**
Clockwise (α)	90.1°	93.6°	92.4°	88.4°
Counterclockwise (β)	88.1°	88.6°	98.3°	81.1°

Upon tests results', it can be concluded that the robot tends to drift to the left. However, the deviation angle is relatively small compared to 90°. Over short distances (less than 1 meter), and with the large size of the robot that is equal to 45.5 centimeters, the deviation does not significantly affect the robot's displacement accuracy. It corresponds to only 6.66% of the robot length.

Over a longer trajectory, and referring to the straight-line test (Figure 2.7), the robot presents an angle deviation of $\tan^{-1}(\theta) = 0.8/11.6 = 3.95°$ to the left. Thus, to have an accurate mapping coverage and stable robot's motion, an auto-correction by a rotation of 3.95° clockwise needs to be applied.

2.4.2 RSSs Combining by Averaging

According to the literature, most common calibration databases use the averaged RSS value computed at a particular distance from the transmitting antenna [26]-[30]. In this framework, [28] puts forward an RSS based localization system using wireless sensor networks. Experiment is performed in a laboratory of 77 square meters. The obtained optimal positioning error is of 2 meters. [29] proposes a new synchronization protocol between the offline and online stages of the auto-fingerprinting based on averaging RSSs. The location accuracy of the proposed indoor localization system reaches 2 meters. In the same context, [30] also presents a system using the average of the RSS values as combining technique; performance of the proposed architecture is analyzed to achieve a location accuracy of 1.22 meters. Thus, we adopt the average technique as RSS combining method in our conventional indoor localization system.

During the offline and online stages, 200 and 20 RSS values are respectively collected at each position. They are combined via the averaging technique. Figure 2.11 presents the flowchart of the localization system based on average RSSs.

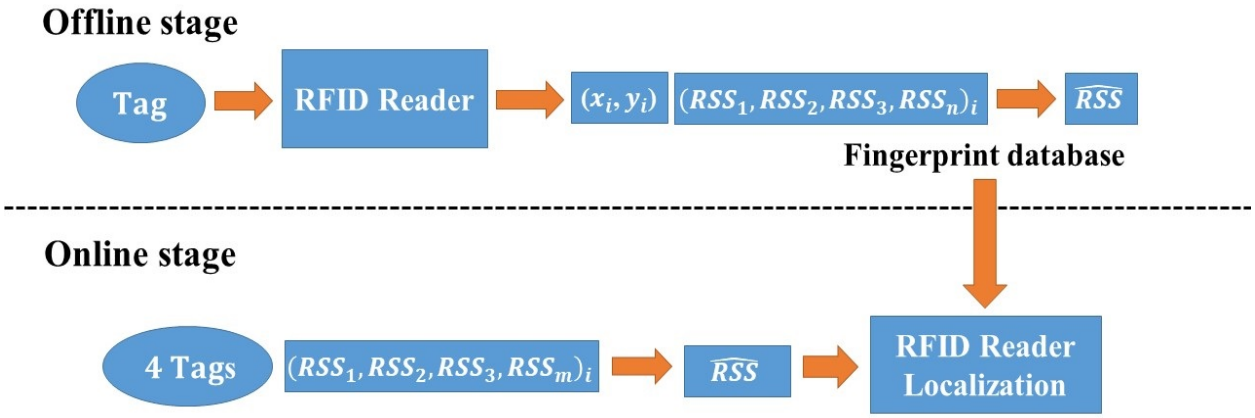

Figure 2.11 Flowchart of the ILS based on the Average Technique

2.4.3 Calibration and Distance Estimation by One Slope Propagation Model

To estimate the tag-reader distance from the received power, we need to apply a signal propagation model. Up to date, the One Slope propagation Model (OSM) is still the most commonly used in indoor localization applications [31] because of its simplicity.

OSM consists in a deterministic analysis that can only be applied in few rather simple cases.

In free space, according to Friis formula [33], the received power P_{r_out} by an antenna at a distance d from a transmitter can be represented by:

$$P_{r\_out}(d) = P_t . G_t . G_r . \left(\frac{\lambda}{4\pi d}\right)^2 \quad (2.3)$$

Where P_t is the transmitted power in watt, G_t is the transmitting antenna gain, G_r is the receiving antenna gain, λ is the wavelength in meters, and d is the distance in meters.

In the logarithmic scale, the received power P_{0_out} at 1 meter in dBm can be expressed as follows:

$$P_{0\_out}(d = 1) = 10 . \log(P_t . G_t . G_r . \left(\frac{\lambda}{4\pi}\right)^2) \quad (2.4)$$

And, the received power in outdoor, in dBm can be expressed as follows:

$$P_{r\_out}(d) = P_{0\_out} - 20 . log_{10}(d) \quad (2.5)$$

Where P_{r_out} is the received power, P_{0_out} is the received power in the free space at distance 1 meter from the transmitter.

Indoors, the attenuation factor varies between 1.6 and 5 [32]. This variation is due to NLoS and multipath effects.

In our case, the conventional ILS applies the OSM defined as follows:

$$P_r(d) = P_0 - 10 . n . log_{10}(d) + X \quad (2.6)$$

With $P_r(d)$ is the received power in dBm, P_0 is the received power at 1 meter in dBm. n defines the attenuation coefficient. The term X describes the standard deviation of the received power values throughout the corresponding area.

2.4.4 Multilateration

As defined in chapter 1, section 1.3.3, multilateration is the process that estimates a target location based on the estimation of distances from several reference points [34]. Within the proposed RFID based localization system, the reader position is determined based on multi tags-reader distances estimation and using RSS values collected by the RFID reader. However, indoor, RSSs are inversely proportional to the tag–reader distance and the random noise factor [35]. Each estimated distance is represented by a circle around the fixed associated tag. The intersection of the different circles provides a common point or a coverage area of the received signals as shown in Figure 2.12.

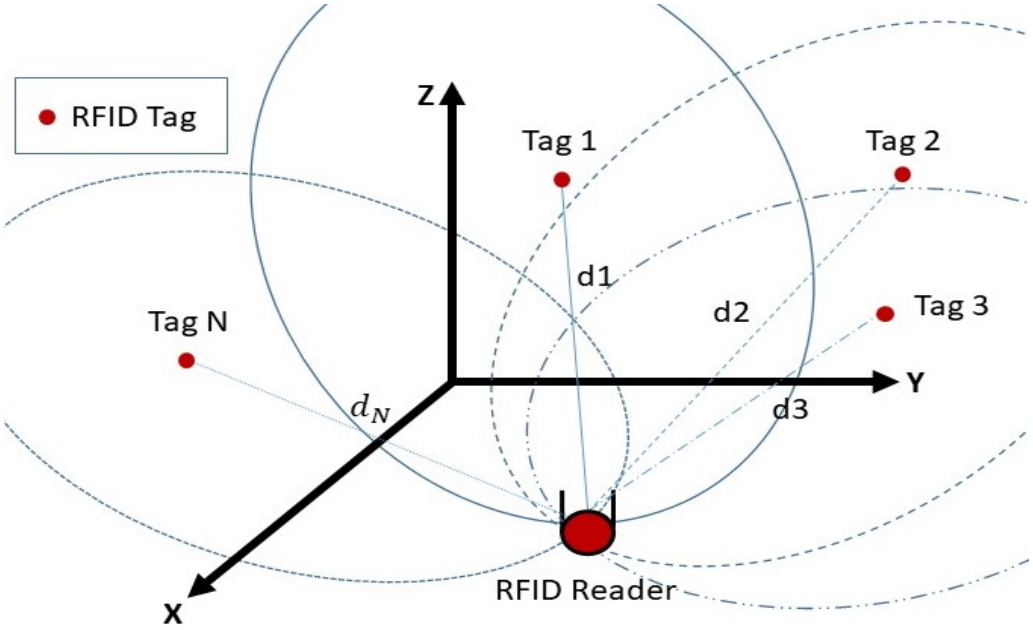

Figure 2.12 Positioning by Multilateration

According to the Euclidean distance formula, nonlinear equations are formulated as follows:

$$(a - x_i)^2 + (b - y_i)^2 + (c - z_i)^2 = {d_i}^2 \quad (2.7)$$

P(a,b,c) represents the unknown reader's location. (x_i, y_i, z_i) represents the i^{th} known tag coordinates, and d_i represents the distance between the reader and the i^{th} tag.

The multilateration technique is based on distances to N reference RFID tags (N>3), assumed fixed in space and located at known coordinates (x_i, y_i, z_i). A movable RFID reader is located at an unknown position P(a,b,c). The high number of tags may improve the

localization accuracy compared to the trilateration approach, where only three fixed tags are needed, but position is determined based on three distances instead of N.

Expanding and regrouping terms in equation (2.7) we obtain:

$$A.\begin{pmatrix} a \\ b \\ c \end{pmatrix} = B \tag{2.8}$$

With

$$A = 2((x_{i+1} - x_i) \quad (y_{i+1} - y_i) \quad (z_{i+1} - z_i)) \tag{2.9}$$

And

$$B = (d_1^2 - d_{i+1}^2 - [(x_1^2 - x_{i+1}^2) - (y_1^2 - y_{i+1}^2) - (z_1^2 - z_{i+1}^2)]) \tag{2.10}$$

Where i is the index of the deployed RFID tags i.e, i ∈ {1, 2, …, (N-1)}.

The solution of equation (2.8), that corresponds to the intersection of the circles, determines the reader's coordinates as follows:

$$\begin{pmatrix} a \\ b \\ c \end{pmatrix} = A^{-1}B \tag{2.11}$$

In our system, we are working in a two-dimensional plane as four deployed RFID tags and the reader are at the same height. Given the asymmetrical shape of the classroom walls (Figure 2.1), we chose to reduce the effects of the ground and the ceiling reflections which are rather symmetric. In this spot, the RFID tags are fixed horizontally at the center of each wall, and at the same reader's height of 1.25 meters from the ground.

Thus, the applicate parameter can be omitted. For instance, P(a,b) represents the unknown reader's location. (x_i, y_i) represents the i^{th} known tag coordinates, and d_i represents the distance between the reader and the i^{th} tag (Figure 2.13).

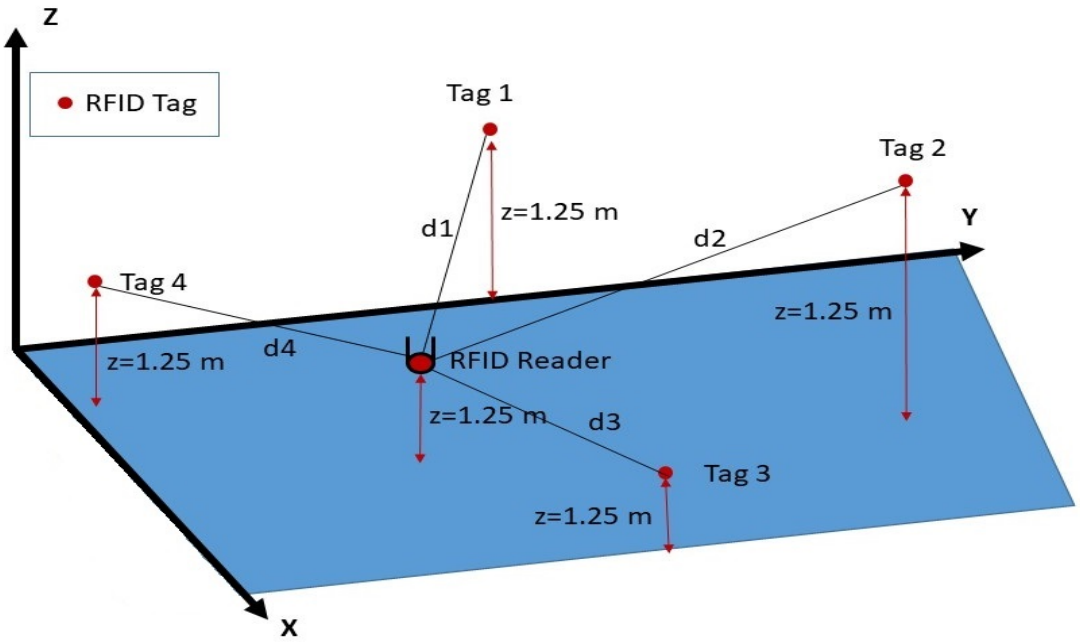

Figure 2.13 Positioning by Multilateration in Two-dimensional Layout

Only three RFID tags, fixed on three walls, could be used to locate the reader. We rather used four tags, fixed horizontally at the centers of the four walls respectively, in order to improve more the positioning accuracy. Hence, four quadratic equations are considered to estimate the RFID reader position given by:

$$\binom{a}{b} = A^{-1}B \tag{2.12}$$

With

$$A = 2((x_{i+1} - x_1) \quad (y_{i+1} - y_1)) \tag{2.13}$$

And

$$B = (d_1^2 - d_{i+1}^2 - [(x_1^2 - x_{i+1}^2) - (y_1^2 - y_{i+1}^2)]) \tag{2.14}$$

i is the index of the deployed RFID tags i.e, $i \in \{1, 2, 3\}$.

2.5 RFID Equipment

The ILS used active UHF-RFID tags and a reader that operate at 433 MHz, as this frequency offers a larger communication range than that provided by the 2.4 GHz band used in most indoor localization systems and is less affected by multipath fading [36].

The RFID equipment is proprietary of Ela-Innovation; it does not comply with RFID standards. Figure 2.14 (a) shows the “Coin ID” tag. This UHF RFID tag can be detected from as far as 20 meters indoors. It presents a fast identification time (less than 1 second). Moreover, it operates according to an active identification process in periodic transmission. More precisely, transmission is non-continuous, the signal emission time is around 1 millisecond and the time difference between two consecutives transmissions is around 200 milliseconds. In the same context, this active RFID tag is powered by a 3 Volt battery. Its antenna has an omnidirectional radiation pattern [37].

The RFID reader is illustrated in Figure 2.14 (b). It is an “UTP Diff 2”, powered by a 6 V battery and can be configured using onboard instructions as well as a software interface, that does not include any anti-collision protocol.

It worth recalling that 200 and 20 RSS values are respectively collected at each position, during the offline and online stages. As the transmission is non-continuous, the 20 acquisitions are collected in 4 seconds, within the online stage. Whereas, around 40 seconds are needed to collect the 200 samples, in the offline stage. Due to the transmission intermittence and long acquisition duration, the propagation channel, between the tag and the reader, can be considered as non-stationary.

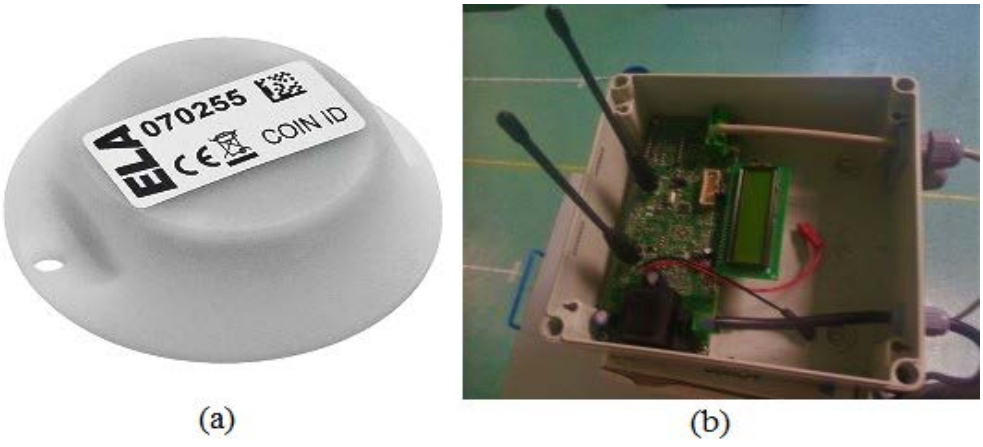

Figure 2.14 (a) Coin ID RFID tag and (b) UTP Diff 2 RFID reader

Ela Manufacturer provides Figure 2.15 that can be used to deduce the relationship between the RSS values collected by the reader and the received power in dBm. The received power in dBm is expressed as follows:

$$P_{dBm} = 30.84 - 0.632 * RSS \quad (2.15)$$

Where P_{dBm} is the received power in dBm. *RSSI* is the received signal strength in decimal.

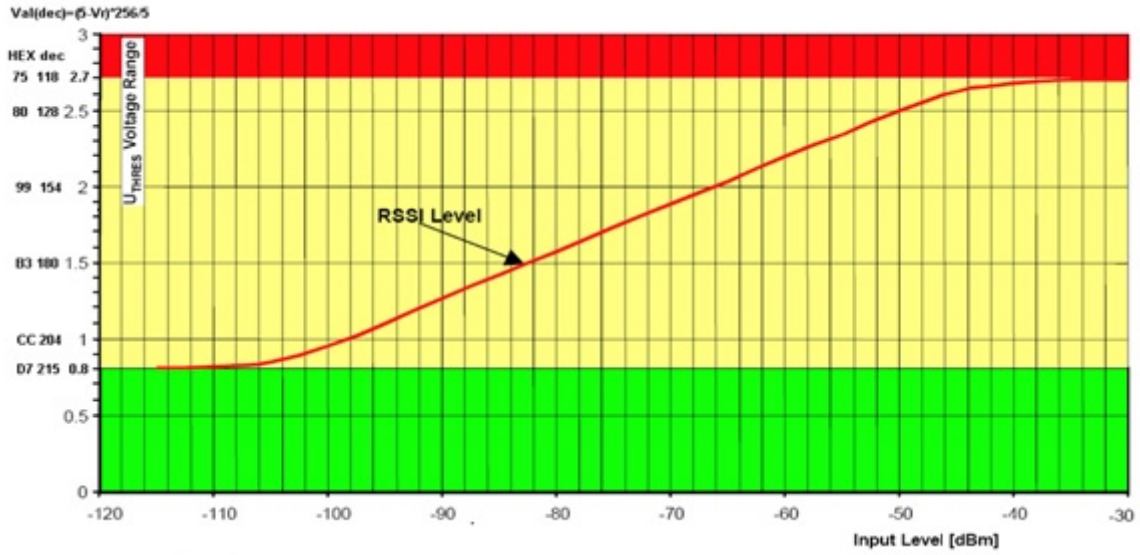

Figure 2.15 RSSI vs Power [dBm]

It can be noticed, on Figure 2.15, that RSS values vary linearly in the range between 128 to 204. In our further processing, RSS values out of this linear range are filtered out.

Besides, it is worth mentioning that the step between two adjacent RSS values is equivalent to 0.6 dB. Thus, the quantization error, based on the RFID reader dynamic range, is equivalent to $\pm$ 0.3 dB.

2.6 Summary

In this chapter, the major drawbacks of RFID-based ILSs and associated solutions are presented. A conventional system is then described. It is divided into two stages: offline and online. The offline stage is focused on building a radio map for the indoor environment. Whereas, the RFID reader position is determined during the online stage. Both, offline radio map and online distances estimation are done using the average technique for RSSs combining. The simplest and most used indoor propagation model (OSM) followed by the multilateration technique are also shown. Finally, the RFID equipment is described.

The conventional system is our baseline; it will be improved in the following chapters in the aim to feature cost effective RFID tags deployment, along with low RSS variability, as well as enhanced radio map reliability and location accuracy.

Bibliography

[1] S. Siachalou, S. Megalou, A. Tzitzis, E. Tsardoulias, A. Bletsas, J. Sahalos, and A. G. Dimitriou, “Robotic Inventorying and Localization of RFID Tags, Exploiting Phase-Fingerprinting,” in Proc. IEEE International Conference on RFID Technology and Applications (RFID-TA), Pisa, Italy, pp. 362–367, Sep. 2019.

[2] A. Motroni, P. Nepa, V. Magnago, A. Buffi, B. Tellini, D. Fontanelli, and D. Macii, “SAR-based indoor localization of UHF-RFID tags via mobile robot,” in Proc. IEEE International Conference on Indoor Positioning and Indoor Navigation (IPIN), Nantes, France, pp. 1-8, 2018.

[3] J. Wu, M. Zhu, B. Xiao, and Y. Qiu, “The improved fingerprint-based indoor localization with RFID/PDR/MM technologies,” in Proc. IEEE 24th International Conference on Parallel and Distributed Systems (ICPADS), Singapore, pp. 878-885, 2018.

[4] A. Aguilar-Garcia, S. Fortes, R. Barco, and E. Colin, “Enhancing localization accuracy with multi-antenna UHF RFID fingerprinting,” in Proc. IEEE International Conference on Indoor Positioning and Indoor Navigation (IPIN), Banff, AB, Canada, pp. 1-9, 2015.

[5] L. M. Ni, D. Zhang, and M. R. Souryal, “RFID-based localization and tracking technologies,” IEEE Wireless Communications, vol. 18, no. 2, p. 45-51, 2011.

[6] Z. Gao, Y. Ma, K. Liu, X. Miao, and Y. Zhao, “An Indoor Multi-Tag Cooperative Localization Algorithm Based on NMDS for RFID,” IEEE Sensors Journal, vol. 17, no. 7, pp. 2120–2128, 2017.

[7] H. Zou, H. Wang, L. Xie, L., and Q. S. Jia, “An RFID indoor positioning system by using weighted path loss and extreme learning machine,” in Proc. IEEE 1st International Conference on Cyber-Physical Systems, Networks, and Applications (CPSNA), Taipei, Taiwan, pp. 66-71, 2013.

[8] L. Ma, M. Liu, H. Wang, Y. Yang, N. Wang and Y. Zhang, “WallSense: Device-free indoor localization using wall-mounted UHF RFID tags,” Sensors, vol. 19, no. 1, p. 68, 2019.

[9] F. Seco and A. R. Jiménez, “Autocalibration of a wireless positioning network with a FastSLAM algorithm,” in Proc. IEEE International Conference on Indoor Positioning and Indoor Navigation (IPIN), Sapporo, Japan, pp. 1-8, 2017.

[10] Ni, L., Y. Liu, and Y. Lau. “LANDMARC: Indoor Location Sensing Using Active RFID,” in Proc. IEEE 1st International Conference on innovative Computing Information and Control, vol. 3, no. 2, pp. 407-415. 2003.

[11] D. Cui, and Q. Zhang, “The RFID data clustering algorithm for improving indoor network positioning based on LANDMARC technology,” Cluster Computing, vol. 22, no. 3, pp. 5731-5738, 2019.

[12] E. Ferraz, P. Seixas, C. Carvalho, “Three-dimensional location in RFID systems with mobile reader,” in Proc. International Conference on Artificial Intelligence and Advanced Manufacturing, Dublin, Ireland, pp. 1-6, 2019.

[13] Z. Dian, L. Kezhong, and M. Rui, “A precise RFID indoor localization system with sensor network assistance,” China Communications, vol. 12, no. 4, pp. 13–22, 2015.

[14] H. Zou, L. Xie, Q. S. Jia, and H. Wang, “Platform and algorithm development for a RFID-based indoor positioning system,” Unmanned Systems, vol. 2, no. 3, pp. 279-291, 2014.

[15] M. El-Absi, F. Zheng, A. Abuelhaija, A. H. Abbas, K. Solbach, and T. Kaiser, “Indoor Large-Scale MIMO-Based RSSI Localization with Low-Complexity RFID Infrastructure,” Sensors, vol. 20, no. 14, p. 3933, 2020.

[16] M. Liu, M., H. Wang, Y. Yang, Y. Zhang, L. Li, J. Xu, and N. Wang, “RFID indoor localization system for tag and tagfree target based on interference,” in Proc. IEEE 19th International Conference on Advanced Communication Technology (ICACT), South Korea · PyeongChang, Korea, pp. 372-376, 2017.

[17] X. Zhu, W. Qu, T. Qiu, L. Zhao, M. Atiquzzaman, and D. O. Wu, “Indoor Intelligent Fingerprint-Based Localization: Principles, Approaches and Challenges,” IEEE Communications Surveys & Tutorials, vol. 22, no. 4, pp. 2634-2657, 2020.

[18] J. Wang, J. Xiong, H. Jiang, X. Chen, and D. Fang, “D-Watch: Embracing “Bad” multipaths for device-free localization with COTS RFID devices,” IEEE/ACM Transactions on Networking, vol. 25, no. 6, pp. 3559-3572, 2017.

[19] Y. Ma, B. Wang, S. Pei,Y. Zhang,S. Zhang, and J. Yu, “An indoor localization method based on AOA and PDOA using virtual stations in multipath and NLOS environments for passive UHF RFID,” IEEE Access, vol. 6, pp. 31772-31782, 2018.

[20] H. Jiang, C. Peng, and J. Sun, “Deep Belief Network for Fingerprinting-Based RFID Indoor Localization,” in Proc. IEEE International Conference on Communications (ICC), Shanghai, China, pp. 1-5, 2019.

[21] P. Roy, and C. Chowdhury, “A Survey of Machine Learning Techniques for Indoor Localization and Navigation Systems,” Journal of Intelligent & Robotic Systems, vol. 101, no. 3, pp. 1-34, 2021.

[22] A. Loganathan, N. S. Ahmad, and P. Goh, “Self-adaptive filtering approach for improved indoor localization of a mobile node with zigbee-based RSSI and odometry,” Sensors, vol. 19, no. 21, p. 4748, 2019.

[23] Adept MobileRobots (2011) Pioneer 3-DX Datasheet. http://www.mobilerobots.com/Libraries/Downloads/Pioneer3DX-P3DX-RevA.sflb.ashx.

[24] S. Park and S. Hashimoto, “Autonomous Mobile Robot Navigation Using Passive RFID in Indoor Environment,” IEEE Trans. Ind. Electron., vol. 56, no. 7, pp. 2366–2373, 2009.

[25] J. Borenstein, and L. Feng, “UMBmark - A method for measuring, comparing, and correcting dead-reckoning errors in mobile robots,” Tech. Report UM-MEAM-94-22 (2nd ed.) University of Michigan, 1994.

[26] M. Kaczmarek, J. Ruminski, and A. Bujnowski, “Accuracy analysis of the RSSI BLE Sensor Tag signal for indoor localization purposes,” in Proc. IEEE Federated Conference on Computer Science and Information Systems (FedCSIS), pp. 1413-1416, Gdańsk, Poland, 2016.

[27] W. Xue, W. Qiu, X. Hua, and K. Yu, “Improved Wi-Fi RSSI measurement for indoor localization,” IEEE Sensors Journal, vol. 17, no 7, pp. 2224-2230, 2017.

[28] P. Barsocchi, S. Lenzi, S. Chessa, and G. Giunta, “A novel approach to indoor RSSI localization by automatic calibration of the wireless propagation model,” in Proc. IEEE 69th Vehicular Technology Conference, Barcelona, Spain, pp. 1-5, 2009.

[29] H. Yan, T. Peng, H. Liu, and Y. Ding, “Indoor Position Method of Industrial Robot Based on Wifi Fingerprint Position Technology,” in Proc. IEEE 1st International Conference on Industrial Artificial Intelligence (IAI), Shenyang, China, pp. 1-6, 2019.

[30] Z. Farid, I. U. Khan, E. Scavino, and M. A. A. Rahman, “A WLAN Fingerprinting Based Indoor Localization Technique via Artificial Neural Network,” International Journal of Computer Science and Network Security (IJCSNS), vol. 19, no. 7, p. 157, 2019.

[31] S. Bertoldo, M. Paredes, L. Carosso, M. Allegretti, and P. Savi, “Empirical indoor propagation models for LoRa radio link in an office environment,” in Proc. IEEE 13th European Conference on Antennas and Propagation (EuCAP), Krakow, Poland, pp. 1-5, 2019.

[32] J. Miranda, R. Abrishambaf, T. Gomes, P. Gonçalves, J. Cabral, A. Tavares, and J. Monteiro, “Path loss exponent analysis in wireless sensor networks: Experimental evaluation,” in Proc. IEEE 11th International Conference on Industrial Informatics (INDIN), Bochum, Germany, pp. 54-58, 2013.

[33] A. F. Molisch, “Wireless communications,” vol. 34, John Wiley & Sons, New York, USA., 2012.

[34] M. Bouet and A. L. Dos Santos, “RFID Tags: Positioning Principles and Localization Techniques,” in Proc. IEEE 1st Wireless Days (IFIP), Dubai, United Arab Emirates, pp. 1-5, 2008.

[35] Q. Wang; I. Balasingham, M. Zhang, and X. Huang, “Improving RSS based ranging in LOS-NLOS scenario using GMMs.” IEEE Commun. Lett., vol. 15, no. 10, pp. 1065–1067, 2011.

[36] P. Tuset-Peiró, A. Anglès-Vazquez, J. López-Vicario, and X. Vilajosana-Guillén, “On the suitability of the 433 MHz band for M2M low-power wireless communications: propagation aspects,” Transactions on Emerging Telecommunications Technologies, vol. 25, no. 12, pp. 1154–1168, 2014.

[37] Ela Innovation, SA. (2014) Ela Innovation active RFID tag and reader manufacturer. Available online: https://elainnovation.com/ (accessed on April 2021).

Chapter 3 Environment and Hardware Modeling

3.1 Introduction

Indoor scenarios represent one of the most complex geometries with exterior walls, windows, doors, etc. On shelves software like WinProp are well adapted to study the coverage of propagating signals in such indoor environments, hence reducing the need for costly measurements.

Considering exhaustively all materials' parameters such as Fresnel parameters and all empirical loss coefficients, predictions of the propagative behavior of signals can be provided in a precise way. It is important to keep in mind that indoor building materials are prerequisite to simulate the environment. Hence, an accurate 3D environment was designed and validated by an in-depth comparison of received power values obtained via a campaign of real measurements.

This chapter focuses on presenting the accurate environment model. Tools used to design the 3D layouts will be introduced in section 3.2. In section 3.3, two indoor environments are well presented with all modeling details. In section 3.4, the different steps for simulation, including the simulated RFID tag's antenna, reader antenna and configured indoor environments, will be expanded. In section 3.5, a comparison between the power values collected by the reader through simulations and real measurements is dressed. Finally, the summary of this chapter is presented in section 3.6.

3.2 WinProp tool

There are several commercial software that predict signals propagation indoors such as EDX [1], Ranplan [2] and WinProp [3]. Most of these tools provide fast simulations, thanks to the preprocessing of the indoor materials' properties that is required for the prediction [4].

WinProp simulator has been selected to model the indoor environment and the RFID hardware based on its reasonable license cost and its features to import CAD files for electromagnetic simulations, as well as it provides accurate and fast propagation models in addition to the empirical and semi-deterministic methods for radio coverage and network planning. Moreover, [5] presents a satisfactory realistic results showing good agreement between simulations and measurements.

Winprop contains several tools (WallMan, AMan, ProMan) and different features that provide a wide interface for the user to present simulations. WallMan is used to design the environment and define the building database. AMan is mainly focused on antennas configuration. Then, signals coverage is characterized with ProMan. ProMan also includes empirical and semi-empirical models e.g. 3D Ray-Tracing and the Dominant Path Model (DPM).

These propagation models differ depending on the prediction accuracy and the computational resources. Performance of this software is reported in the literature as follows: [5] characterizes signals behavior over the 700 MHz band with different propagation models. According to the presented results, Ray-Tracing provides more accurate modeling than that by other methods. [6] verifies WinProp capability to correctly predict the propagation characteristics of the 5G radio coverage at millimeter-wave bands in different urban city centers. In this context, [7] compares empirical or Ray-Tracing propagation models to real measurements. It shows that the new approach, based on 3D vector building databases, exceeds the accuracy of the Dominant path propagation model.

3.3 Environments for Tests

We aim to characterize signals behavior in two considered indoor environments, using active RFID tags operating at 433MHz. The RFID equipment used is already presented in chapter 2, section 2.6.

Experiments are carried out in the following environments: an empty classroom on the fourth floor and a hall on the ground floor of the Engineering School EFREI-Paris.

It is worth recalling that the classroom has typical dimensions, with an area of approximately 63.75 square meters (8.5 x 7.5 square meters). Although unfurnished, this environment may still be considered as complex for RF signals propagation due to its asymmetrical walls. It also contains some unmovable metallic objects such as the heater (with 8 meters of length and 1 meter of height) with sharp blades, LCD projector, fire detector, and speakers (Figure 3.1).

Figure 3.1 Indoor site of experiments in the classroom

The hall is an indoor area of 205 square meter, with a traditional ceiling, as shown in Figure 3.2. It is also complex for RF signals propagation because of the geometrical shape (shape of L), and the presence of some metallic objects such as big heaters, billboard, fire detectors and doors.

Figure 3.2 Indoor site of experiments in the hall

3.4 Simulation Setup

As previously mentioned, WinProp contains several tools that allow to get accurate simulations. The workflow for a typical indoor propagation simulation is represented as follows: Subsection 3.4.1 introduces WallMan, where the geometry of the considered environment is created. In subsections 3.4.2 and 3.4.3, AMan and Feko perform to produce the RFID tag's antenna pattern and reader's antenna pattern, respectively. These patterns can be exported in the correct format to be used for the RF coverage scenario. Finally, simulations, of the propagation model and illustrations of the received power done by ProMan, are explained in subsection 3.4.4.

3.4.1 Environment Properties

The use of AutoCAD is helpful to design the indoor environment with small details. To get an accurate configuration, each object or material is drawn carefully and classified under different layers.

For instance, fourteen different layers in the considered classroom were introduced: concrete walls, plywood walls and ceiling, doors, LCD projector, six lamp boxes, three speakers, one fire detector, duct, big heater, pillar, windows and their frames and boards in aluminum, as illustrated in Figure 3.3.

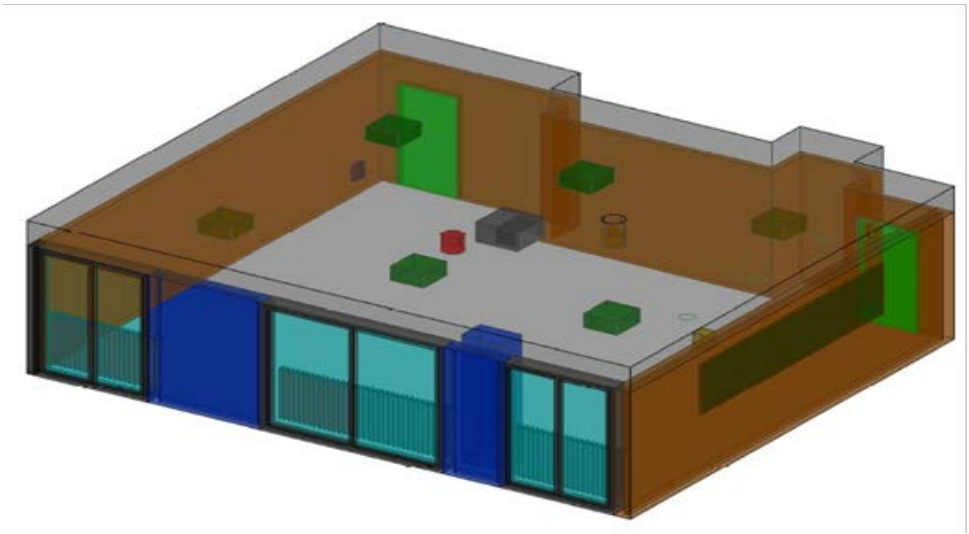

Figure 3.3 3D Layout of the classroom environment

Furthermore, eight different layers in the considered hall environment were introduced: concrete walls, plywood walls and ceiling, doors, twelves lamp boxes, two fire detector, big heaters, windows and their frames, as illustrated in Figure 3.4.

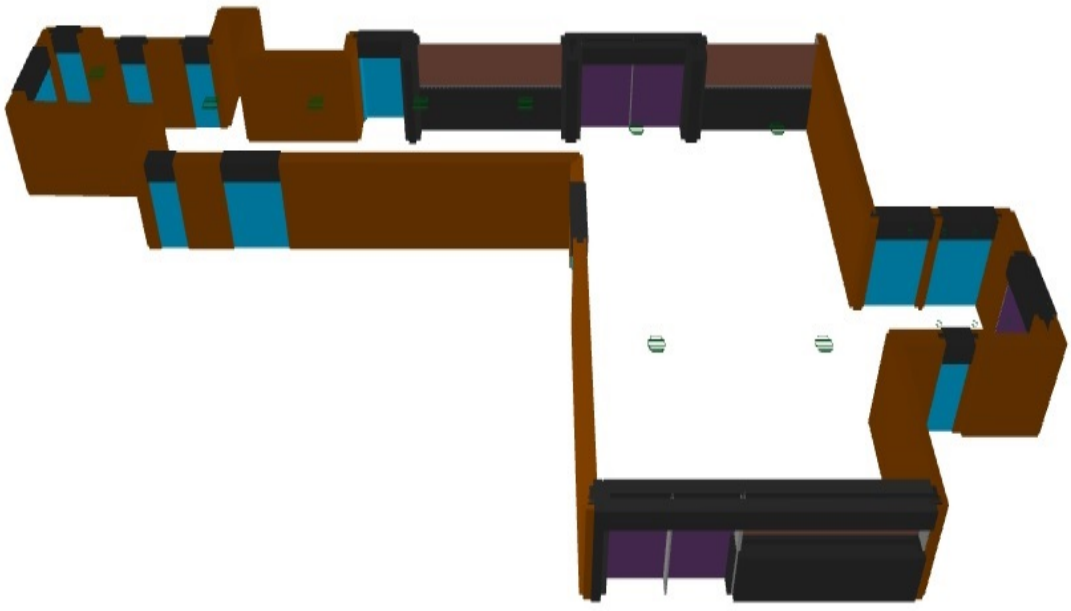

Figure 3.4 3D Layout of the hall environment

Through WallMan, the layers' database is converted from the Cad file to generate a database for each environment; each layer, already defined through AutoCAD, corresponds to a specific material.

Figure 3.5 presents the flowchart to design the 3D simulated environment via WallMan.

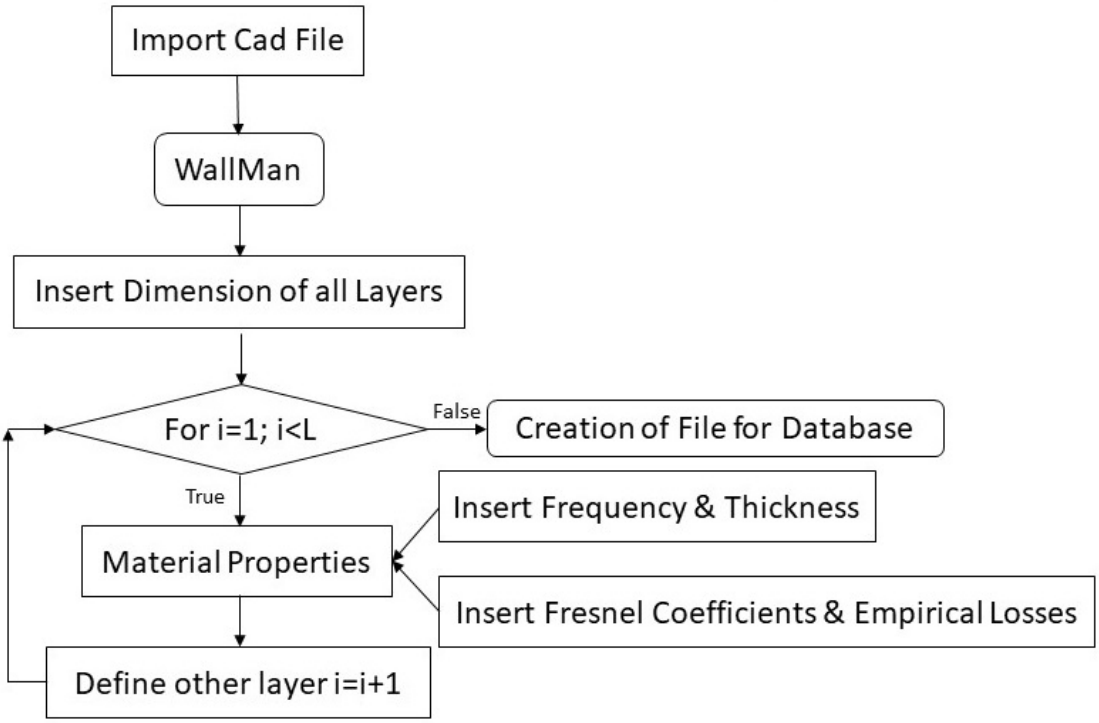

Figure 3.5 Flowchart for the generation of vector databases

While generating the environment database, empirical losses and Fresnel parameters that correspond to each material are defined depending on the material thickness and the frequency used. As already mentioned, up to fourteen different layers constitute the considered indoor environments. Table 3.1 exposes the Fresnel parameters of the main present materials.

Table 3.1 Fresnel coefficients of the materials in the two environments

Materials	**Fresnel Coefficients**		
	Relative Dielectric Permittivity (ε_r)	**Relative Magnetic Permeability (μ_r)**	**Conductivity [s/m] (σ)**
Concrete	2.3	1	0.004
Plate	4	1	0.02
Iron	1	10^5	$1.04*10^7$
Aluminum	9.3	1	$3.5*10^7$
Wood	3	1	0.005
Glass	6	1	0.001
Copper	4.2	1	$5.8*10^7$

Then, materials constituting the environment and subdivisions such as: walls, doors, windows, and others are characterized by their electrical properties (transmission, reflection, scattering and diffraction coefficients).

WinProp offers an extensive library where properties are defined for different frequency bands and materials. Table 3.2 states the empirical transmission and reflection losses corresponding to each material at 433 MHz.

Table 3.2 Empirical Losses of the included materials in both environments

Materials/Layer	Empirical Losses [dB]	
	Transmission	**Reflection**
Wood	1.45	13.63
Iron	92.57	0.05
Plate	4.3	9.52
Copper	59.57	0.04
Glass	1.7	7.53
Aluminum	56.31	0.05
Concrete	5.2	7.51

In addition to transmission and reflection, diffraction and scattering are also taken into consideration.

Diffraction describes the propagation variation between illuminated and shadowed regions when there are edges or wedges that participate to the diffraction process. It is important when edges and wedges dimensions are closed to a factor of the wavelength. We are working in the UHF frequency band; diffraction is significant. Two types of diffractions are considered: the Geometric Theory of Diffraction (GTD) [8] and the Uniform Theory of Diffraction (UTD) [9]-[11]. Empirical formulas are also included when applying empirical propagation models.

Scattering is directly related to the roughness and finite surfaces with small dimensions compared to the wavelength [12]. In our case, several surfaces are included in the indoor simulated model such as those of the heater and the LCD projector. Scattering will have a direct effect by reducing the reflected energy in the expected direction [13].

After defining all Fresnel parameters and empirical losses coefficients for the materials that constitute the considered indoor environments, four views (x-z, y-z, x-y and 3D view) appear on the main panel, as illustrated in Figure 3.6 and Figure 3.7, respectively. Finally, the two configurations, containing the vectors database, will be created and saved under the extension *.dbi.

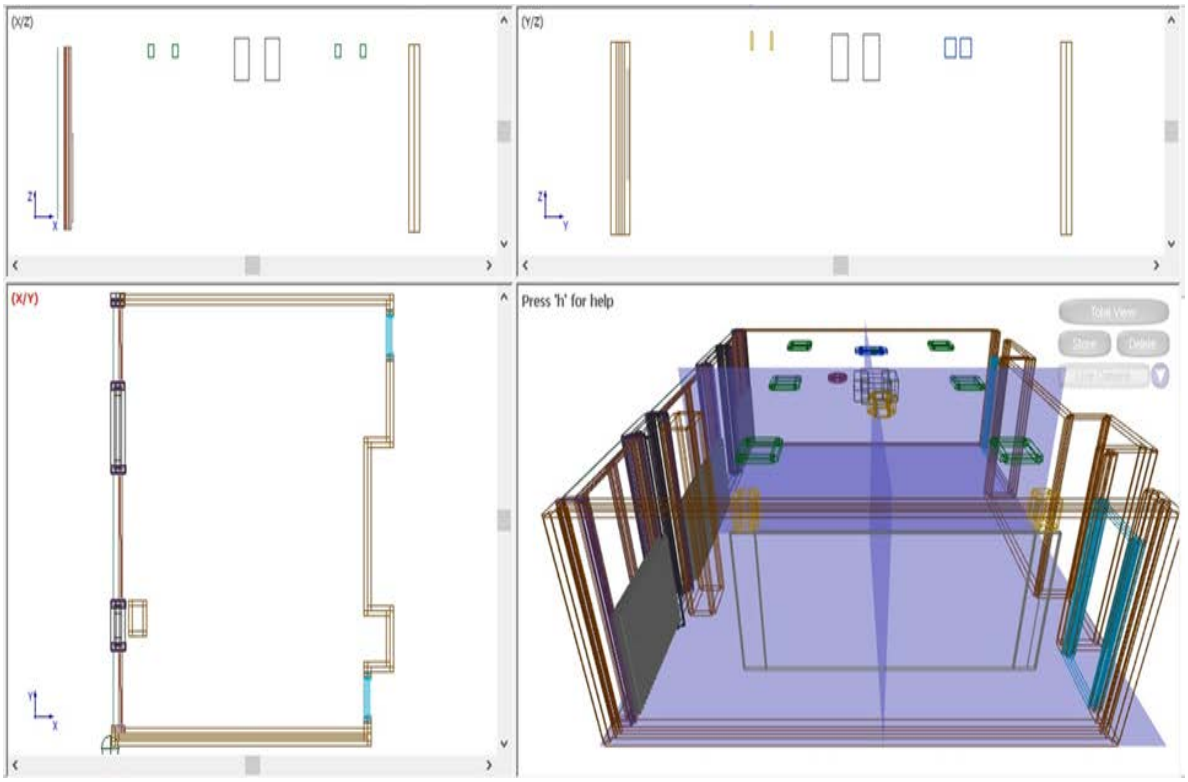

Figure 3.6 x-z, y-z, x-y and 3D view of the classroom in WallMan

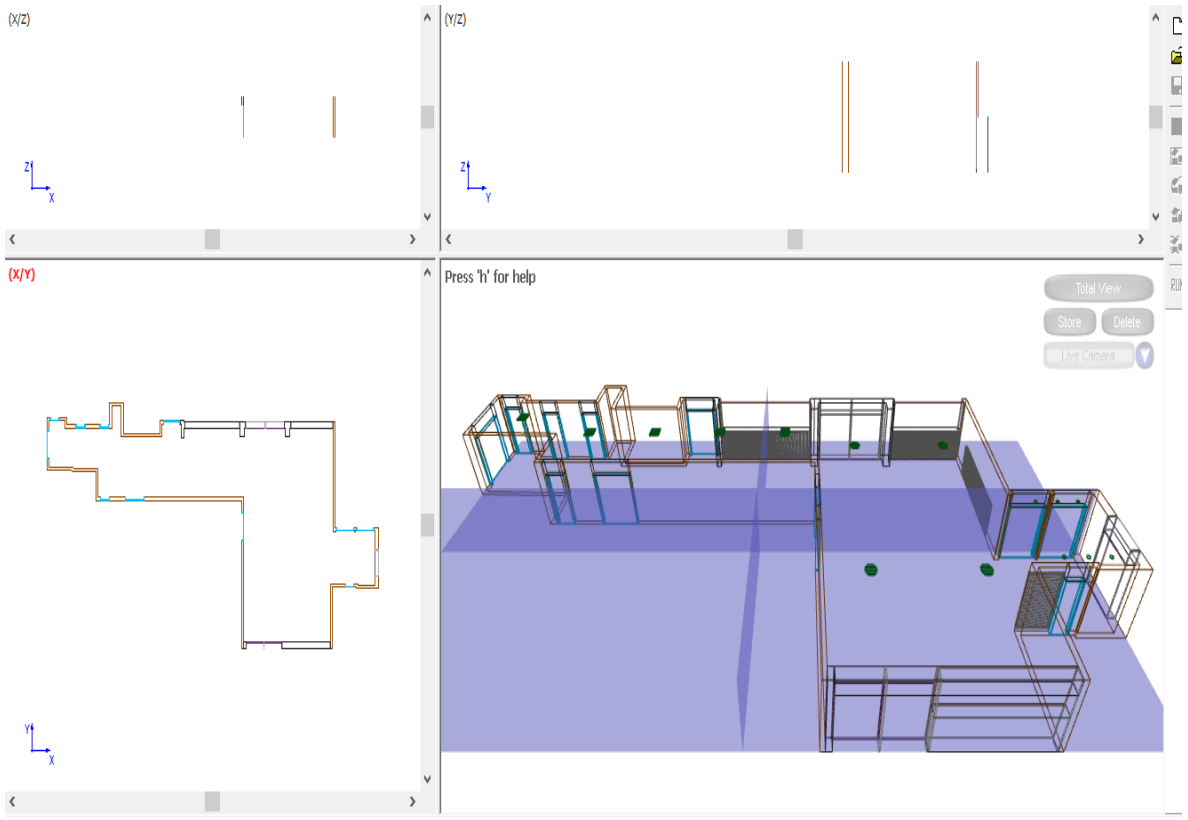

Figure 3.7 x-z, y-z, x-y and 3D view of the hall in WallMan

3.4.2 Tag's Antenna Model

As it is well known, signals propagation relies on the antenna's radiation pattern. To predict the signal coverage, the pattern must be described accurately within the radio network planning tool.

Through AMan, which is a graphical antenna pattern editor, the tag's antenna is designed. Its radiation pattern is taken into consideration in order to obtain signals propagation closest to the reality.

Vertical and horizontal antenna patterns are available from manufacturers; they describe the antenna's radiation in ideal environments (Figure 3.8).

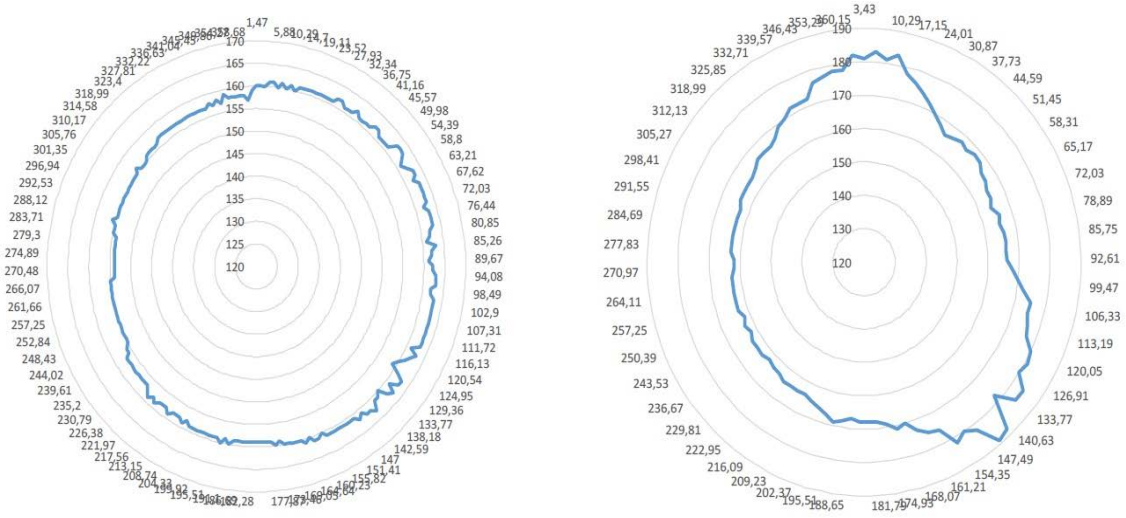

Figure 3.8 Horizontal and vertical radiation patterns of the tag's antenna

Patterns, that are in the form of *. jpeg files, are used as inputs for AMan. Then, two binary files, with extensions *.ahb and *.avb, for the vertical and horizontal radiation patterns are created.

AMan offers several algorithms for the 2D to 3D patterns conversion:

- Arithmetic Mean (AM)
- Bilinear Interpolation (BI)
- Weighted Bilinear Interpolation (WBI)
- Horizontal Projection Interpolation (HPI)
- Exponential Interpolation (EXP)

HPI is the most common and accurate algorithm used for centered and non-centered radiation pattern beams. This algorithm considers any shape of antenna and tracks the maximum gain direction. Any beam tilt will be better handled by the HPI.

For the conversion patterns settings, we selected the HPI algorithm 2x2D to 3D, through AMan, that will be used for the RF propagation model. Hence, the 2D vertical and horizontal tag antenna patterns are combined to generate the 3D pattern under the extension *.apb, as presented in Figure 3.9. The red color represents the 3D radiation pattern of the tag's antenna and the gray color is the grid envelop of this pattern.

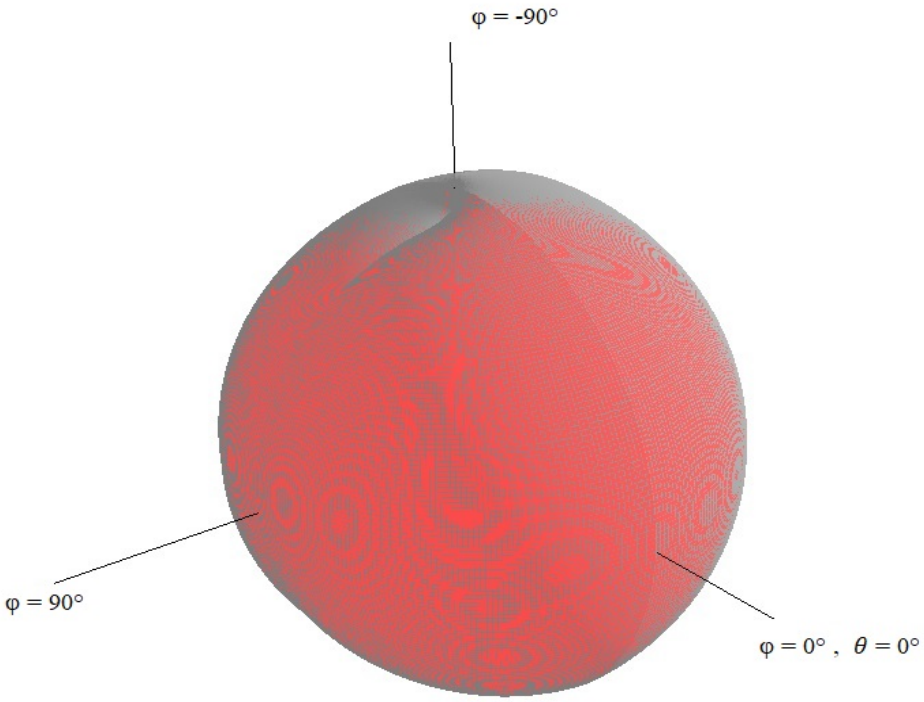

Figure 3.9 3D radiation pattern of the tag antenna with AMan

3.4.3 Reader's Antenna Model

Feko is an electromagnetic solver combining several numerical methods in the frequency and time domains. Direct and indirect hybridization between numerical methods are also available to solve electrically big structures. Feko offers a panel of numerical methods/solvers included in one interface (Figure 3.10). Depending on the complexity and the electrical structure size, one can adapt a dedicated numerical method. Simulation of complex and electrically large scenarios can also be solved by using full hybridization between numerical algorithms. Feko is mainly based on the Method of Moments (MoM), which is a

numerical computational method of solving linear partial differential equations that have been formulated as integral equations i.e. in the boundary integral form [14].

In our case, the MoM is used to model the RFID reader. It is based on the full-wave method without any convergence algorithm; this makes it accurate as far as the meshing is well defined.

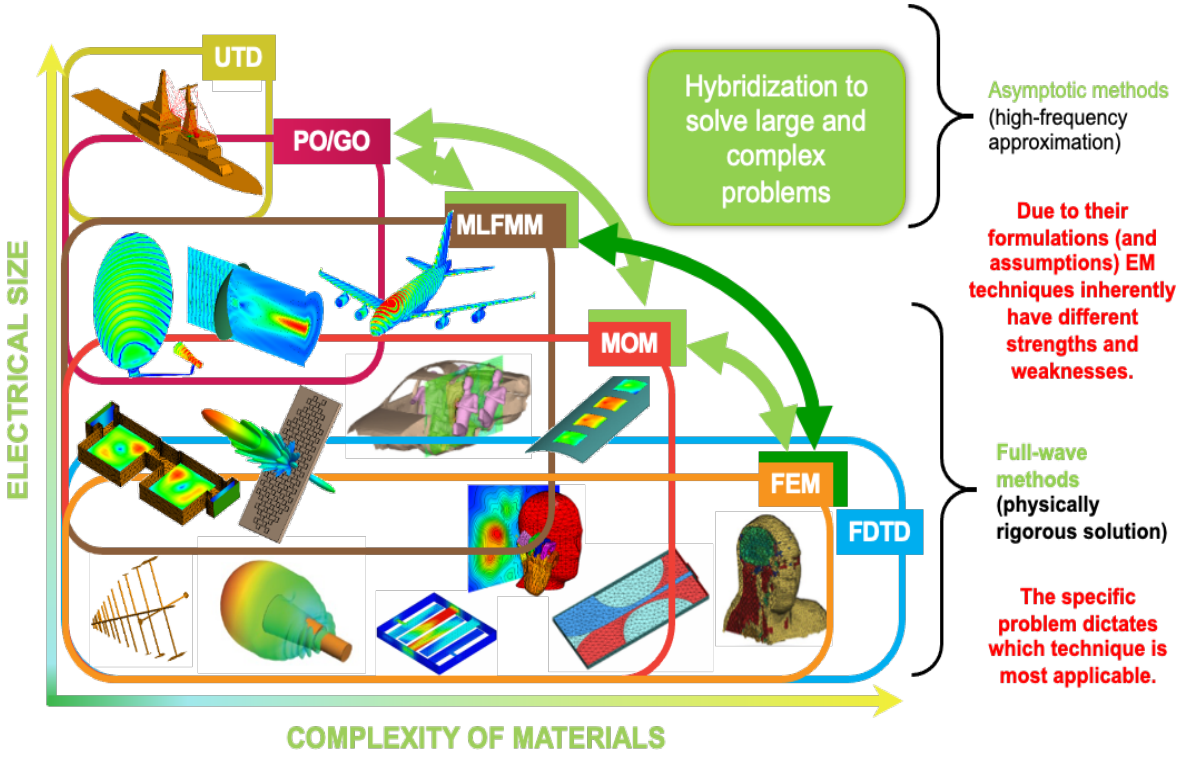

Figure 3.10 Feko numerical methods overview [15]

Based on the Ela Innovation RFID reader datasheet [16], reverse engineering has been achieved to design the reader antenna model. Using Feko, the antenna is configured and the characteristics of the reader are used as inputs to the simulator.

The RFID reader antenna consists in two monopoles mounted on the ground plane and excited in the spatial diversity mode: when one monopole is receiving, the other one is loaded and vice versa. The RFID reader box is made from plastic materials with the following characteristics: Relative Dielectric Permittivity ε_r = 4 and losses tan δ = 0.02.

The reader meshing is based on equilateral triangles to represent the geometrical cad and assign a basis function to each triangle node (Figure 3.11). This meshing type is the default one used in Feko for MoM with mesh size of $\lambda/16$, which is related to this solver algorithm to have accurate current sampling.

Currents are then calculated on the node of each triangle using the MoM [14]; the sum of these currents will contribute to the calculation of the radiated field [15]. This sum is based on three types of currents:

- Linear currents on the antenna segments
- Electric current on the metallic triangles, e.g. currents on the antenna's ground plane
- Magnetic current in the dielectric triangles, e.g. currents on the plastic box.

A locally refined mesh has been applied around the RFID reader antennas where the antenna source or feeding is located as currents are highly varying in this zone (Figure 3.11).

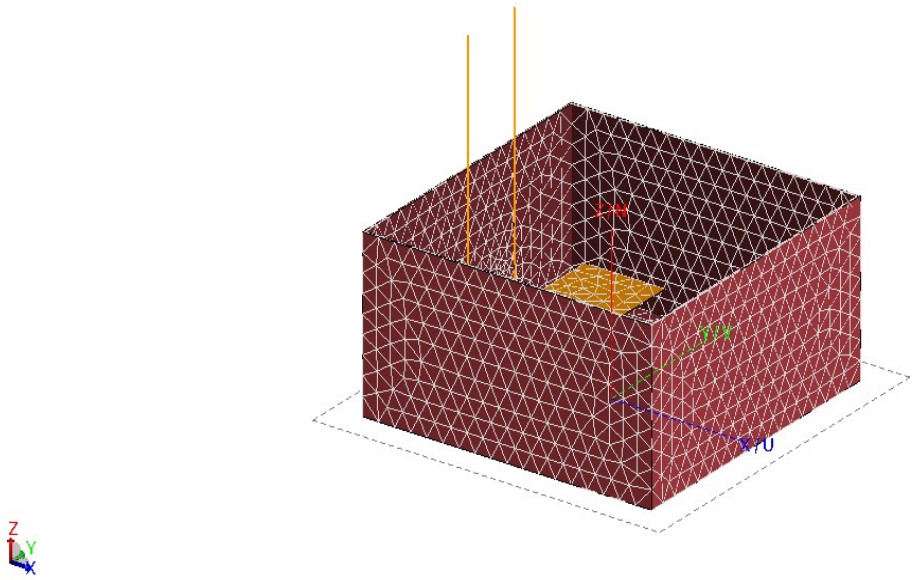

Figure 3.11 Meshed structure for the RFID reader box

The radiation pattern of the RFID reader antenna has a dissymmetric shape due to the proximity of the loaded antenna. When one antenna is excited, the other antenna is 50 Ω loaded and vice versa. Since the loaded antenna is not radiating, it will behave as a metallic object beside the radiating antenna. This leads to an unsymmetrical radiation pattern shape.

This pattern will be exported in *.ffe format (ASCII format) compatible with WinProp and will be used as a receiving antenna (called Mobile Station in WinProp).

As shown in Figure 3.12 and Figure 3.13, the antennas' pattern is not similar to the omnidirectional one. It is designed based on ELA Innovation reader datasheet [16].

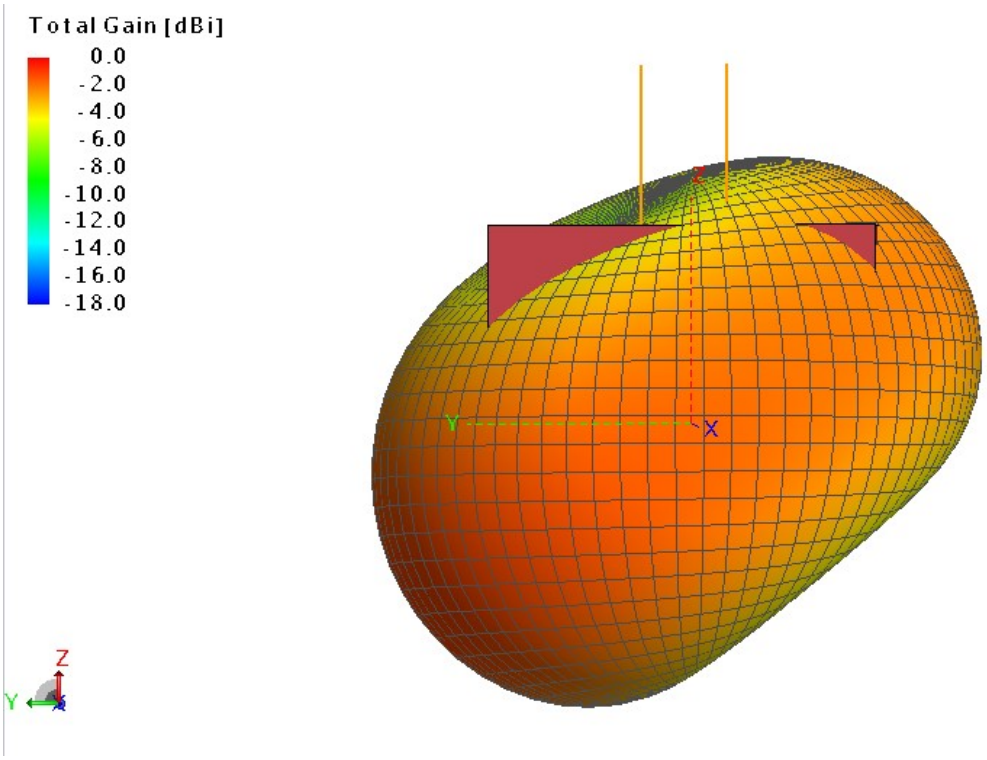

Figure 3.12 3D radiation pattern of the RFID reader antenna 1

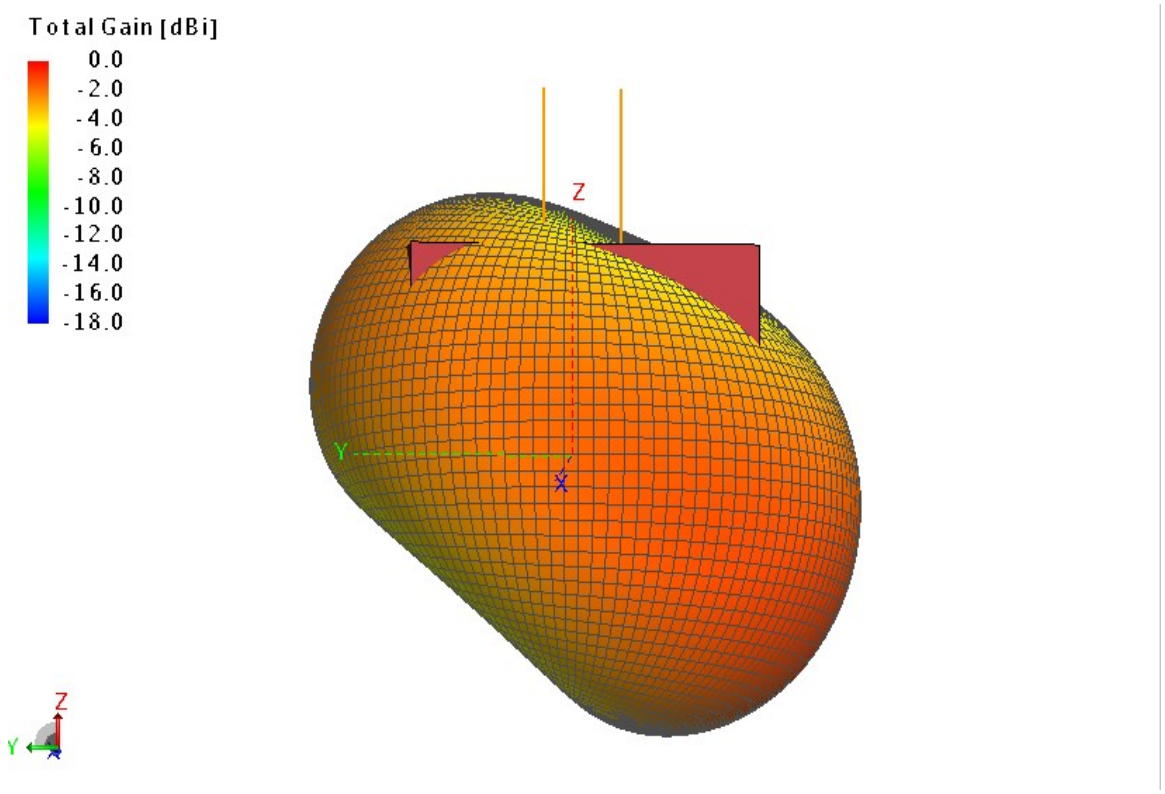

Figure 3.13 3D radiation pattern of the RFID reader antenna 2

3.4.4 Propagation Manager (ProMan)

The main tool in WinProp is ProMan (Propagation Manager). ProMan is where the simulation project settings are defined and edited, and where results are illustrated.

In ProMan, different propagation models exist in order to simulate signals propagation in an indoor environment; for instance, the Modified Free Space Model (MFSM) or the One Slope propagation Model (OSM) already presented in the chapter 2, subsection 2.3.3. This is the most common propagation model; a simple linear formula determines the path loss. However, the position and dimensions of walls, obstacles and material's properties are relatively ignored as a prior database. The Multi-Wall Multi-Floor (MWMF) model includes only losses introduced by walls and floors; it is applicable for an entire floor or building.

Other propagation models need to be used to predict the signal coverage indoors, while not only considering all losses (already defined through WallMan) but also reflections, diffractions, and scattering. The most accurate existing propagation models for indoor scenarios founded in ProMan, are the Dominant Path (DPM) and the Ray-Optical Models.

3.4.4.1 The Dominant Path Model

Indoors, the signal propagates through different paths to reach the receiver. Figure 3.14 illustrates an example of many possible rays between the transmitter and receiver. Using DPM, the computation of the received power depends on the accuracy of the indoor scenario description already defined in WallMan. This model performs with light computational resources.

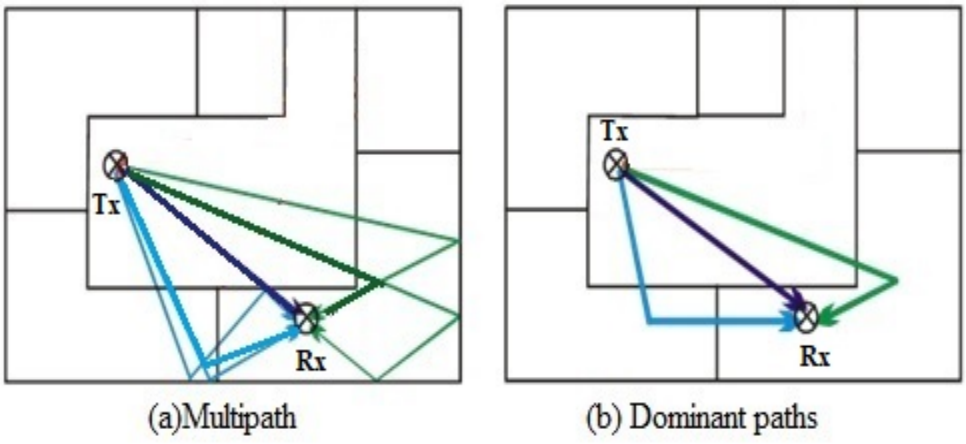

Figure 3.14 Multipath propagation and the dominant path indoor

Consider that the transmitter Tx is fixed in a specific position, as illustrated in Figure 3.15. The indoor environment description is used to determine whether corners are concave or convex.

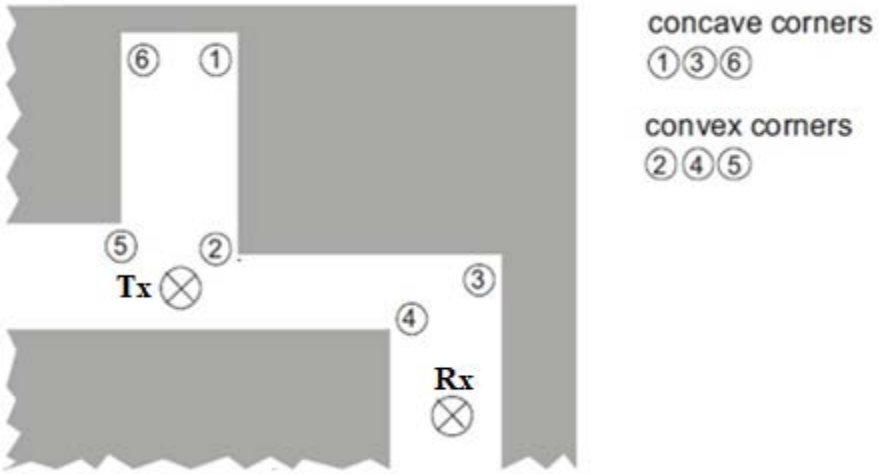

Figure 3.15 Scenario with transmitter Tx, receiver Rx and different types of corners [7]

To reach the receiver Rx, the Dominant Path model's (DPM) algorithm is focused on tracking the best path for the signal, as presented in Figure 3.16. The tree structure starts with corners visible from the transmitter Tx. Each time the receiver Rx is found in the tree, corners along the path can be determined by following the branches back to the transmitter Tx. More precisely, DPM considers only the most relevant path that contributes to the dominant path. According to [17], it is applied in an office building. One can deduce that not all rays and interactions, between the transmitter and receiver, are explored. Only the dominant path is used; this will lead to a reduced computational complexity at the expense of accuracy, especially in NLoS scenarios.

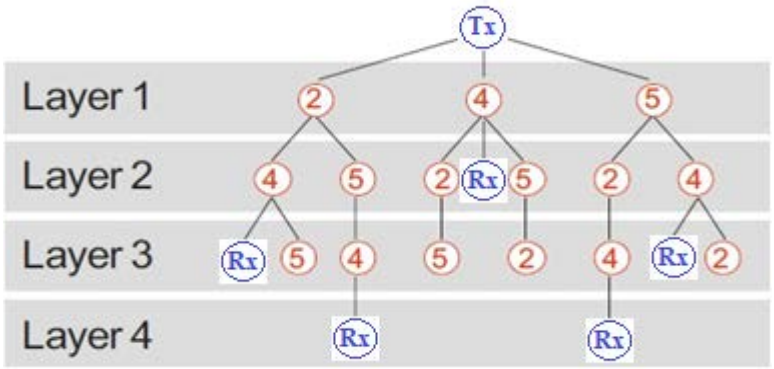

Figure 3.16 Tree structure of the DPM [7]

3.4.4.2 Ray-Optical Models

There are two different approaches to determine the Ray-Optical propagation paths between transmitter and receiver: Ray-Tracing and Ray-Launching [18].

The Ray-Tracing model computes the power at each receiving point with a constant resolution and uses the image principle to determine the reflection point (Figure 3.17).

Whereas, the Ray-Launching performs a constant angle increment for the ray shooting. Depending on the Ray-Launching angle of increment, some details can be neglected or in other word not illuminated by the rays. This fact can lead to a lower accuracy. Figure 3.17 illustrates the difference between the Ray-Tracing and the Ray-Launching models.

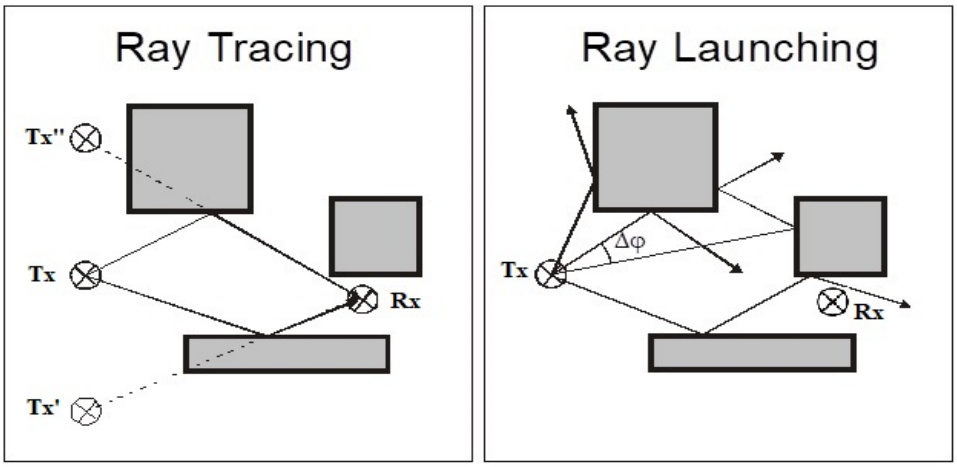

Figure 3.17 Ray-Tracing Versus Ray-Launching model [18]

Meanwhile, WinProp presents several advanced options to accelerate the Ray-Tracing model such as:

- Phase resolution
- Number of paths and interactions (reflection, transmission, diffraction and combined reflection and diffraction)
- Length of wedges for diffraction
- Tiles resolution for scattering.

In addition, WinProp provides two types of Ray-Tracing models: Standard Ray-Tracing (SRT) and Intelligent Ray-Tracing (IRT).

- *Standard Ray Tracing (SRT)*

The Standard Ray-Tracing model performs a rigorous 3D Ray-Tracing prediction; it results in very high accuracy because it takes into consideration the effect of the environment on the propagation parameters. This model requires a large computational time.

- *Intelligent Ray Tracing (IRT)*

The Intelligent Ray-Tracing model is used to accelerate the classical ray optical models such as SRT. This model is based on a preprocessing of the environment properties. All walls of the indoor building are divided into tiles, and all wedges are subdivided into horizontal and vertical segments.

3.4.4.3 Summary for the different Propagation Models

Table 3.3 presents the different indoor propagation models available in WinProp with their characteristics.

Table 3.3 Comparison between the WinProp Indoor Propagation models

Models	Materials Properties	Walls Properties	Computation time	Preprocessing	Accuracy
MFSM or OSM	Not Considered	Not Considered	Short	Not Required	Low
DPM	Considered	Considered	Short	Not Required	Trade-off
SRT	Considered	Considered	Large	Not Required	High
IRT	Considered	Considered	Short	Required	High

After presenting the characteristics of the indoor propagation scenarios, the Ray-Tracing model, that considers all materials properties, is applied in our use cases. Particularly, we used Standard Ray-Tracing for its high accuracy. Despite the high efficiency of the Intelligent Ray-Tracing, it requires preprocessing of the environment database via WallMan. Hence, if there is any modification in that database, it must be modified through the original one. And, a new preprocessing is requested. Flexibility and better control of the database were required in our research. This pushed us to use the SRT as the best trade-off between accuracy and flexibility.

3.4.5 Principle of the Ray-Tracing Model

Within the Optical-Ray Tracing model, all rays are followed until they hit an obstacle. Afterwards, reflection or transmission or both will occur, depending on the obstacle materials [20]. The direction of the new ray is determined by Snell's law [21]. Losses due to rays

reflections' depend on the thickness and the material characteristics of the hit obstacle at the respective frequency [22]. The relationship between the optimum thickness of the material and the angles of incidence is expressed by:

$$d = \frac{p.c}{2\sqrt{\varepsilon_r - sin^2\,\theta - sin^2\,\alpha - \frac{sin^2\,\theta\, sin^2\,\alpha}{\varepsilon_r}}} \tag{3.1}$$

d is the thickness of the material; θ and α are the angles of incidence in azimuth and elevation planes; p is an integer constant for each optimal thickness; c is the light celerity in free space and ε_r is the relative dielectric permittivity of the material.

Diffracted rays can be considered when applying the Uniform Theory of Diffraction method (UTD) [9]-[11]. In addition to the reflection and transmission behavior, losses inside the materials must be considered for better accuracy.

To better understand the signals propagation behavior, a review of the reflection and transmission coefficient, in terms of the incident angle and various obstacles within the environment, is useful. Hence, it is necessary to characterize electrically the various materials existing in the environment. For instance, a plane electromagnetic wave, crossing to the planar interface between two regular semi-infinite areas 1 and 2, gives rise to two waves: reflected and transmitted (or refracted). According to Snell's law, applied to the EM propagation through the dielectric slab [23], the reflection and transmission coefficient for the Transverse Electric (TE) mode are calculated as follow:

$$R_{TE} = \frac{\mu_2^2\sqrt{\varepsilon_1}cos\,\theta_i - \sqrt{\mu_1\mu_2\varepsilon_2 - \mu_1^2\,\varepsilon_1 sin\,\theta_i^2}}{\mu_2^2\sqrt{\varepsilon_1}\,cos\,\theta_i + \sqrt{\mu_1\mu_2\varepsilon_2 - \mu_1^2\,\varepsilon_1 sin\,\theta_i^2}} \tag{3.2}$$

And,

$$T_{TE} = \frac{2\mu_2\sqrt{\varepsilon_1\varepsilon_2}\,cos\,\theta_i}{\mu_2\sqrt{\varepsilon_1\varepsilon_2}\,cos\,\theta_i + \sqrt{\mu_1\mu_2\varepsilon_2^2 - \mu_1^2\varepsilon_1\varepsilon_2\,sin\,\theta_i^2}} \tag{3.3}$$

Concerning the Transverse Magnetic (TM) mode, the incident wave is perpendicular to the plane of incidence. The reflection and transmission can also be defined by:

$$R_{TM} = \frac{-\varepsilon_2\sqrt{\mu_1\mu_2}\cos\theta_i + \sqrt{\mu_2^2\varepsilon_1\varepsilon_2 - \mu_1\mu_2\varepsilon_1^2\sin\theta_i^2}}{\varepsilon_2\sqrt{\mu_1\mu_2}\cos\theta_i + \sqrt{\mu_2^2\varepsilon_1\varepsilon_2 - \mu_1\mu_2\varepsilon_1^2\sin\theta_i^2}} \quad (3.4)$$

And,

$$T_{TM} = \frac{2\mu_2\sqrt{\varepsilon_2\varepsilon_1}\cos\theta_i}{\varepsilon_2\sqrt{\mu_1\mu_2}\cos\theta_i + \sqrt{\mu_2^2\varepsilon_1\varepsilon_2 - \mu_1\mu_2\varepsilon_1^2\sin\theta_i^2}} \quad (3.5)$$

With θ_i is the angle of incidence; ε_i and μ_i are the dielectric permittivity and the magnetic permeability of the material. It is worth mentioning that indices 1 and 2 correspond to the two regular semi-infinite areas.

Recall that, to get accurate simulations, the environment properties, the empirical transmission and reflection coefficients should be well defined in WallMan. Through ProMan, the computation of the signal propagation takes into consideration all these parameters.

3.4.6 Indoor Radio Coverage

In this subsection, the model of the classroom and the hall, where the proposed system and approaches will be tested, is analyzed. As previously stated in section 3.4.1, the behavior of the radio channel in indoor scenarios heavily depends on the complexity of the environment. The defined materials parameters' in WallMan and the creation of the tag's antenna via AMan are imported to ProMan, in order to study the signal propagation in the designed environment. Figure 3.18 represents the algorithm that should be followed to examine the signals propagation in the indoor environment.

Furthermore, the calculation's resolution and the attenuation coefficient corresponding to the environment need to be also defined as inputs. As already mentioned in section 3.4.4, WinProp includes several indoor propagation models. The use of 3D Ray-Tracing is preferable, thanks to the high accuracy and materials dependency.

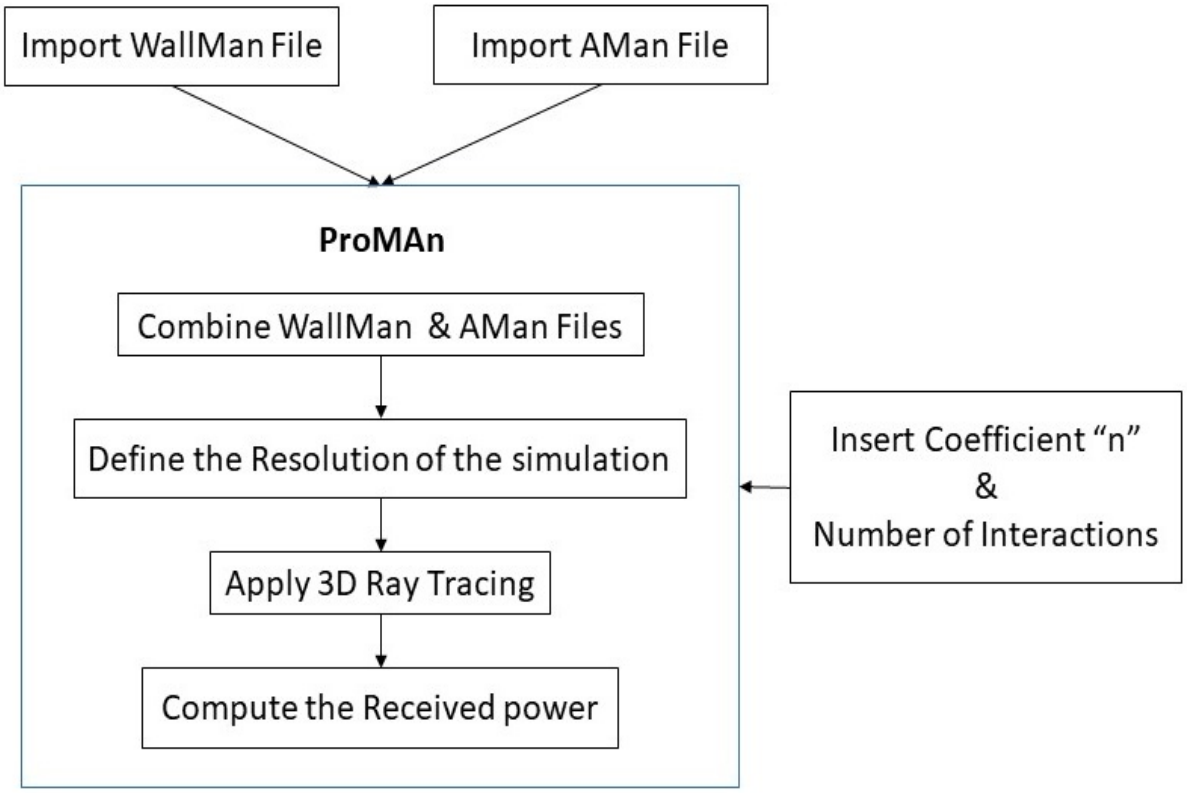

Figure 3.18 Flowchart for the coverage prediction and network planning with ProMan

After following steps for the indoor environment configuration, RFID simulated tags are fixed on the walls, as illustrated in Figure 3.19 and Figure 3.20. The reader pattern is used as a received gain at each pixel (receiving point), depending on the directions and the resolution of the received rays. Finally, obtained results by simulations, using the 3D SRT propagation model, will be compared to those obtained by measurements in the following section.

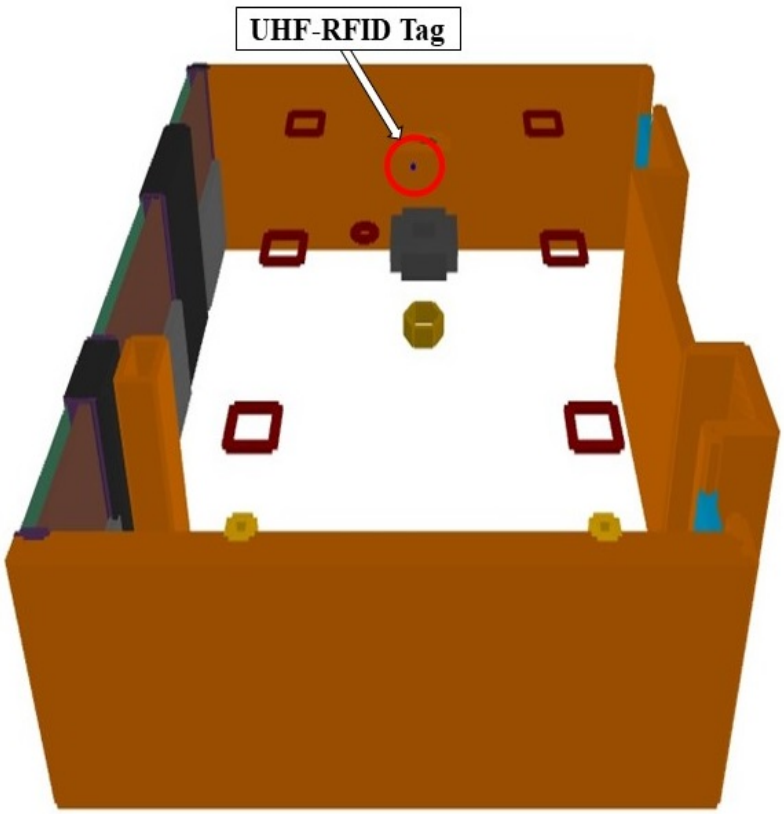

Figure 3.19 3D Layout of the Simulated classroom by ProMan

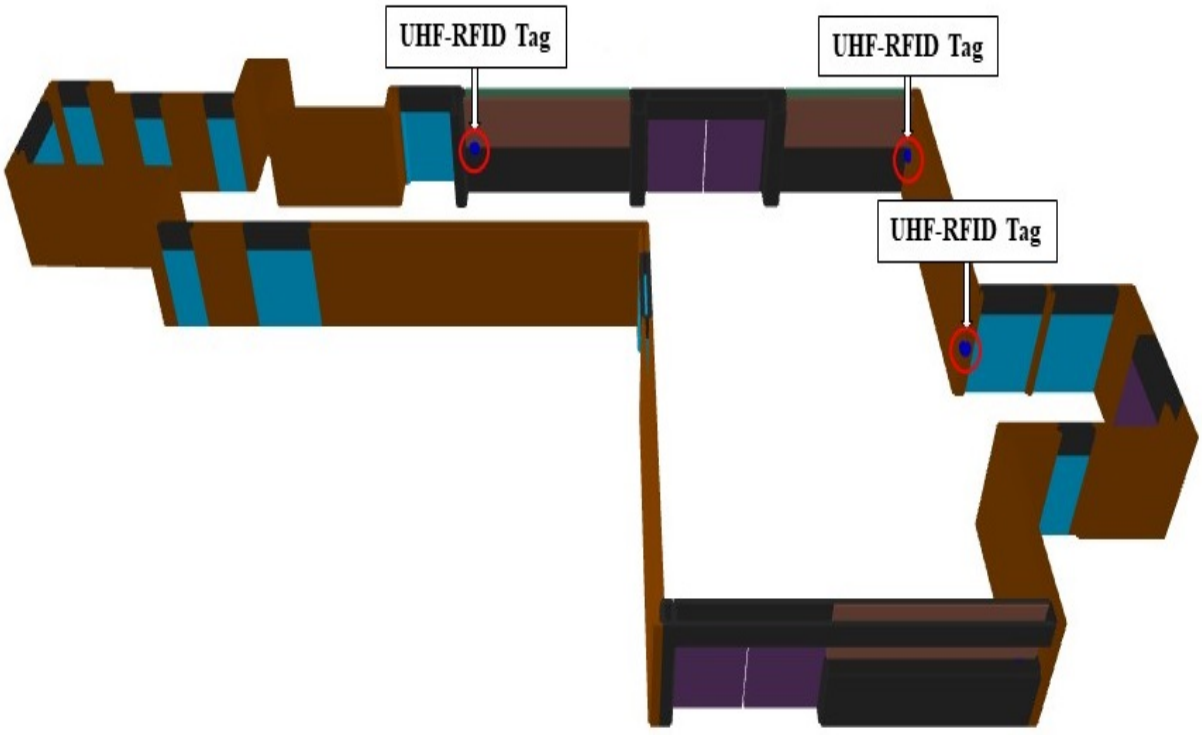

Figure 3.20 3D Layout of the Simulated hall presented by ProMan

3.5 Simulations versus Measurements

In this section, modeling, using an active RFID tag, is analyzed and compared to the real environments at EFREI Paris. Simulations are realized using WinProp based on 3D SRT as a propagation model. The received power values are collected every 50 centimeters in the classroom and the hall environments. After estimating the tag-reader distance, distance errors are compared with those practically measured, in order to validate the models accuracy. Subsections 3.5.1 and 3.5.2 present the simulation results compared to the measured ones.

3.5.1 Tests in the Classroom

In the classroom environment, the received power values are collected every 50 centimeters starting from the front wall, at sixty-four reference positions covering the whole classroom environment, during the offline stage. These positions are distributed over seven tracks A30 till A150 to characterize the signal behavior in terms of the (tag-reader) distance, as illustrated in Figure 3.22. The space separating two successive positions is constant and different than that considered within the online stage.

The OSM, already described in subsection 2.4.3, is applied to determine the estimated distance. Figure 3.21 presents the block diagram of the distance error calculation.

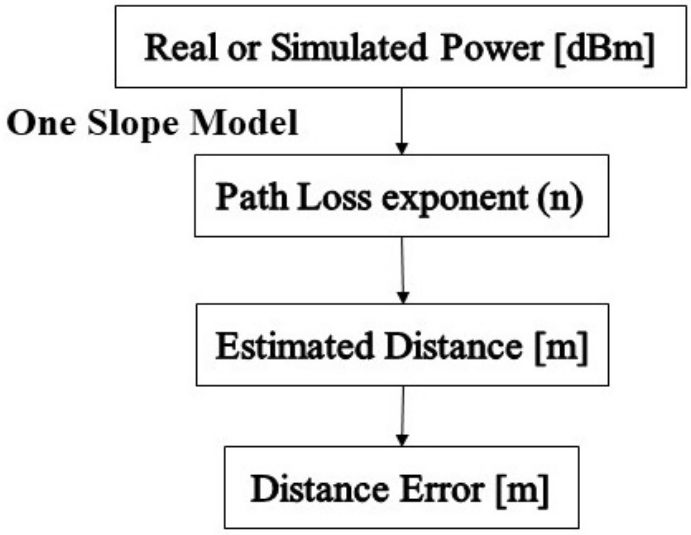

Figure 3.21 Block diagram of the distance error calculation

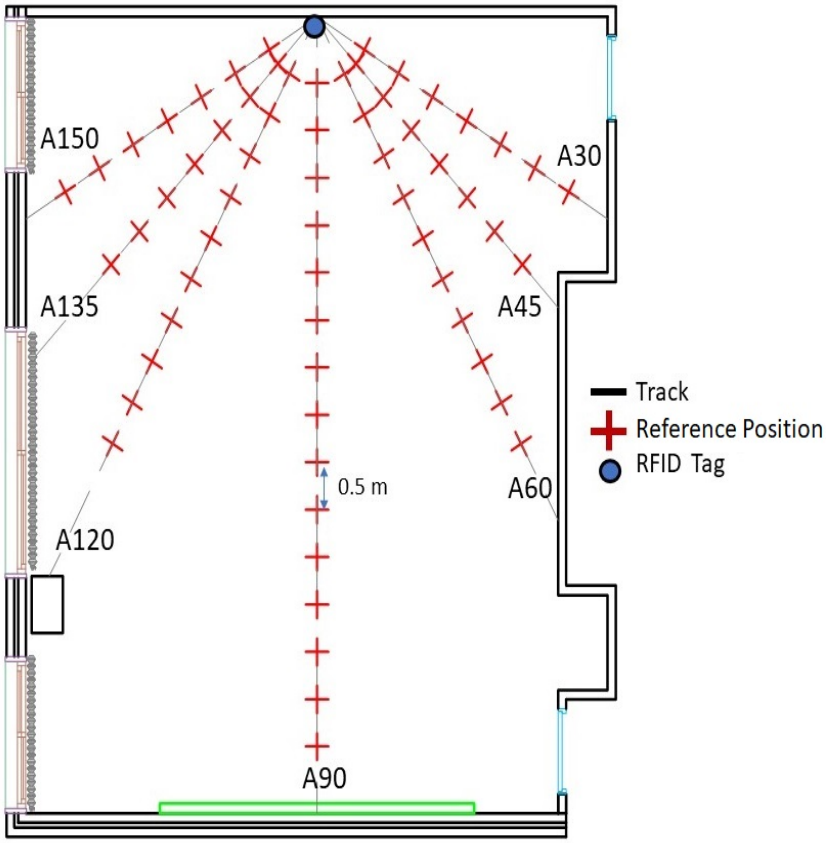

Figure 3.22 2D Layout of the classroom

As a preliminary comparison, the received power values collected over track A90 are analyzed and compared with those obtained by simulation over the same track (Figure 3.23). The estimated (tag-reader) distance errors over A90 are presented in Figure 3.23.

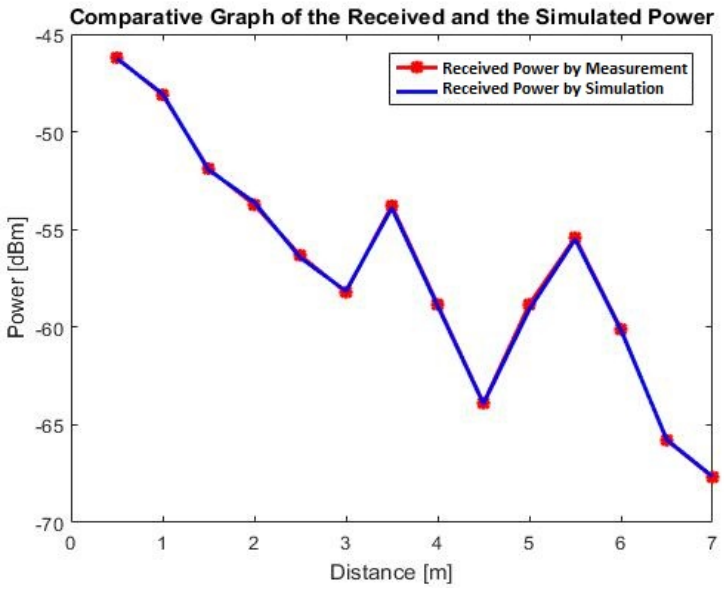

Figure 3.23 Measured and simulated Power values over the central track A90 of the classroom

Following the block diagram of the distance error calculation in the experimental and the simulated scenarios (Figure 3.21), and after applying the OSM to estimate the tag-reader distance, the distance error is determined by subtracting the estimated distance from the real one. Table 3.4 shows the measured and simulated (tag-reader) distance errors over the track A90.

Table 3.4 Measured and Simulated Estimated Distance Errors over the central track A90 of the classroom

Distance [m]	Measurements Distance Errors [m]	Simulations Distance Errors [m]
0.5	0	0
1	0.22	0.21
1.5	0.82	0.83
2	1.23	1.2
2.5	1.98	2.03
3	2.67	2.67
3.5	1.25	1.28
4	2.98	3.01
4.5	4.13	4.15
5	2.97	3.1
5.5	1.67	1.72
6	3.6	3.62
6.5	4.9	4.86
7	5.1	5.07
MDE [m]	**2.4**	**2.41**

According to the Mean Distance Error (MDE) presented in Table 3.4, it can be noticed that measurements and simulations present very close results.

The following experiment is performed over the seven tracks A30 till A150 of the classroom environment (Figure 3.22). The estimated (tag-reader) distance errors are determined, by applying the OSM, over each track independently for both scenarios (real and simulation). Figure 3.24 presents the Cumulative Distribution Function (CDF) for the real and simulated estimated distance errors over the sixty-four considered positions.

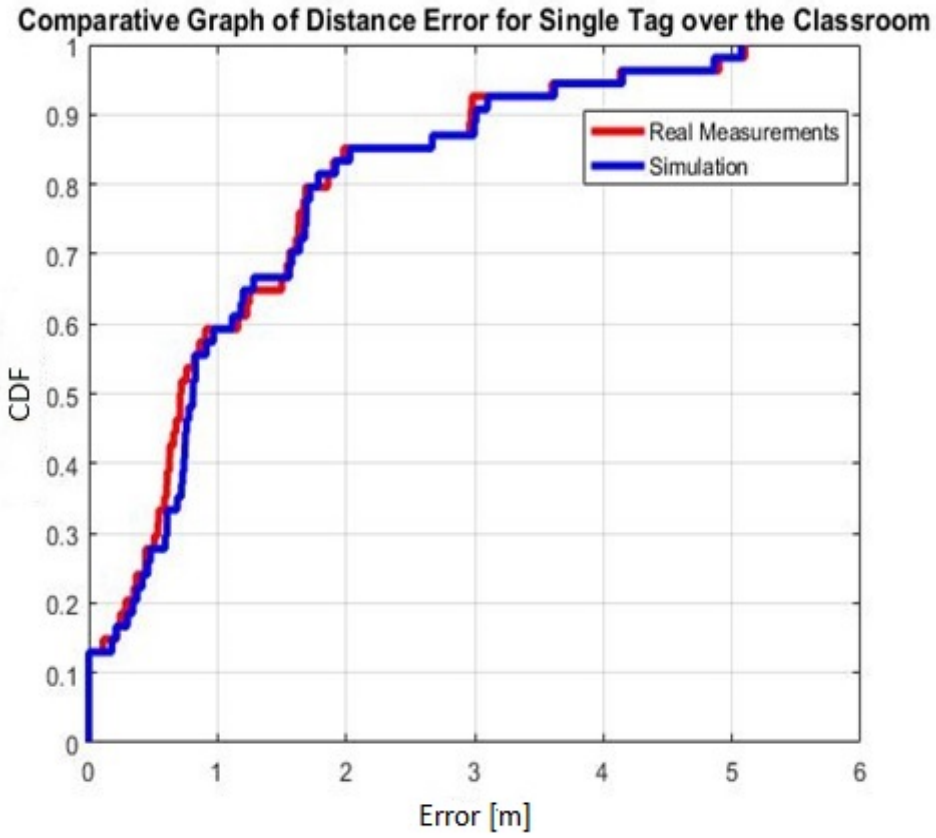

Figure 3.24 CDF of estimated distance errors for the real measurements and simulations

Based on Figure 3.24, the achieved performance is 3.4 meters in the classroom environment. It can be noticed that the distance error at 90% CDF for the simulated data is 10 centimeters lower than for the real one. Thus, knowing the transmitted signal level and defining well all materials parameters are sufficient to estimate the signal propagation. Moreover, this simulated model can reduce the need for costly measurements and increases the simplicity of the coverage process.

3.5.2 Tests in the Hall Environment

In order to better assess our modeling, five RFID simulated tags are mounted on the walls of the hall at 1.3 meters of height. Measurements are made on a regularly spaced distance of 50 centimeters in the hall environment over the two tracks A90 and A'90, as illustrated in Figure 3.25.

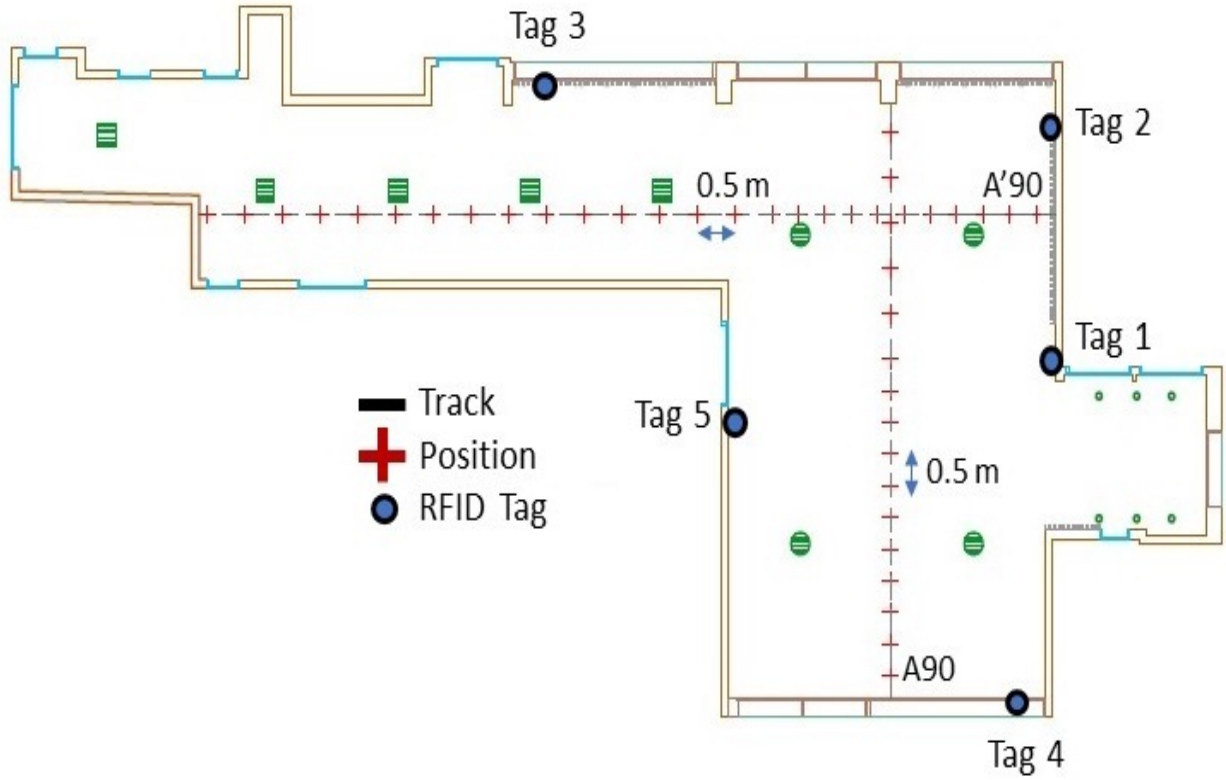

Figure 3.25 2D Layout of the hall

The RFID reader was moved forward to collect RSS samples at forty-one positions over A90 and seventy-six positions over A'90. The collected received power values are analyzed and compared with those obtained by simulation over the same tracks. More precisely, the difference between the real and simulated power values as well as the standard deviation are calculated. To assess the accuracy of the simulated hall configuration, it is necessary to achieve a difference, between the received power values and the simulated ones, less than 0.1 dB and not exceeding 0.5 dB. Beyond this limit, the simulation will lose its precision. Some major adjustments on the environment modeling are recommended in order to improve the received power matching. Table 3.5 illustrates the Standard Deviation (Std) of the received simulated power for each tag, over the two tracks as well as the number of positions where the Received Power Difference (RPD) exceeds 0.5 dB over A90 and A'90.

Table 3.5 Measured and Simulated Received Power Analysis over A90 and A'90

Tag Number	Track A90		Track A'90	
	RPD > 0.5 dB	Std [dB]	RPD > 0.5 dB	Std [dB]
Tag 1	5	0.1122	11	0.1824
Tag 2	2	0.2634	3	0.3891
Tag 3	3	0.2566	9	0.2635
Tag 4	5	0.3805	7	0.4105
Tag 5	15	0.4746	13	0.5146

Based on results in Table 3.5, it can be noticed that the standard deviation exceeds 0.3 dB with tags 4, 5 over track A90, and with tags 3, 4 and 5 over track A'90. This deviation is due to many factors such as some metallic objects placed in the hall (around tags 2, 3, 4 and 5) and NLoS between the transmitting tag and the reader (for tags 4 and 5). In this context, the differences between the real and the simulated received power, that exceed 0.5 dB at some positions over the two tracks, are mainly due to the NLoS and the neglection of some small details that couldn't be took in consideration. Despite the high accuracy of 3D Standard Ray-Tracing, this model is still limited for large environments like our hall, where the prediction positions are far away from the transmitting antennas.

3.6 Summary

The chapter presented the models of two indoor environments as well as those of the RFID equipment that will be used in our solution. Numerical methods such as the HPI algorithm for the RFID tag configuration, and MoM for the RFID reader modeling, were clearly elaborated. For instance, the radiation pattern of the RFID tag antenna is configured through AMan. The RFID reader is designed by FEKO software and then used within WinProp to get accurate values of the power received by the reader. Besides, all material parameters that constitute the classroom and hall environments, are defined. The signal propagation characteristics, at 433 MHz, are analyzed with a single RFID tag fixed on the wall of the classroom environment, and with five tags over the hall. Simulations were achieved using the 3D Ray-Tracing model of WinProp. Experimental and simulated results had similar behavior with a maximum deviation of 10 centimeters over the classroom environment. However, differences over the hall environment exceed 0.5 dB at particular positions due to the obstructed NLoS.

Finally, it has been noticed that our measurement campaign in the hall was not sufficient and representative for indoor positioning. Hence, the following research is conducted only in the classroom environment.

Bibliography

[1] EDX Wireless, available online: http://www.edx.com/. Accessed on Mars 2021.

[2] Ranplan, available online: http://www.ranplan.co.uk/. Accessed on Mars 2021.

[3] WinProp, Wave Propagation and Radio Network Planning Software (part of Altair HyperWorks), available online : http://altairhyperworks.com/WinProp. Accessed on January 2021.

[4] Z. Yun, M. F. Iskander, and Z. Zhang, "A fast ray tracing procedure using space division with uniform rectangular grid," Electronics Letters, vol. 36, no. 10, pp. 895-897, 2000.

[5] J. C. e Silva, N. A. Lemos, M. D. C. de L. M. Frazao, and A. F. dos Santos, "Characterization of coverage of signals in 700 MHz band in indoor environments," in Proc. SBMO/IEEE MTT-S International Microwave and Optoelectronics Conference (IMOC), Porto de Galinhas, Brazil, pp. 1–5, 2015.

[6] R. Hoppe, G. Wolfle, P. Futter, and J. Soler, "Wave propagation models for 5G radio coverage and channel analysis," in Proc. IEEE 6th Asia-Pacific Conference on Antennas and Propagation (APCAP), Xi'an, China, pp. 1–3, 2017.

[7] R. Wahl, G. Wölfle, P. Wertz, P. Wildbolz, and F. Landstorfer, "Dominant path prediction model for urban scenarios," in Proc. 14th IST Mobile and Wireless Communications Summit, Dresden, Germany, 2005.

[8] J. B. Keller, "Geometrical theory of diffraction", Journal of the Optical Society of America, vol. 52, no. 2, pp 116-130, Feb. 1962.

[9] S. W. Lee and G. Deschamps, "A uniform asymptotic theory of electromagnetic diffraction by a curved wedge", IEEE Trans. Antennas and Propagation, vol. 24, no. 1, Jan. 1976.

[10] R. G. Kouyoumjian and P. H. Pathak, "A Uniform Geometrical Theory of Diffraction for an edge in a perfectly conducting surface", in Proc. IEEE, vol. 62, no. 11, pp. 1148-1161, Nov. 1974.

[11] J. Deschamps, S. Boersma and S. W. Lee, "Three-dimensional half-plane diffraction solution and testing of uniform theories", IEEE Trans. Antennas and Propagation, vol. 32, no. 3, March 1984.

[12] R. Nityanada "Diffraction at a straight edge: a gem from Sommerfeld's work in classical physics," Resonance, vol. 20, no 5, pp. 389-400, 2015.

[13] X. D. He, K. E. Torrance, F. X. Sillion, and D. P. Greenberg, "A comprehensive physical model for light reflection," ACM SIGGRAPH computer graphics, vol. 25, no 4, pp. 175-186, 1991.

[14] C. W. Gibson, "The method of moments in electromagnetics." CRC press, 2014.

[15] Altair Engineering, available online: https://altairhyperworks.com/product/Feko/. Accessed on Mars 2021.

[16] Ela Innovation, SA. (2014) Ela Innovation active RFID tag and reader manufacturer. Available online: https://elainnovation.com/. Accessed on April 2021.

[17] G. Wölfle, R. Wahl, P. Wertz, P. Wildbolz, and F. Landstorfer, "Dominant path prediction model for indoor scenarios," in Proc. German Microwave Conference (GeMIC), Ulm, Germany, 2005.

[18] B. E.Gschwendtner, G. Wölfle, B. Burk, and F. M. Landstorfer, “Ray tracing vs. ray launching in 3-D microcell modelling,” 1995.

[19] Altair Engineering. Available online: https://altairuniversity.com/free-ebooks/. Accessed Mars 2021.

[20] M. Lott, Y. Fifield, D. Evans, and S. Hulyalkar, “Radio Channel Caracteristics for Typical Environments at 5.2 GHz,” in Proc. ACTS Mobile Communication Summit, Aalborg, Denmark, pp. 252-257, 1997.

[21] H. D. Hristov. “Fresnel Zones in Wireless Links, Zone Plate Lenses and Antennas,” s.l, Artech House, 2000.

[22] D. J. Kozakoff, “Analysis of radome-enclosed antennas,” Artech House, Chapter 5, 2010.

[23] C. A. Balanis, “Advanced engineering electromagnetics,” John Wiley & Sons, Chapter 5, 2012.

Chapter 4 Improved Location Accuracy by RSS Digital Processing and Propagation Modeling

4.1 Introduction

It is well known that RSS based localization systems suffer from multipath effects that affect the location accuracy. In [1], a statistical data analysis, of the received signals, covers different aspects such as the skewed distribution of RSS values and its variability. The location determination performance is improved by selecting the optimal Access Point (AP) that provides the widest coverage and the most stable received signal.

Moreover, as mentioned in chapter 2, subsection 2.4.2, most common ILSs use the averaging technique to combine the RSS acquisitions. For this reason, this technique was applied in our conventional ILS, within both stages. However, the use of the averaging technique to combine RSS samples seriously limits the location accuracy. Instead, the Maximum Likelihood Estimator (MLE) is applied on the sets of RSS to enhance the proposed ILS's stability and narrow the location uncertainty.

Concerning propagation modeling, Cost 231, Winner II, ITU-R 2135 and Multi Walls Multi Floors (MWMF) are the most known models [2]-[8]. These models tend to focus on a particular characteristic like temporal fading or inter-floors losses. Therefore, none of the empirical indoor propagation models, found in the literature, have yet successfully created an accurate signals coverage. A specific challenge is to provide a new empirical propagation model providing reliable estimations of the indoor propagation parameters. Hence, two approaches, the Dual One Slope Model (DOSM) and Dual One Slope with Second Order Model (DOSSOM) will be proposed in order to represent better signals behavior. However, these two propagation models do not cover the full range of the considered scenario. To overcome this issue, the extraction of accurate calibration parameters is optimized by the Weighted Average Attenuation Factor (WAAF). This approach is proposed to improve the system reliability by covering the whole indoor environment.

It is worth recalling that our positioning system is divided into offline and online stages: the offline involves an environmental calibration phase. It is needed to determine the propagation channel attenuation parameters. During the online stage, the RFID reader position

is then estimated, by applying the new propagation channel model (DOSM or DOSSOM) associated with WAAF and followed by Multilateration.

First, in section 4.2, RSS sets collected within the offline stage are examined. To examine and overcome the fluctuations impact, different RSS combining techniques are adopted; the conventional averaging as well as the Maximum Likelihood Estimator (MLE) as combining technique are elaborated in section 4.3. Indoor propagation models found in the literature, as well as the proposed approaches (DOSM and DOSSOM) are then introduced and analyzed in sections 4.4 and 4.5, respectively. The Weighted Average Attenuation Factor (WAAF) applied for an accurate environmental calibration is presented in section 4.6. Section 4.7 is dedicated to capitalize the overall proposed ILS. It is followed by localization assessments, based on the multilateration technique, in section 4.8. Once the complete proposed ILS validated by positioning errors results', section 4.9 ends the chapter with a detailed conclusion.

4.2 RSS Datasets

This subsection is dedicated to study the RSS fluctuations in the classroom during the offline stage. The received samples, at sixty-four reference positions distributed over the seven tracks A30 until A150 (Figure 4.1) are examined.

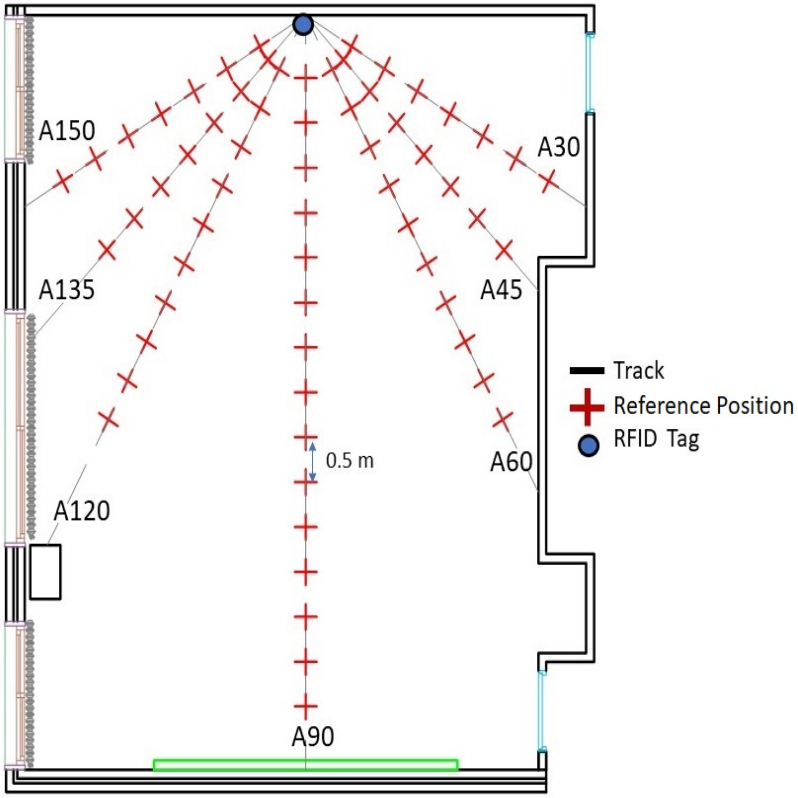

Figure 4.1 Two-dimensional Layout of the classroom environment (Offline Stage)

Following the same steps as for our conventional ILS presented in chapter 2, subsection 2.4.2, 200 samples of the RSS are acquired every 50 centimeters (Figure 4.1). These samples will be used in order to determine the attenuation parameters of the propagation model.

The variations of the received signals are illustrated in Figure 4.2, over each track respectively.

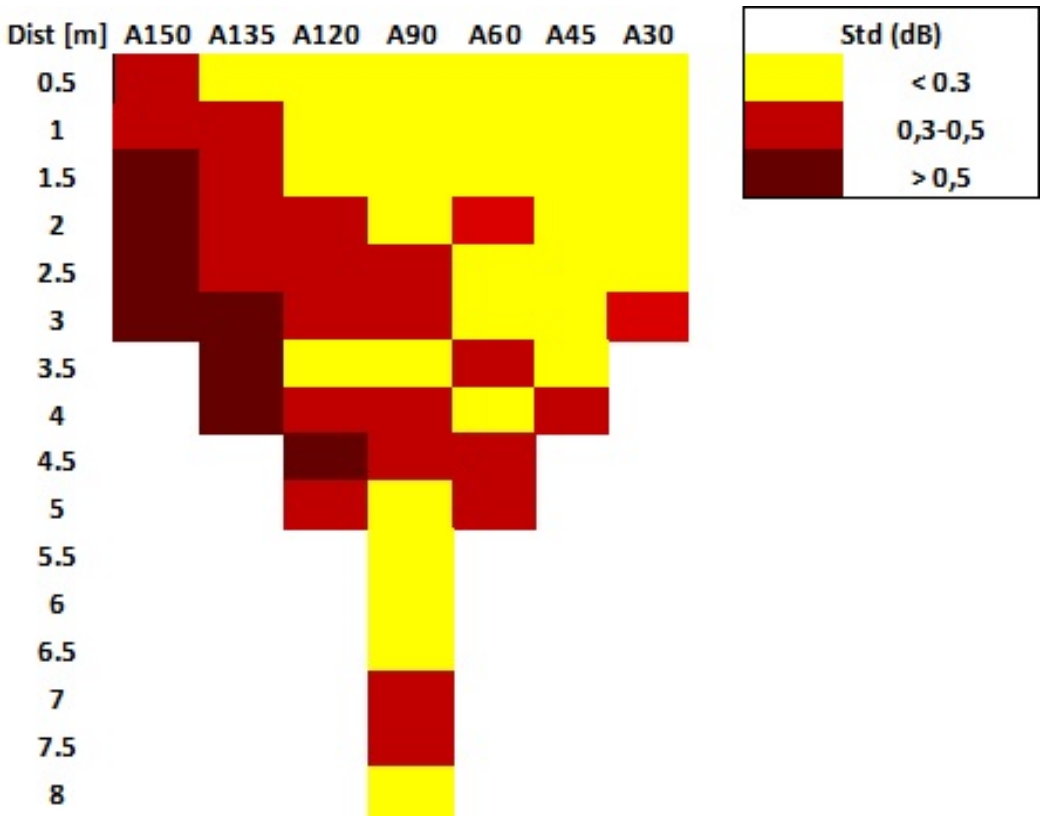

Figure 4.2 RSS Standard Deviation over the classroom

Several factors may affect the received power deviation, e.g. the environment complexity, as well as the channel non-stationarity.

It is worth to recall that the tags' transmission is intermittent. As mentioned in section 2.5, 40 seconds are needed to collect the 200 samples, in the offline stage. Hence, the propagation channel, between the tag and the reader, can be considered as non-stationary. This channel variance may induce RSS variability.

In addition, the RFID reader quantization error is equivalent to $\pm$ 0.3 dB [9]. Hence, the standard deviation values are divided into three categories: the first one is where the standard deviation is less than the quantization noise. The second category illustrates the deviation values between 0.3 and 0.5 dB. Greater than this limit, another category should be considered, in order to identify the critical signals propagation areas.

In this context, it can be noticed that RSS acquisitions fluctuate widely when the RF signals are strongly affected by the indoor environment. More precisely, the largest standard deviations, obtained over tracks A30 and A45, are mainly induced by the corner in front of these two tracks.

Concerning track A90, the maximal standard deviation is less than that of other tracks because most of the emitted signals are far from walls, heater, and pillar, then, signals propagation is nearly LoS over this track.

However, we observe that signals are strongly affected over tracks A120, A135 and A150. Hence, it is necessary to compare the RSS distributions over these three tracks with that of one of the least affected tracks. Figure 4.3 shows four histograms of the RSS acquisitions that were collected at the same tag-reader distance (3 meters) over four different tracks, during the offline stage.

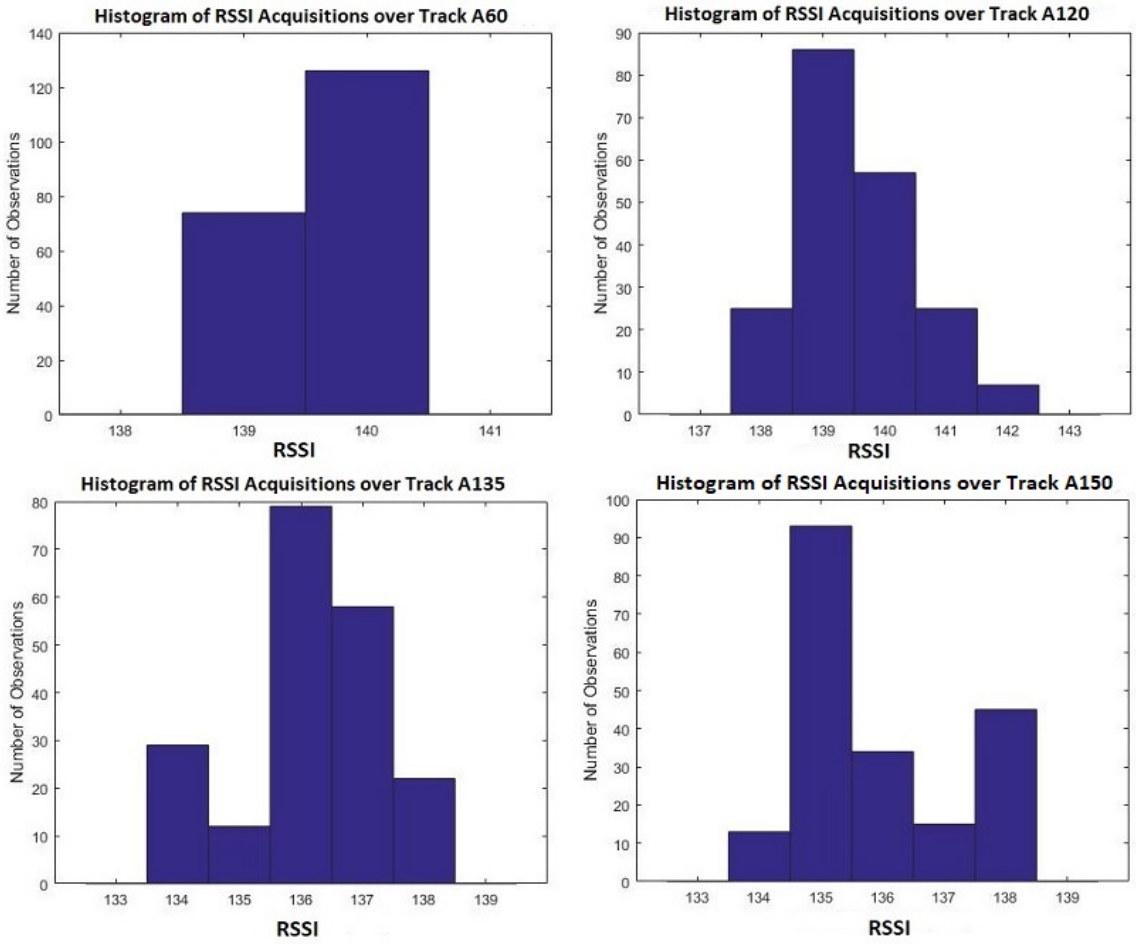

Figure 4.3 Histograms of 200 RSSI collected at 3 meters over 4 different tracks

Histograms illustrated in Figure 4.3 show the distribution of the RSS measurements, at a same distance, over four different tracks A60, A120, A135 and A150. It can be noticed that the RSS acquisitions fluctuate greatly and don't follow a normal distribution. For instance, RSS measurements over track A60 are clustered and span a small range between 139 and 140 that correspond to a received power of -56.94 and -57.58 dBm [9], respectively. In this case, it could still be reasonable to apply the averaging technique to combine the RSS acquisitions.

However, those over tracks A120, A135 and A150 spread and appear to span a wider range. RSS values over track A120 vary between 138 and 142 corresponding to -56.32 and -58.84 dBm. In the same context, the RSS acquisitions over tracks A135 and A150 are spread between 134 and 138 which correspond to -53.79 and -56.32 dBm, respectively. These wide distributions over tracks A120, A135 and A150 are mainly due to the signals reflection and scattering created by the big heater (Figure 4.1). Therefore, accrediting only averaging as RSS combining technique will lose the high-order statistical information in the raw data. Thus, the location system accuracy would be compromised. To improve the system's reliability, the use of the MLE in order to determine the RSS value with the highest probability of occurrence is promising.

4.3 RSS Combining Techniques

4.3.1 RSS Combining by the Conventional Averaging

As already elaborated in chapter 2, subsection 2.4.3, several ILSs found in the literature apply the averaging technique to combine the received RSS_i values. The mean $\widehat{RSS}$ is given by:

$$\widehat{RSS} = \frac{1}{K}\sum_{i=1}^{K} RSS_i \tag{4.1}$$

With K is the number of RSS values collected at each position and RSS_i is the i^{th} received signal strength at each position.

4.3.2 RSS Combining by the MLE

The maximum likelihood of a variable is the value having the highest probability of occurrence, while observing a given set of that variable [10]. MLE is used for different applications [11], [12]. For instance, [11] adopts the MLE in artificial intelligence to understand the language, by predicting the most consistent sequence with the highest probability of occurrence. Considering one sequence predictions of the target sequence y with parameters θ, MLE aims to train the sequence prediction models by minimizing the negative log-likelihood of the probability $p_\theta(y|x)$ as follows:

$$L_{MLE}(\theta) = -log\, p_\theta(y|x) \tag{4.2}$$

With y = $\{y_1, y_2, \dots, y_l\}$ is the sequences set and x is the source type such as phrase, sentence or passage of human language or even an image.

In [12], the MLE is used to estimate and remove the frequency offsets at the ground station, in order to get successful communications with a satellite. Given a block of *N* samples of the received noisy signal, the MLE produces the frequency value that maximizes the periodogram, as follows:

$$\hat{f}_{MLE} = \underset{\lambda}{argmax}\, I(\lambda) \tag{4.3}$$

Where $I(\lambda)$ is the plot of the periodogram function for a noiseless signal, λ is the wavelength.

In our case, to improve the calibration phase's reliability and the localization accuracy, the effect of the RSS values deviation must be mitigated through the associated combining technique providing the most reliable value of RSS in both offline and online stages. Hence, for further processing, the RSS samples are combined with the Maximum Likelihood Estimator (MLE) which is a statistical approach that computes the distribution probability factor of the received power values [13].

Given *K* acquisitions at each position, the MLE determines the RSS value that maximizes the likelihood with the real power captured by the RFID reader; this RSS value is that with the highest probability of occurrence.

$$RSS = [RSS_1, RSS_2, \dots . . RSS_K] \tag{4.4}$$

With *K* is the size of RSS acquisitions at the corresponding position.

The MLE of RSSs is defined as:

$$RSS_{MLE} = arg\, max\, p(RSS_K) \tag{4.5}$$

Where argmax is the operator that gives the RSS with the greatest probability of occurrence. *p* represents the RSS probability.

RSS observations are combined via MLE in both offline and online stages. Figure 4.4 summarizes the MLE approach.

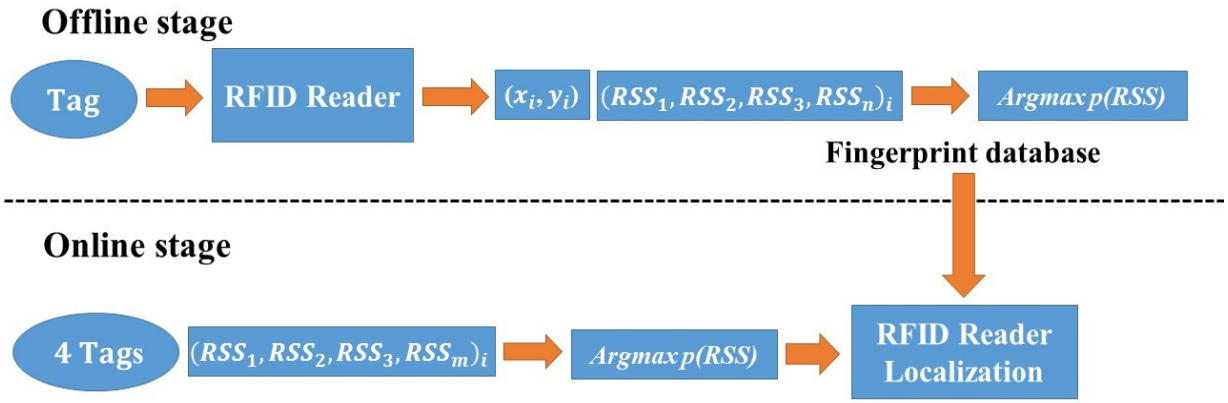

Figure 4.4 RSS values combined by MLE in offline and online stages

The values $\widehat{RSS}$ within the conventional system and RSS_{MLE} within the proposed solution are converted to power values in dBm.

The comparison, between the performance of averaging and the MLE combining techniques, will be elaborated, through indoor localization assessment, in section 4.8.

4.4 Empirical Indoor Propagation Models

Several propagation models have been performed in different indoor environments, such as houses, corridors, and offices. Empirical models are those based on observations and measurements. These models are mainly used to predict the path loss in different scenarios such as LoS or NLoS.

The empirical models Cost 231, WINNER II, ITU-R M2135, Multi Walls Multi Floors, the Attenuation Factor Classic (AFC) Model and the Second Order Polynomial Propagation Model, have been studied. They will be presented in the following subsections.

4.4.1 COST 231 Model

COST 231 is a One Slope Model (OSM) described in [6] and already presented in chapter 2, subsection 2.4.3. The received power expression is given by:

$$P_r\,(d) = P_0 + 10nlog_{10}\left(\frac{d}{d_0}\right) + X \tag{4.6}$$

Where $P_r\,(d)$ is the received power in dBm at a distance *d* in meters, P_0 is the received power at the distance d_0 in dBm and *n* is the path loss exponent. The term *X* describes the standard deviation of the received power values throughout the corresponding area.

4.4.2 WINNER II D112 V1.2 Model

Referring to [7], the WINNER II channel model was proposed for indoor, indoor to outdoor, outdoor to indoor and outdoor scenarios. Initially, it was applied at 2 and 5 GHz. Then, it was extended over the frequency range 2 to 6 GHz. Two models were proposed; the first is for LoS (Without any obstacles). The path loss is then calculated following equation (4.7):

$$PL(d) \;=\; 18.7log_{10}(d) + 46.8 + 20log_{10}\left(\frac{f_c}{5}\right) \tag{4.7}$$

The second one is for NLoS. The transmitter and receiver are in different rooms. In this case, path loss is given by equation (4.8). The number of crossings through walls and floors is taken into consideration.

$$PL(d) = 20log_{10}(d) + 46.4 + 20log_{10}\left(\frac{f_c}{5}\right) + 12n_W + F_L \tag{4.8}$$

$$F_L = 17 + 4(n_f - 1) \tag{4.9}$$

Where f_c is the frequency in GHz, *d* is the distance between the transmitter and the receiver in meters, n_W is number of walls and n_f is number of floors.

4.4.3 ITU-R 2135 Model

Based on real measurements carried out in China, WINNER II model was modified and validated by the ITU-R M.2135 [8]. ITU-R are specified in the frequency range from 2 GHz to 6 GHz. Four different scenarios have been studied: indoor hotspot, urban, suburban, and rural. In the indoor hotspot scenario, it is adopted for a floor of 6 meters of height, including a big hall and 16 rooms. Path loss is given by equation (4.10) for LoS and by equation (4.11) for NLoS:

$$PL(d) = 16.9log_{10}(d) + 20log10\,(f) + 32.8 \quad (4.10)$$

$$PL(d) = 43.3log_{10}(d) + 20log10\,(f) + 11.5 \quad (4.11)$$

Where $PL(d)$in dB, f is the frequency in GHz, d is the distance between the transmitter and receiver in meters.

4.4.4 The Multi Wall Multi Floor Model

The Multi Wall Multi Floor (MWMF) model was validated for two different frequencies 5 and 5.8 GHz [3]. The path loss is computed as in equation (4.12). Within buildings, this propagation model incorporates a linear component of loss, proportional to the number of walls penetrated, plus a more complex term which depends on the number of floors penetrated, producing a loss that increases more slowly as additional floors are included.

$$PL_{MWF}(d) = PL_0 + 10nlog_{10}(d) + \sum_{i=1}^{I}\sum_{k=1}^{K_{wi}} L_{wik} + \sum_{j=1}^{J}\sum_{k=1}^{K_{fj}} L_{fjk} \quad (4.12)$$

Where $PL_{MWF}(d)$ is the path loss in dB at a distance d in meters. L_{wik} is the loss of the k^{th} crossed wall of type i in dB, K_{wi} is the number of crossings through walls of type i, I is the number of walls' type i, L_{fjk} is the loss of the k^{th} penetrated floor of type j in dB, K_{fj} is the number of crossings through walls of type j and J is the number of floors' type j.

4.4.5 Attenuation Factor Classic Model

The Attenuation Factor Classic Model (AFC) model is an empirical indoor office path loss model. [14] presents the path loss measurements conducted in a modern office building using a 5.25 GHz carrier frequency. It is presented in different propagation conditions, e.g. in rooms and corridors. In rooms, it is expressed by (4.13):

$$PL(d) = 47.8 + 10nlog_{10}(d) \tag{4.13}$$

For corridors, the two-slopes model is shown in (4.14):

$$PL(d) = \begin{cases} 53.2 + 25.8log_{10}(d) & d \leq 9\ m \\ 56.4 + 29.1log_{10}(d) & d > 9\ m \end{cases} \tag{4.14}$$

As defined previously, $PL(d)$ is the path loss in dB, *d* is the distance in meters and *n* is the path loss exponent.

4.4.6 Second Order Polynomial Propagation Model

The Second Order Polynomial Propagation Model (SOPPM) seems to be the best way to calibrate an environment according to flat/home configurations such as walls, furniture and other obstacles [15]. It presents a better fit that allows to obtain the set of propagation parameters that mitigate the difference between real measurements and estimations. It is defined in equation (4.15):

$$PL(d) = a(d)^2 + b(d) + c \tag{4.15}$$

Where $PL(d)$ is is the path loss in dB, at a distance *d* in meters. *a*, *b*, and *c* are constant parameters of the second order polynomial model.

4.5 Proposed Empirical Indoor Propagation Models

Empirical investigation has been a common methodology to study radio waves propagation and path loss modeling. Our approach follows this practice. A series of measurements were conducted in the classroom environment in order to determine the propagation channel attenuation coefficients. The received power is then depicted and matched

with different propagation models in a way to justify the use of a two slopes model. Figure 4.5 illustrates the received power measurements over track A90 (central line in Figure 4.1).

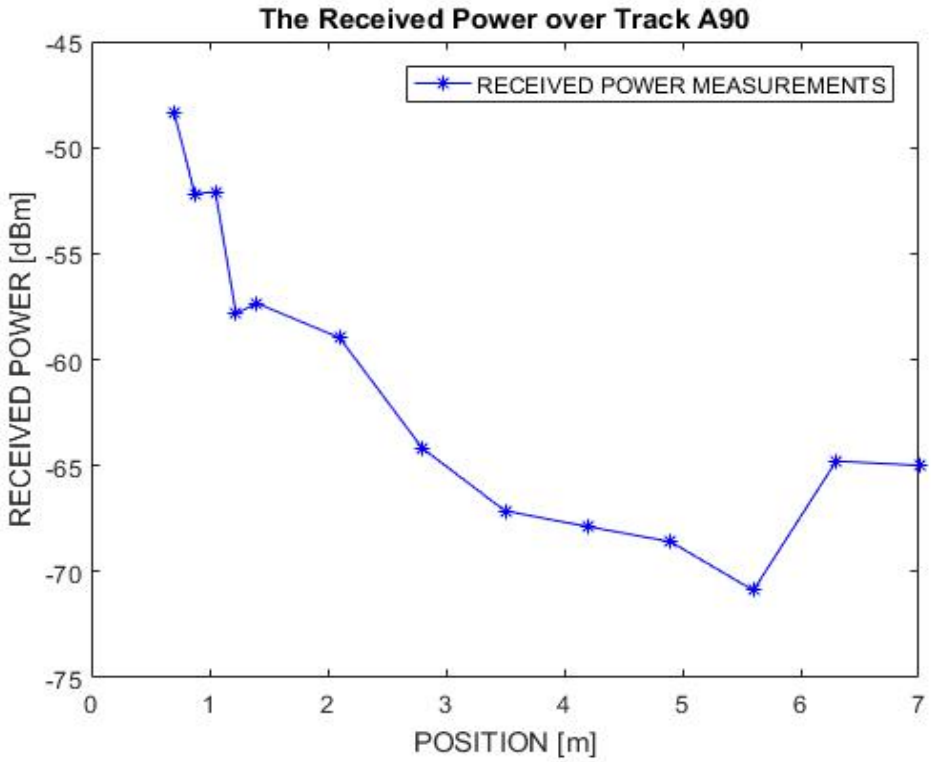

Figure 4.5 Received Power measurements over track A90

According to Figure 4.5, received signals, over track A90 positions, largely vary. Signals' fluctuation is one of the major issues causing inaccuracy of propagation models. Thus, to get an accurate signals propagation representation in indoor environments, two empirical models will be introduced in subsections 4.5.1 and 4.5.2. The first one is the Dual One Slope Model (DOSM) that applies the OSM twice performing a regression on two successive segments. The second one is the Dual One Slope with Second Order Model (DOSSOM). This model uses the OSM followed by the SOPPM. Subsection 4.5.3 illustrates the received power through the existing and proposed indoor propagation models. Distances estimation principle, elaborated in subsections 4.5.4 and 4.5.5, presents the Mean Estimated Distance Errors (MDE) obtained with the known and the proposed indoor propagation models.

4.5.1 Dual One Slope Propagation Model

According to recent experiments presented in [16], the received power decays sharply when the measurement range is up to 1.5 meters. Then, the signal starts to decay slowly. In our case, the propagation model has also two different slopes, one for tag-reader distances shorter

than 3λ and another one for distances greater than 3λ, which is equal to 2.1 meters. The proposed empirical Dual One Slope Propagation Model (DOSM) that fitted the collected received power for each track, is defined in the following equations (4.16):

$$P_r(d) = \begin{cases} P_0 - 10.n_{1T_i}.log_{10}(d) + X_{1T_i} & d \leq 3\lambda \\ P_0{}' - 10.n_{2T_i}.log_{10}(d) + X_{2T_i} & d > 3\lambda \end{cases} \quad (4.16)$$

$P_r(d)$ is the received power in dBm at the distance *d* in meters, P_0 is the received power at 1 meter in dBm. P_0 is the received power at 3λ in dBm. *i* is the track index. The terms n_{1T_i} and n_{2T_i} are the path loss exponent of the corresponding slope. X_{1T_i} and X_{2T_i} are lognormal constants corresponding to the received power variations throughout the first and the second part of each track modeled by one slope.

4.5.2 Dual One Slope with Second Order Polynomial Model

As previously mentioned, measured power values are separated into two slopes, since the received power highly decrease for tag-reader distances shorter than 3λ (which is equal to 2.1 meters) and vary slightly for distances greater than 3λ. A detailed analysis is described and illustrated in section 4.5.3, where the different propagation models are assessed.

The Dual One Slope with Second Order Polynomial Model (DOSSOM) is hence given by:

$$P_r(d) = \begin{cases} P_0 - 10.n_{T_i}.log_{10}(d) + X_{T_i} & d \leq 3\lambda \\ P_0' - a_{T_i}.log_{10}(d)^2 - b_{T_i}.log_{10}(d) - c_{T_i} & d > 3\lambda \end{cases} \quad (4.17)$$

As previously defined, $P_r(d)$ is the received power in dBm at the distance *d* in meters, P_0 is the received power at 1 meter in dBm. P_0 is the received power at 3λ in dBm. *i* is the track index, X_{T_i} is a lognormal variable for the received power error throughout the first part of each track (Figure 4.1) modeled by the one slope variation. n_{T_i} is the path loss exponent corresponding to the first part of the path.

Thus, the attenuation parameter of the first part of each track T_i is determined as follows:

$$n_{T_i} = \frac{P_r(d) - P_0 - X_{T_i}}{-10log_{10}(d)} \tag{4.18}$$

a_{T_i}, b_{T_i} and c_{T_i} are constant parameters of the second order polynomial model that corresponds to the second part, *i* is the track (Figure 4.1). P_0' is the received power at 3λ. They are determined by forming a squared matrix as follows:

$$\begin{pmatrix} log_{10}(d_1)^2 & log_{10}(d_1) & 1 \\ log_{10}(d_2)^2 & log_{10}(d_2) & 1 \\ log_{10}(d_3)^2 & log_{10}(d_3) & 1 \end{pmatrix} \begin{pmatrix} a_{T_i} \\ b_{T_i} \\ c_{T_i} \end{pmatrix} = \begin{pmatrix} P_r(d_1) - P_0' \\ P_r(d_2) - P_0' \\ P_r(d_3) - P_0' \end{pmatrix} \tag{4.19}$$

Where $d_1, d_2,$ and d_3 are three different real tag-reader distances over the corresponding track.

Let

$$A = \begin{pmatrix} log_{10}(d_1)^2 & log_{10}(d_1) & 1 \\ log_{10}(d_2)^2 & log_{10}(d_2) & 1 \\ log_{10}(d_3)^2 & log_{10}(d_3) & 1 \end{pmatrix} \tag{4.20}$$

And

$$B = \begin{pmatrix} P_r(d_1) - P_0' \\ P_r(d_2) - P_0' \\ P_r(d_3) - P_0' \end{pmatrix} \tag{4.21}$$

The solution of equation (4.19) determines the attenuation parameters of each track as follows:

$$\begin{pmatrix} a_{T_i} \\ b_{T_i} \\ c_{T_i} \end{pmatrix} = A^{-1}B \tag{4.22}$$

4.5.3 Propagation Models Representations

As signals propagating in our case study have a frequency of 433 MHz, the two empirical indoor propagation models OSM and SOPPM, found in the literature and presented in section 4.4, as well as the two proposed models described in the previous subsections 4.5.1 and 4.5.2 are applied on the received power values collected, during the offline stage, over the three tracks A60, A90 and A120 (Figure 4.1). These three tracks were selected because they

include a sufficient number of reference positions to better reflect the signal attenuation in the considered environment. Power variations are shown in Figure 4.6, Figure 4.7 and Figure 4.8 respectively.

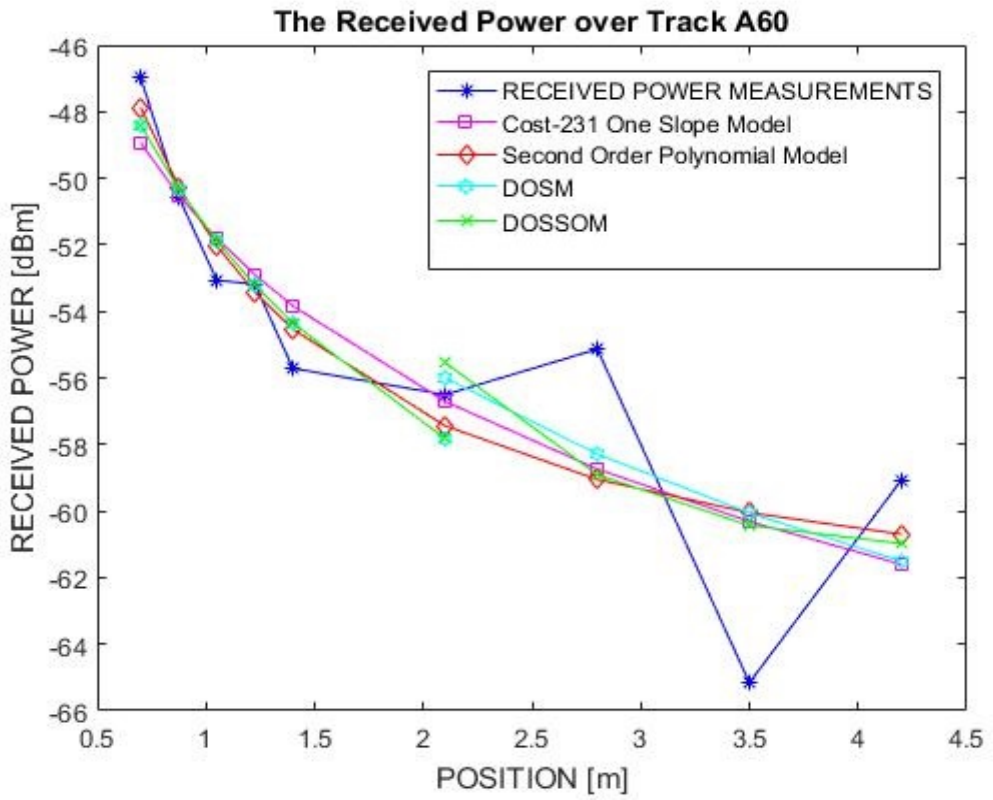

Figure 4.6 Received Power by the different empirical propagation models over the track A60

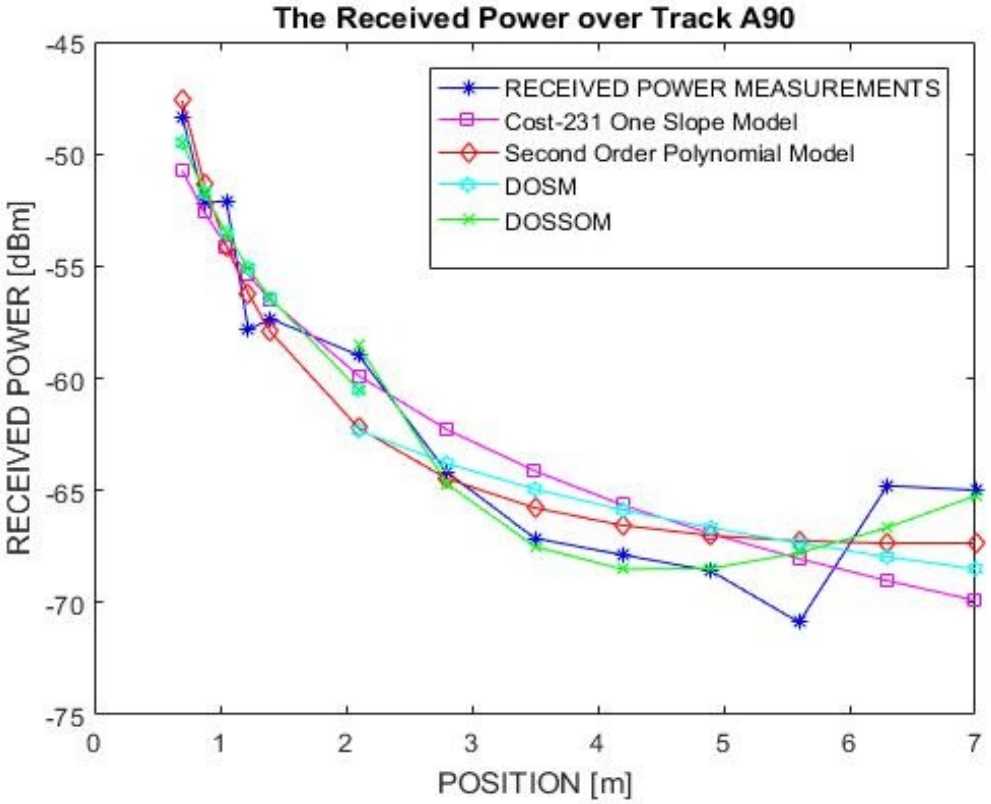

Figure 4.7 Received Power by the different empirical propagation models over the track A90

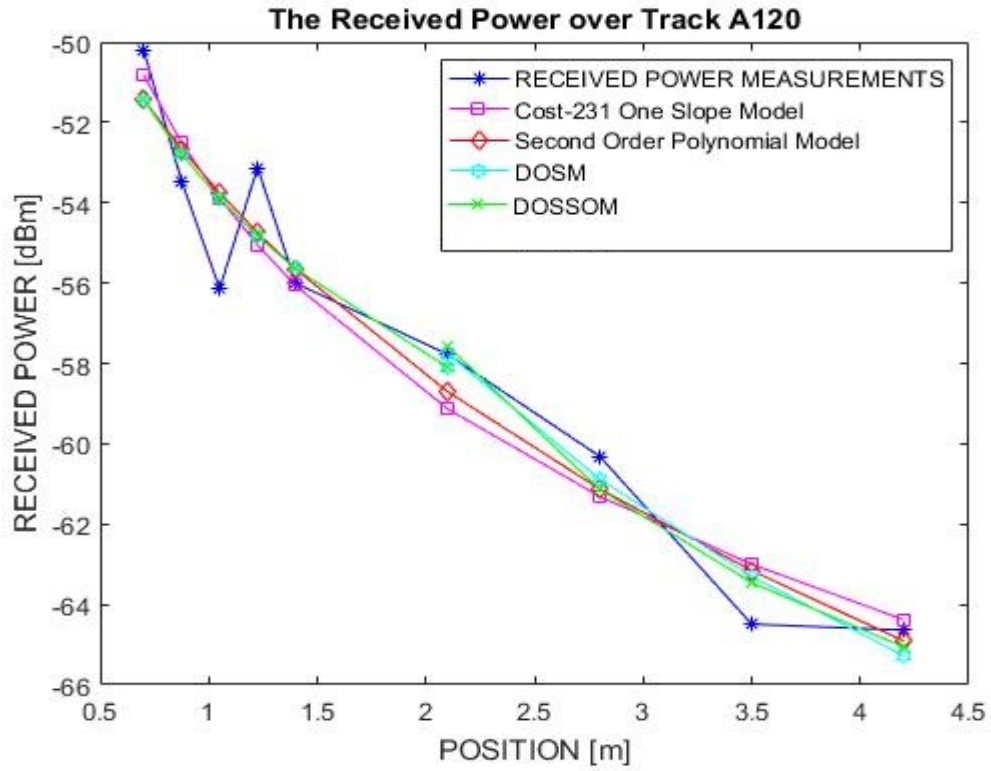

Figure 4.8 Received Power by the different empirical propagation models over the track A120

According to the illustrated Figure 4.6, Figure 4.7 and Figure 4.8, the one slope propagation model performs better when the tag-reader distance small, more precisely while LoS conditions are dominant. Whereas, when the tag-reader distance is significant, the second order propagation model presents a better fit by taking into consideration all signals' fluctuations due to the classroom geometry and materials as well as unmovable furniture, already detailed on chapter 3, subsection 3.4.1.

4.5.4 Distance Estimation

After determining the propagation model parameters, tags-reader distances are estimated during the online phase. The averaged RSS acquisitions are further converted to power values in dBm.

Knowing the power captured by the reader and following equation (4.16) (DOSM model), the distance can be estimated as:

$$\hat{d} = 10^{\left(\frac{P_r(d) - P_0{}' - X_{T_{2i}}}{-10n_{T_{2i}}}\right)} \tag{4.23}$$

Whereas, by applying DOSSOM (equation 4.17), the tags-reader distances can be estimated, by resolving the quadratic relationship:

$$a_{T_i}.(log_{10}(\hat{d})^2 + b_{T_i}.(log_{10}(\hat{d}) + (c_{T_i} - P_0{}' - P_r(d)) = 0 \tag{4.24}$$

$P_r(d)$is the received power captured by the RFID reader in dBm, at the tag-reader estimated distance $\hat{d}$ in meter. $a_{\mathrm{T_i}}$, $b_{\mathrm{T_i}}$ and $c_{\mathrm{T_i}}$ are the propagation channel constants already determined by equations (4.18) and (4.22).

Finally, the distance error ϵ_d can be calculated as follows:

$$\epsilon_d = |d_r - \hat{d}| \tag{4.25}$$

where d_r is the real tag-reader distance.

4.5.5 Distance Error Analysis

In this section, the Mean Distance Errors (MDE) obtained with the different indoor propagation models are studied and analyzed. As already stated, this analysis is assessed during the offline stage in a way to validate the performance of the proposed propagation models (DOSM and DOSSOM). Table 4.1 shows the variation of the MDEs and the 90% Cumulative Density Functions (CDFs) of the distance errors along the three different tracks A60, A90 and A120 respectively.

Table 4.1 MDE with Average RSS over the three tracks A60, A90 and A120

Propagation Models	**Track A60**		**Track A90**		**Track A120**	
	MDE [m]	**CDF 90%**	**MDE [m]**	**CDF 90%**	**MDE [m]**	**CDF 90%**
COST 231	0.99	5.8	2.45	3.7	2.18	5.2
SOPPM	0.67	3.1	1.73	3.5	1.91	4.1
DOSM	0.56	2.7	1.04	0.9	1.11	1.5
DOSSOM	0.51	1.9	0.53	0.91	0.8	1.2

According to Table 4.1, it can be noticed that the obtained MDEs differ from one track to another depending on the signal attenuation and the multipath effects. As already mentioned, track A60 is almost far from materials like the big heater near track A120, where the signals propagation is obviously affected. However, track A60 is mostly affected by the signals' diffraction due to the asymmetrical wall shape (Figure 4.1).

With A60, DOSM and DOSSOM present almost the same performance as SOPPM, due to the limited number of positions. They preform similarly over track A90, due to the limited impact of furniture affecting the signal propagation. However, these two models perform better than to the SOPPM. Concerning, track A120, DOSSOM presents better results by taking into account the signals' fluctuations due to the big heater.

The optimal MDE, obtained with the existing propagation models, is 67 centimeters over track A60. However, the optimal MDEs obtained, over the same track, with DOSM and DOSSOM are 56 and 51 centimeters, respectively. Hence, it can be noticed that the proposed indoor propagation models DOSM and DOSSOM improve the distance estimation by 79.18 percent compared to the distance errors obtained with the COST 231 model over track A90.

Moreover, these proposed models enhance the distance estimation by 23.88 percent compared to results obtained with the best performing model SOPPM that matches perfectly with the received power. Thus, DOSM and DOSSOM are effective propagation models that can improve the accuracy in the proposed localization system.

4.6 Weighted Average Attenuation Factors

In the literature, several studies evaluate the impact of the environment calibration on localization systems accuracy [17]-[22]. However, most of these studies have focused on signals propagation characteristics only [17] and [18]. Work in [17] creates a Ray Launching based simulation model to evaluate an indoor localization system implemented in an office. Positions errors highly depend on the number of considered Bluetooth Low Energy (BLE) devices used to extract the accurate signal attenuation parameters. In the same context, [18] focuses on the calibration of Wi-Fi-based indoor tracking systems to be used by smartphones. Experiment was conducted in a multi-room office laboratory. To build an accurate signal propagation model corresponding to the indoor environment, a novel in-motion calibration methodology is introduced. This calibration uses three different propagation models based on RSS collection, supplemented by a particle filter. According to the presented results, using the in-motion calibration mechanism considerably improves the tracking accuracy. In these studies [17] and [18], some important challenges, such as the fluctuation of RSS measurements and the long durations as well as manpower needed for data collection are not addressed.

Beyond this, some studies focused on avoiding time-consumption for data collection. For instance, [19] develops a new interpolation algorithm to optimize the number of pre-chosen calibrated points to build a radio map. In addition, work in [20] proposes a novel Simultaneous Calibration and Localization (SCAL) algorithm to improve real-time positioning and calibrating accuracy in indoor scenarios. The proposed framework is divided into the Target Localization and Beacon Calibration (TLBC) section and the Global Optimization (GO) section. Positioning accuracy is improved to reach 0.24 meters. Despite the improvement achieved by the proposed solutions [19] and [20], issues like the computational complexity and the system’s cost were not addressed.

Looking at beamforming-based localization approaches, work in [21] applies an adaptive beamforming AoA estimation technique based on the Minimum Variance Distortion less Response (MVDR) algorithm. This technique reaches a sub metric positioning accuracy.

In the same context, [22] presents an Ultra-Wide Band Impulse Radio (UWB-IR) beamforming array targeted for a precise directional positioning and tracking of moving objects in complex indoor environments. This beamforming transmitting array is able to achieve full scanning range from -90 to +90 degrees with a resolution of 5 degrees. Despite the high accuracy achieved in both studies, the use of beamforming for angles estimation requires a complex end-user hardware, which increases the system's cost and complexity.

In our case, to trade-off between the system's performance, complexity and hence cost, we propose an RSS calibration method via the Weighted Average Attenuation Factor (WAAF). It aims to increase the accuracy of the localization system through a better propagation channel model. Compared to the attenuation factor AF90 of our conventional localization system, already introduced in chapter 2, subsection 2.4.4, WAAF approach takes into account all the positions over all tracks, in order to extract accurate attenuation parameters corresponding to the considered environment (Figure 4.1).

In fact, our conventional indoor localization system uses only the calibration parameters of the track A90, that is characterized by the highest number of positions. These attenuation parameters are abbreviated as AF90.

$$AF90 = \left\{ n_{T_{90}};\ a_{T_{90}};\quad b_{T_{90}};\quad c_{T_{90}} \right\} \tag{4.26}$$

The proposed calibration procedure WAAF uses the attenuation parameters corresponding to the seven tracks, and not only those of A90. These parameters are extracted via either DOSM or DOSSOM, which are expressed in two segments. The first segment is for tag-reader distances up to 3λ and the second one is for tag-reader distances greater than 3λ.

Applying WAAF with DOSM, equation (4.16) becomes:

$$P_r(d) = \begin{cases} P_0 - 10.n_{w_1}.log_{10}(d) + X_{w_1} & d \leq 3\lambda \\ P_0{}' - 10.n_{w_2}.log_{10}(d) + X_{w_2} & d > 3\lambda \end{cases} \tag{4.27}$$

The attenuation parameters are then defined in the following equations:

While d $\leq 3\lambda$,

$$n_{w1} = \sum_{i=1}^{7} n_{1T_i} \frac{N'_{Pos/T_i}}{N'_{Total}} \tag{4.28}$$

While d > 3λ,

$$n_{w2} = \sum_{i=1}^{7} n_{2T_i} \frac{N''_{Pos/T_i}}{N''_{Total}} \tag{4.29}$$

With i indicates the track. n_{w1} and n_{w2} are the WAAF corresponding to the first and the second slope of the propagation model, respectively. n_{1T_i} and n_{2T_i} are the slopes associated to each track. N'_{Total} and N''_{Total} represent the respective total number of positions over the two segments. N'_{Pos/T_i} and N''_{Pos/T_i} are the respective number of positions over each track of the corresponding slope.

Furthermore, applying WAAF with DOSSOM, equation (4.17) becomes:

$$P_r(d) = \begin{cases} P_0 - 10.n_{w_1}.log_{10}(d) + X_{w_1} & d \leq 3\lambda \\ P'_0 - A_{w_2}.log_{10}(d)^2 - B_{w_2}.log_{10}(d) - C_{w_2} & d > 3\lambda \end{cases} \tag{4.30}$$

The attenuation parameters are then defined in the following equations:

While d ≤ 3λ,

$$n_{w1} = \sum_{i=1}^{7} n_{T_i} \frac{N'_{Pos/T_i}}{N'_{Total}} \tag{4.31}$$

With i indicates the track. n_{w1} is the weighted average attenuation factor corresponding to the first slope of the propagation model. n_{T_i} is the attenuation factor relative to each track. N'_{Total} represents the total number of positions over the first segment and N'_{Pos/T_i} the respective number of positions over each track.

While d > 3λ,

The weighted average coefficients A_{w2}, B_{w2} and C_{w2}, corresponding to the second order polynomial modeling the second segment of the propagation channel, are then defined as:

$$\begin{cases} A_{w2} = \sum_{i=1}^{7} a_{T_i} \dfrac{N''_{Pos/T_i}}{N''_{Total}} \\ B_{w2} = \sum_{i=1}^{7} b_{T_i} \dfrac{N''_{Pos/T_i}}{N''_{Total}} \\ C_{w2} = \sum_{i=1}^{7} c_{T_i} \dfrac{N''_{Pos/T_i}}{N''_{Total}} \end{cases} \quad (4.32)$$

With i indicates the track. a_{T_i}, b_{T_i} and c_{T_i} are the constants associated to each track. They are given by equation (4.22) in sub-subsection 4.5.2.

$N"_{Total}$ represents the total number of positions over the second segment and $N"_{Pos/T_i}$ the respective number of positions over each track.

It can be noticed that WAAF coefficients are directly proportional to the number of calibrated positions. This procedure takes into account all positions in order to cover the whole environment.

To evaluate the accuracy improvement thanks to WAAF calibration, a comparison between Estimated Distance Errors obtained, by applying the conventional RSS average combining technique, with AF90 and WAAF attenuation factors is elaborated.

It is worth recalling that, within the online stage, RSSs are collected every 70 centimeters $\cong \lambda$, over the three tracks A60, A90 and A120, selected for the validation of the proposed calibration procedure improvements'.

Hence, examined estimated distance errors at two tag-reader distances of $2.8 \cong 4\lambda$ and $3.5 \cong 5\lambda$ meters, are illustrated in Table 4.2. These are the nearest distances to 3 meters; value where the RSS fluctuations were studied in section 4.2.

Table 4.2 Comparison of the Estimated Distance Errors via AF90 and WAAF Attenuation Factors

Tracks	**Tag-Reader Distance [m]**	**Estimated Distance Errors [m]**	
		AF90	WAAF
A60	2.8	0.71	0.58
	3.5	0.83	0.72
A90	2.8	0.63	0.54
	3.5	0.68	0.63
A120	2.8	0.83	0.41
	3.5	0.75	0.48

It can be noticed that the suggested WAAF calibration approach improves the estimated distance errors compared to the conventional one, that is based on the attenuation parameters of the central track (A90) only.

Finally, once the RSS combining approach by the MLE is introduced and the WAAF calibration technique is elaborated, the following section is dedicated to present the overall proposed ILS.

4.7 Complete Proposed ILS System

In short, the proposed ILS based on MLE with WAAF is divided into two stages: offline and online stage.

During the offline stage, a defined number of RSS values are collected. These samples are combined via the MLE. This combined RSS value is then converted into received power in dBm. In order to determine the attenuation parameters that cover the whole classroom environment, the proposed empirical indoor propagation model DOSM or DOSSOM, associated with the weighted average constant parameters is applied.

The attenuation parameters using DOSM propagation with WAAF are previously defined in equations (4.28) and (4.29). In addition, the attenuation coefficients using DOSSOM propagation with WAAF are already expressed in equations (4.31) and (4.32).

Within the online stage, another defined number of RSS samples are collected at each unknown location and combined with the same technique (MLE) used during the calibration phase. The best RSS sample is further converted into received power in dBm. The RFID reader

position is then estimated by applying either the defined propagation model DOSM or DOSSOM, followed by multilateration.

The DOSM propagation model with WAAF is already presented in equation (4.27). Moreover, the DOSSOM propagation with WAAF is also previously expressed in the equation (4.30).

The complete proposed localization system is thus summarized by the following block diagram (Figure 4.9):

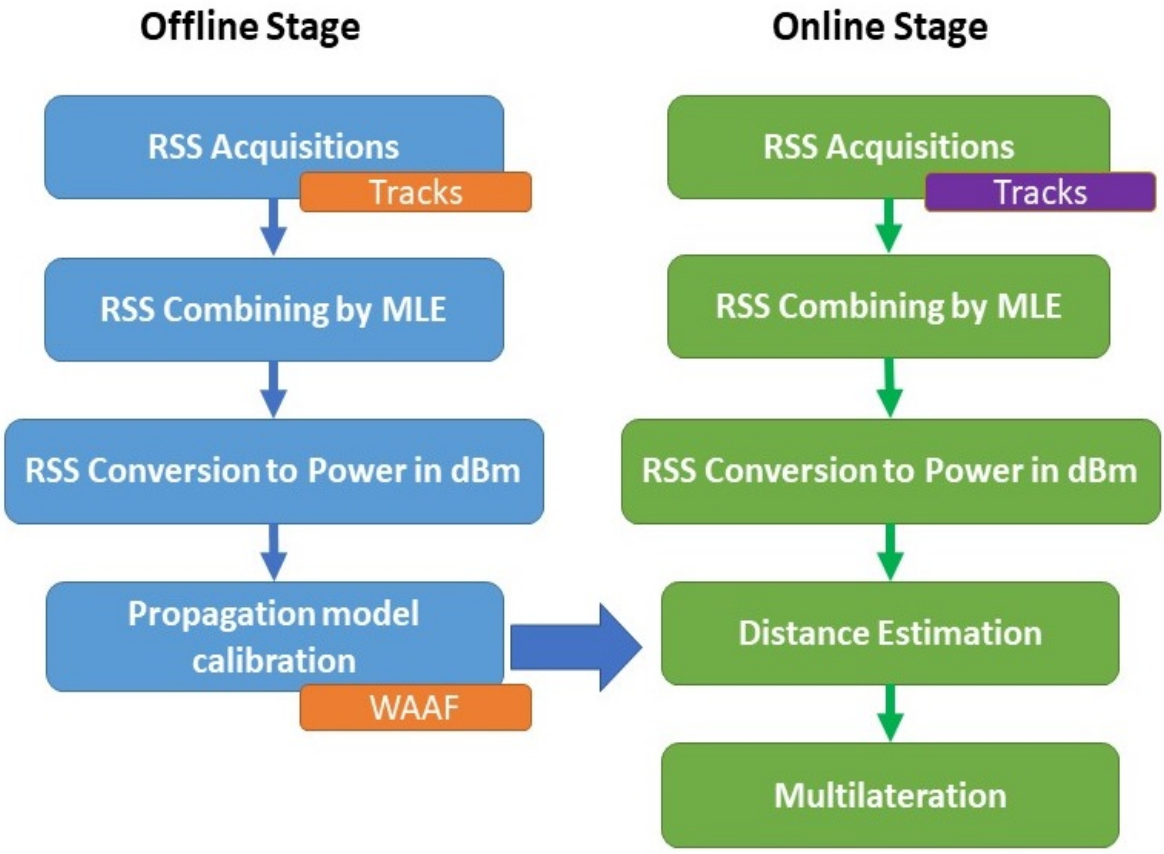

Figure 4.9 Block diagram of the complete ILS based on MLE with WAAF

4.8 Localization Assessment

This section evaluates the complete proposed localization system.

Within the online stage, localization is achieved with four active RFID tags deployed in the 63.75 square meters' classroom environment i.e. with a deployment density of 0.062 RFID tags per square meter. Each tag is attached on the center of each wall of the classroom environment as illustrated in Figure 4.10.

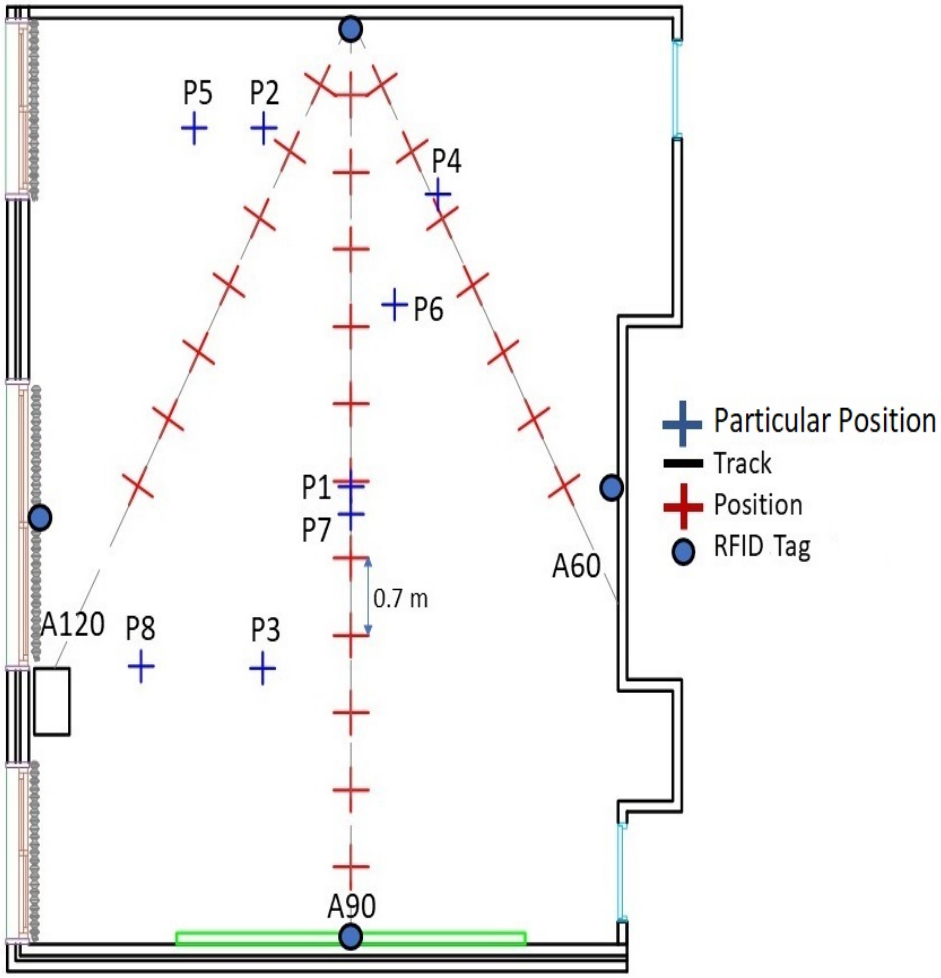

Figure 4.10 Two-dimensional layout of the classroom environment (Online Stage)

The position error is estimated at thirty-two different positions. Among these positions, twenty-four are uniformly distributed in the space, with a distance of 70 centimeters $\cong \lambda$, over the three tracks A60, A90 and A120. This step differs from the one used within the calibration stage (50 centimeters) in order to evaluate our system's accuracy on tracks.

Eight particular positions are chosen out of the considered tracks, to assess the effects of the classroom geometry and structure as well as those produced by the metallic elements distributed within. P1 and P7 were selected to check the impact of the LCD projector on the positioning error. P3 and P8 reflect the influence of the pillar on the left side of the classroom. P5 and P2 assess the heater's effect. Finally, P4 and P6 are between tracks A60 and A90, on the right side of the classroom, where the impact of the metallic objects is less compared to other areas.

Twenty samples of the RSS are acquired at each position; they are combined by the conventional averaging as well as by the Maximum Likelihood Estimator (MLE), in both the calibration and the positioning stages.

Moreover, tags-to-reader distances were estimated using one of the propagation models DOSM and DOSSOM, considering the two calibrations approaches: that with the basic attenuation parameters of the central track A90 (AF90) and that with the Weighted Average Attenuation Factor (WAAF) defined in the section 4.6.

Then, by applying the multilateration technique, the position of the RFID reader is estimated.

Positions errors', obtained by performing the MLE in both stages, were determined and compared to those obtained while combining the RSS samples by averaging.

4.8.1 Location assessment via AF90 vs WAAF

The following shows the location accuracy, using the RSS averaging technique within the offline and online stages, in order to evaluate the positioning improvement thanks to the proposed WAAF calibration approach.

Figure 4.11 and Figure 4.12 illustrate the CDF of the positions errors' achieved through the two different attenuation factors: AF90 and WAAF. Experiments were conducted with the two introduced indoor propagation models DOSM and DOSSOM.

Figure 4.11 presents the CDF of the obtained positions errors' with the two calibration parameters AF90 and WAAF while applying the DOSM as indoor propagation model.

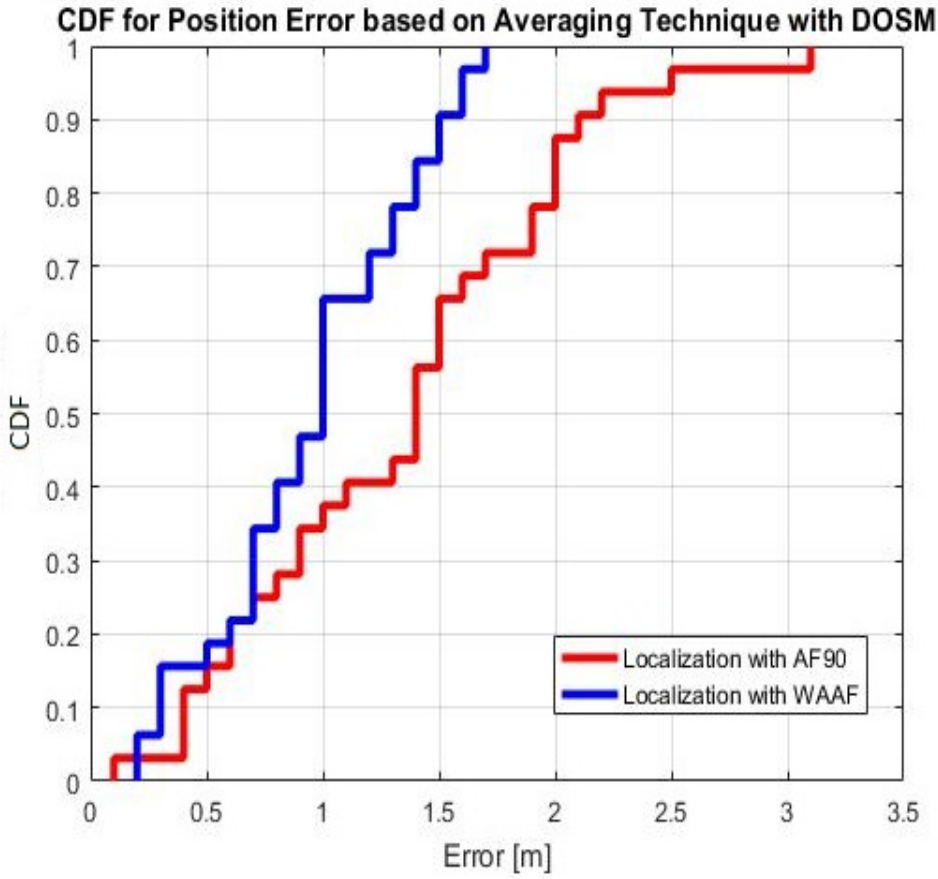

Figure 4.11 Comparative CDF for the positions errors with DOSM

According to Figure 4.11, positions errors', reached at 90% CDF, are 2.2 and 1.5 meters with AF90 and WAAF, respectively. The localization accuracy increases by 31.81 percent while applying DOSM with WAAF compared to that obtained by only DOSM.

Figure 4.12 compares the CDF of the positions errors' obtained while applying the DOSSOM as a propagation model.

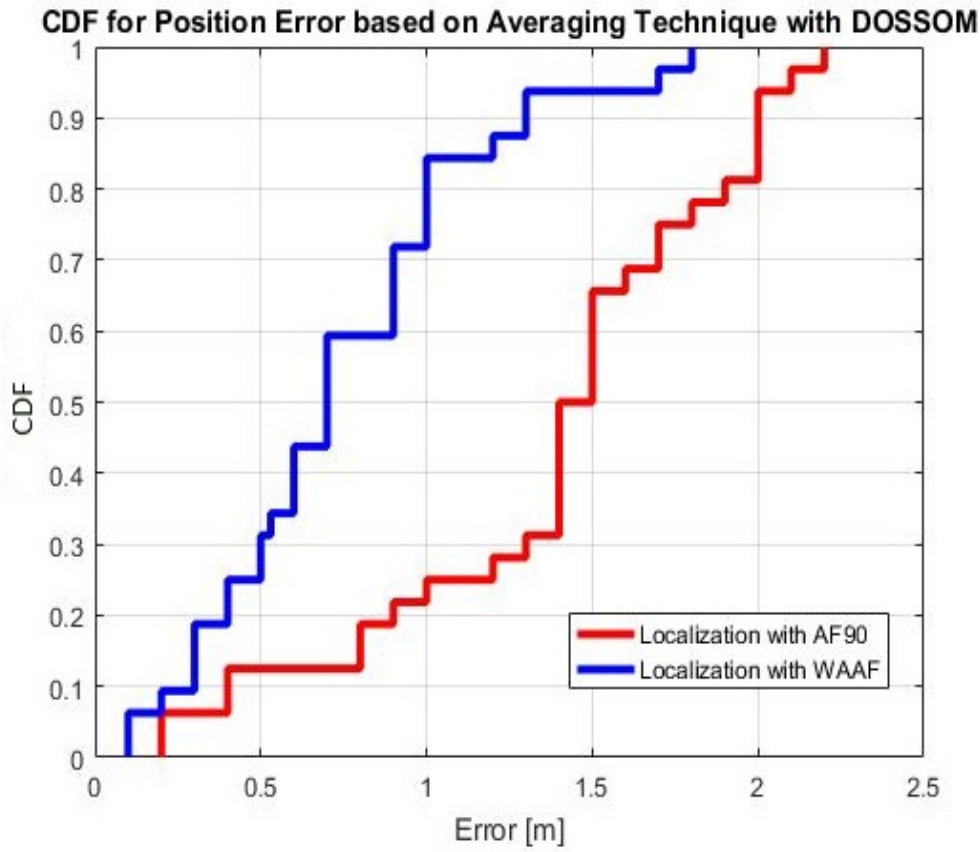

Figure 4.12 Comparative CDF for the positions errors with DOSSOM

According to the CDF presented in Figure 4.12, the positions errors' of the localization system based on the averaging technique, achieved at 90% CDF, are 2 and 1.3 meters while applying AF90 and WAAF, respectively.

In short, the DOSSOM with WAAF calibration improves the position accuracy of 35 percent, as compared to DOSSOM.

Overall, the suggested indoor localization architecture improves the position accuracy by up to 41 percent hence reducing the position error from 2.2 to 1.3 meters.

4.8.2 Location Assessment by Averaging versus MLE

In this sub-section, experiments were conducted, using the calibration parameters AF90 and WAAF independently within the offline stage, in order to investigate the localization performance via averaging and MLE as RSS combining techniques.

As previously mentioned in section 4.3, these techniques are used to combine the received power acquisitions in both offline and online stages.

Obtained CDF, presented in Figure 4.13 and Figure 4.14, illustrate the positions errors' achieved through the two different attenuation factors: AF90 and WAAF. Experiments were performed with the proposed indoor propagation models DOSM and DOSSOM.

Figure 4.13 presents the CDF of the obtained positions errors' using the calibration parameters AF90 and WAAF independently while applying DOSM.

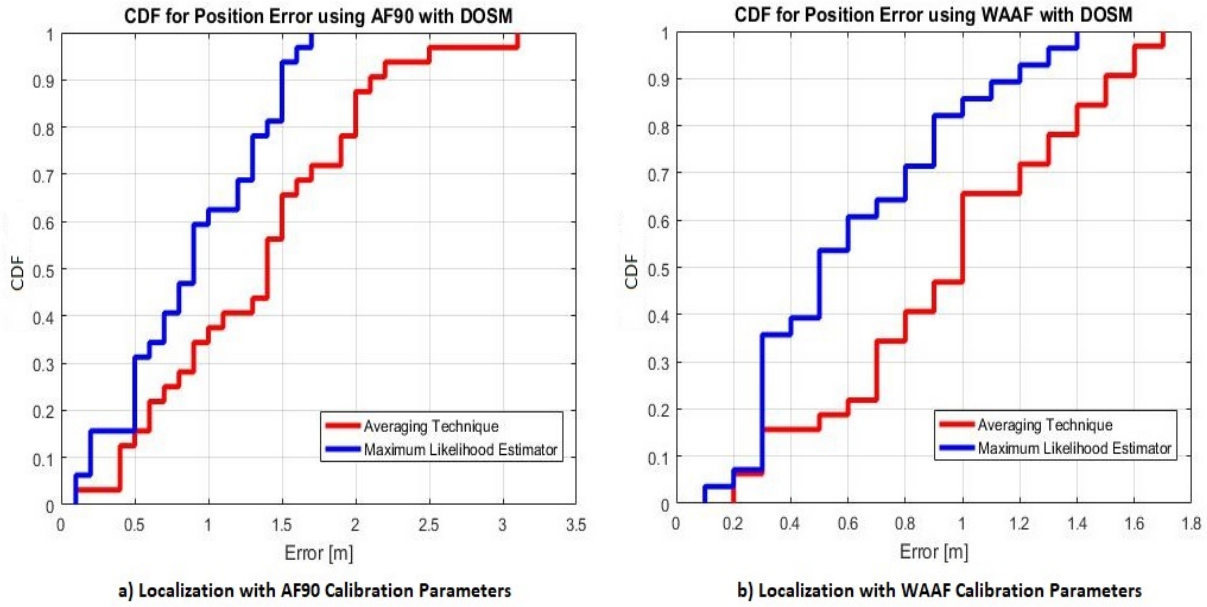

Figure 4.13 CDFs for the positions errors with the average and MLE using DOSM

According to Figure 4.13 (a), the obtained positions errors', at 90% CDF with calibration parameters AF90, are 2 and 1.5 meters with the averaging technique and the MLE, respectively. The location accuracy achieved with the MLE is increased by 20 percent while using the calibration parameters of the central track AF90 and DOSM.

Figure 4.13 (b) represents the CDF of the positions errors' using DOSM with WAAF. The positions errors', at 90% CDF, are 1.5 and 1.1 meters with the averaging technique and

the MLE respectively. The location accuracy using MLE increases by 26.66 percent while applying DOSM with WAAF.

Finally, Figure 4.14 compares the CDF of the positions error obtained using the two calibration parameters of AF90 and WAAF independently with the DOSSOM as empirical propagation model.

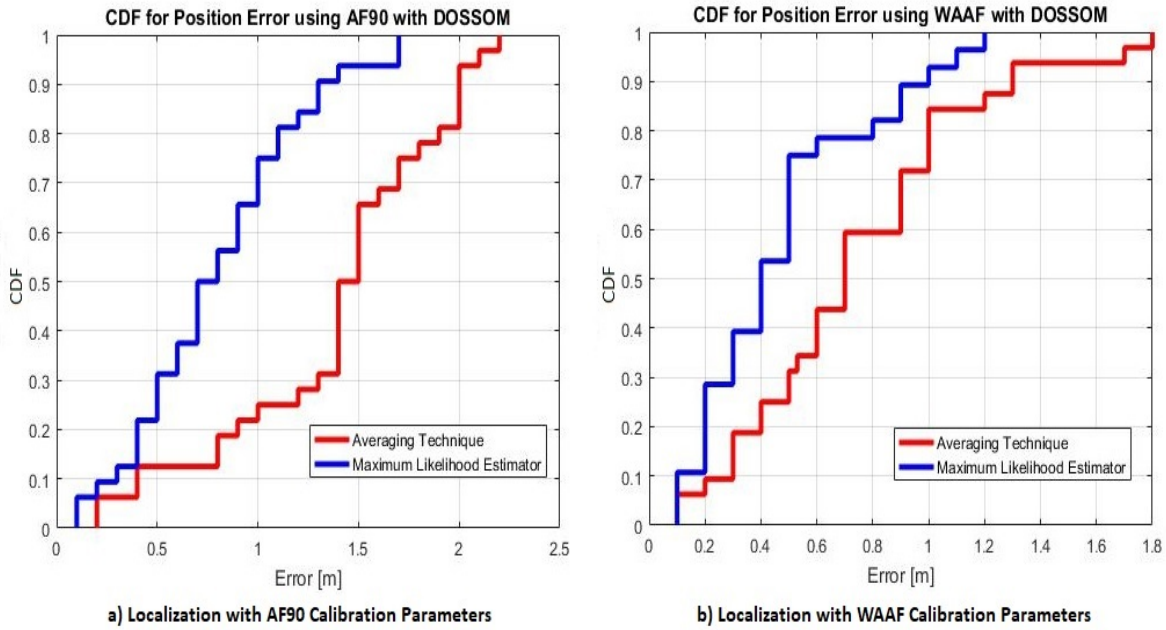

Figure 4.14 CDFs for the positions errors with the average and MLE using DOSSOM

Based on Figure 4.14 (a), it can be noticed that the positions errors', achieved at 90% CDF, are 2 and 1.3 meters with the averaging technique and MLE respectively. Hence, the localization system based on MLE increases the location accuracy for 35 percent while using the calibration parameters of the central track AF90 with DOSSOM.

However, the location accuracy, achieved at 90% CDF, while performing the WAAF calibration parameters is equal to 1.25 meters and 90 centimeters with the average technique and MLE (Figure 4.14 (b)). Thus, the efficiency of the MLE with the WAAF is well demonstrated and validated for indoor localization purposes. MLE and WAAF procedures increase the location accuracy by 28 percent.

Overall, the suggested indoor localization architecture improves the position accuracy by up to 60 percent hence reducing the position error from 2.2 meters to 90 centimeters.

4.9 Summary

The main challenge of the proposed localization system is to mitigate locations error. The MLE is introduced as a combining technique in order to improve the calibration phase's reliability and the localization phase's accuracy. It is applied to combine the RSS samples collected at each position in both offline and online stages. It improves the received signals' stability compared to the typical method, i.e. averaging.

Moreover, two new empirical indoor localization models were proposed. They were compared with those found in the literature, using real measurements in a classroom environment of 63.75 square meters. Experimental results confirm that two propagation models DOSM and DOSSOM present an improvement in estimated distances and positions error.

In addition, the presented WAAF propagation channel modeling shows closest agreement of the predicted path loss in the indoor environment. This approach gives a reliable calibration that considers all multipath parameters.

Concerning the proposed system's accuracy, it was validated during the positioning phase, by applying the proposed propagation models (DOSM or DOSSOM) followed by the multilateration technique and using four active RFID tags only.

Quantitatively, the location error of the suggested system is 90 centimeters, with a cumulative density function at 90%, while deploying 0.062 RFID tags per square meters only. This accuracy will be optimized more, by introducing the constellation approach in the following chapter.

Bibliography

[1] K. Kaemarungsi and P. Krishnamurthy, “Analysis of WLAN’s received signal strength indication for indoor location fingerprinting,” Pervasive and Mobile Computing. vol. 8, no. 2, pp. 292-316, 2012.

[2] S. R. Saunders, “Antennas and Propagation for Wireless Communication Systems,” John Wiley & Sons Ltd, England, 1999.

[3] M. Lott and I. Forkel, “A multi-wall-and-floor model for indoor radio propagation,” in Proc. IEEE 53rd Vehicular Technology Conference (VTC), vol. 1, pp. 464–468, 2001.

[4] A. Zyoud, J. Chebil, M. H. Habaebi, M. R. Islam, and A. K. Lwas, “Investigation of Three Dimensional Empirical Indoor Path Loss Models for Femtocell Networks,” in Proc. IOP Conference Series: Materials Science and Engineering, Bandung, Indonesia, p. 012021, 2013.

[5] A. A. M. Saleh and R. Valenzuela, “A statistical model for indoor multipath propagation,” IEEE Journal on selected areas in communications, vol. 5, no. 2, pp. 128-137, 1987.

[6] COST (European Co-operation in the Field of Scientific and Technical Research), “COST 231 Book,” Final Report. Chapter 4, Propagation Prediction Models, 1999.

[7] IST-4-027756, “WINNER II D1.1.2 V1.2”, WINNER II Channel Models, Part I Channel Models, 2008.

[8] Report ITU-R M.2135-1, “Guidelines for evaluation of radio interface technologies for IMT-Advanced,” 2009.

[9] Ela Innovation, SA. (2014) Ela Innovation active RFID tag and reader manufacturer. Available online: https://elainnovation.com/ (accessed on April 2021).

[10] J. C. Duan, G. Gauthier, and J.-G. Simonato, “On the Equivalence of the KMV and Maximum Likelihood Methods for Structural Credit Risk Models,” Working paper, Rotman School of Management, University of Toronto, 2005.

[11] Z. Li, R. Wang, K. Chen, M. Utiyama, E. Sumita, Z. Zhang and H. Zhao, “Data-dependent gaussian prior objective for language generation.” in Proc. of International Conference on Learning Representations, New Orleans, LA, USA, 2019.

[12] E. Aboutanios, “Estimating the parameters of sinusoids and decaying sinusoids in noise.” IEEE Instrumentation & Measurement Magazine, vol. 14, no. 2, pp. 8-14, 2011.

[13] Z. Abbasi, A. Farahi, and H.H.S. Javadi, “An Improvement in Maximum Likelihood Location Estimation Algorithm in Sensor Network,” International Journal of Computer Science & Engineering Survey (IJCSES), vol. 2, no.1, 2011.

[14] D. Xu, J. Zhang, X. Gao, P. Zhang, and Y. Wu, “Indoor Office Propagation Measurements and Path Loss Models at 5.25 GHz,” in Proc. IEEE 66th Vehicular Technology Conference, Baltimore, Maryland, USA, pp. 844–848,. 2007.

[15] M. Kaczmarek, J. Ruminski, and A. Bujnowski, “Accuracy analysis of the RSSI BLE Sensor Tag signal for indoor localization purposes,” in Proc. IEEE Federated Conference on Computer Science and Information Systems (FedCSIS), pp. 1413-1416, Gdańsk, Poland, 2016

[16] S. F. Wong and X. Ni, “Signal Propagation Model Calibration under Metal Noise Factor for Indoor Localization by Using RFID,” in Proc. IEEE International Conference on

Industrial Engineering and Engineering Management (IEEM), Selangor Darul Ehsan, Malaysia, pp. 978-982, 2014.

[17] J. Pelant, Z. Tlamsa, V. Benes, L. Polak, O. Kaller, L. Bolecek, and T. Kratochvil, "BLE device indoor localization based on RSS fingerprinting mapped by propagation modes," In Proc. 2017 27th International Conference Radioelektronika (RADIOELEKTRONIKA), IEEE, Brno, Czech Republic, 2017, pp. 1-5.

[18] M. Martínez del Horno, I. García-Varea, and L. Orozco Barbosa, "Calibration of Wi-Fi-based indoor tracking systems for Android-based smartphones," Remote Sensing, 2019, vol. 11, no. 9, p. 1072.

[19] M. D. Redžić, C. Brennan, and N. E. O'Connor, "SEAMLOC: Seamless indoor localization based on reduced number of calibration points," IEEE Transactions on Mobile Computing, 2013, vol. 13, no. 6, pp. 1326-1337.

[20] S. Li, Z. Deng, Y. Liu, and E. Hu, "A Novel Simultaneous Calibration and Localization Algorithm Framework for Indoor Scenarios," IEEE Access, 2020, vol. 8, pp. 180100-180112.

[21] N. Bnilam, G. Ergeerts, D. Subotic, J. Steckel, and M. Weyn, "Adaptive probabilistic model using angle of arrival estimation for IoT indoor localization," in Proc. of IEEE International Conference on Indoor Positioning and Indoor Navigation (IPIN), Sapporo, Japan, 2017, pp. 1-7.

[22] M. A. H. Ansari, and C. L. Law, "Beamforming UWB-IR transmitter for NLOS indoor positioning and tracking application," in Proc. of IEEE MTT-S International Wireless Symposium (IWS), Chengdu, China, 2018. pp. 1-4.

Chapter 5 The Constellation of Tags

5.1 Introduction

As discussed in chapter 4, section 4.2, the RSS variability is an essential parameter in indoor localization. This stability could be achieved through signals diversity [1]. The multiple antennas technology was proven to be efficient by improving the spectral efficiency over conventional single antenna systems [2], [3]. The capacity limits of the multiple antennas technology were extensively studied in various practical scattering propagation environments [4]-[6]. Besides, the spatial diversity of the emitted signals is well performed by the Multiple-Input Single-Output (MISO) architecture. These systems introduced many techniques to reduce the effect of multipath fading [5], [6]. In addition, the classical approaches consist of using multiple receiving antennas and performing combining or selection and switching techniques to improve the quality of the received signals. Based on this idea, the concept of using multiple antennas for localization is very challenging. Therefore, our proposed approach is focused on using a group of tags that operate together at the same frequency in our reader-based localization system. We named this configuration: a constellation of tags.

Moreover, several techniques can be used to exploit the antennas signals' diversity [7], [8]. In our work, the MLE is suggested to combine the received signals strength and assess the location accuracy.

This chapter is organized into four sections; section 5.2 presents the constellation approach with different radii, shapes, and number of RFID tags. In section 5.3, the error of distances estimated with the optimal constellation are compared to those obtained with a single tag in two scenarios: real and simulated environments. Then, localization by the proposed system is assessed and analyzed with both the optimal constellation and the single tag configurations, and through the two different RSS combining techniques i.e. averaging and the Maximum Likelihood Estimator, in section 5.4. Finally, the last section focuses on conclusions based on obtained results.

5.2 Constellation of UHF-RFID Tags

We introduce the concept of constellation of RFID tags in indoor localization, aiming to minimize the location uncertainty. As already mentioned in the introduction, the constellation is a set of tags that are close to each other and operating at the same frequency.

Preliminarily, a MISO-based ILS is introduced in this section. Then, the constellation approach is proposed along with its different radii, shapes, and number of tags. By applying the One Slope propagation Model (OSM), mean estimated distance errors of the different constellations are analyzed and compared to each other to reach the optimal constellation of RFID tags.

5.2.1 MISO-Based Indoor Localization System

The MISO architecture is one of the several forms of smart antenna technologies with only one receiving antenna. Performance of wireless communication systems can be improved by adopting multiple antennas at the transmitting side [3]. Few papers present works using MISO for localization purposes [9]. Most traditional researches are focused on the channel capacity [10].

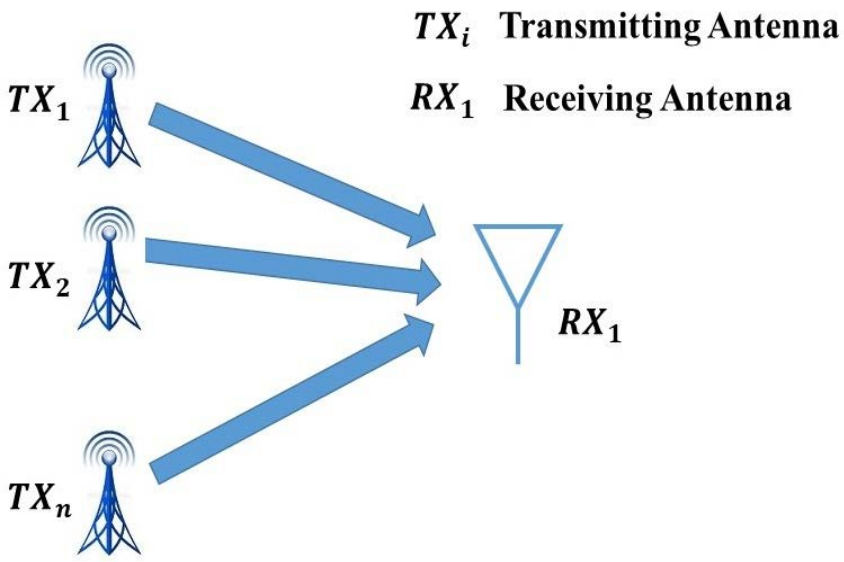

Figure 5.1 MISO Communication System

Notwithstanding these previous studies, [11] proposes a comparative study of RSSI-based localization algorithms for Wireless Sensor Networks (WSNs) indoors using spatial diversity. They show that the Single Input Multiple Output (SIMO) and MISO systems present similar performances. Obtained results indicate that the usage of a multiple antennas system significantly improves the localization accuracy to 87 centimeters in an indoor environment of 400 square meters. Additionally, [12] proposes an ILS based on a single-frequency continuous-wave Doppler radar sensor. It was implemented under the form of SIMO architecture with redundant receiving channels. The method was validated by simulations. Two different trajectories were recovered in a simulated environment scenario of 0.8 x 0.8 square meters.

Accuracy errors, between the estimated and the actual trajectories, were 11.4 and 14.1 centimeters respectively. Despite good performance, [11] implemented the WSN in a homogenous indoor environment and [12] validated their approach without any interference and by simulations only. In the following, we present a technique to improve the accuracy of our low-cost RFID localization system in a classroom environment. The complexity of this classroom is attributed to its geometry and to the materials that constitute this environment, as previously discussed in chapter 3, sub-section 3.4.1.

5.2.2 Constellation of Active UHF-RFID Tags for Reader Localization

As previously mentioned in chapter 2, section 2.4, the RFID reader-based localization system includes tags used as anchor or beacons and a reader to locate. The suggested constellation of tags can have different shapes and may include a variable number of tags. For instance, Figure 5.2 presents the constellation of four active RFID tags for reader localization. First, our work was focused on investigating the optimal constellation's radius and shape as well as on the optimal number of tags constituting it. As multiple transmitting antennas can reduce multipath by benefiting from signals' diversity, different experiments with the constellation of RFID tags will be analyzed, in the following subsections, in order to increase the location accuracy.

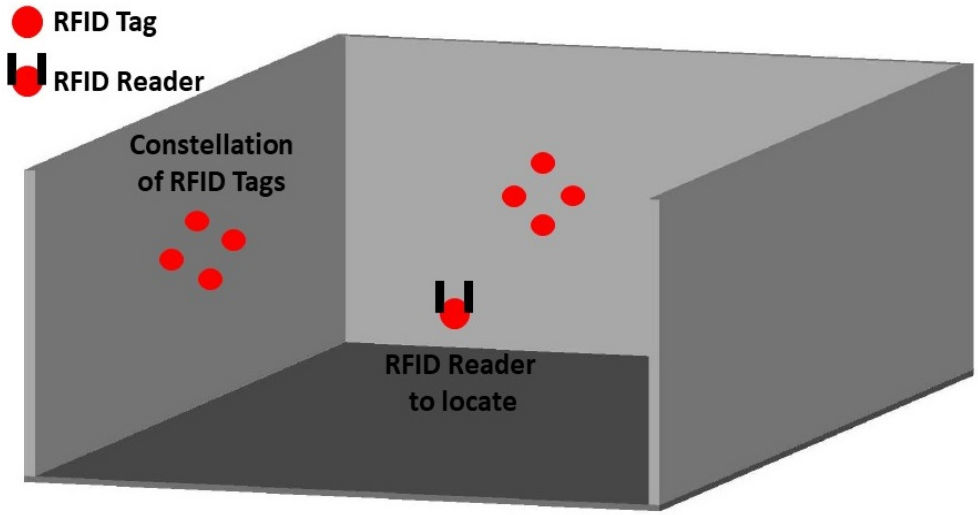

Figure 5.2 Constellation of four RFID tags

5.2.3 Optimal Constellation's Radius

In this subsection, different radii of the constellation are empirically examined over track A90. The experiment was conducted in the classroom at EFREI-Paris spaced of 63.75 square meters, where Figure 5.3 shows the layout of the scenario.

The center of the constellation was on the center of the front wall. The RFID reader was moving forward with a step equal to 50 centimeters to collect the RSS at each reference position as presented in Figure 5.3.

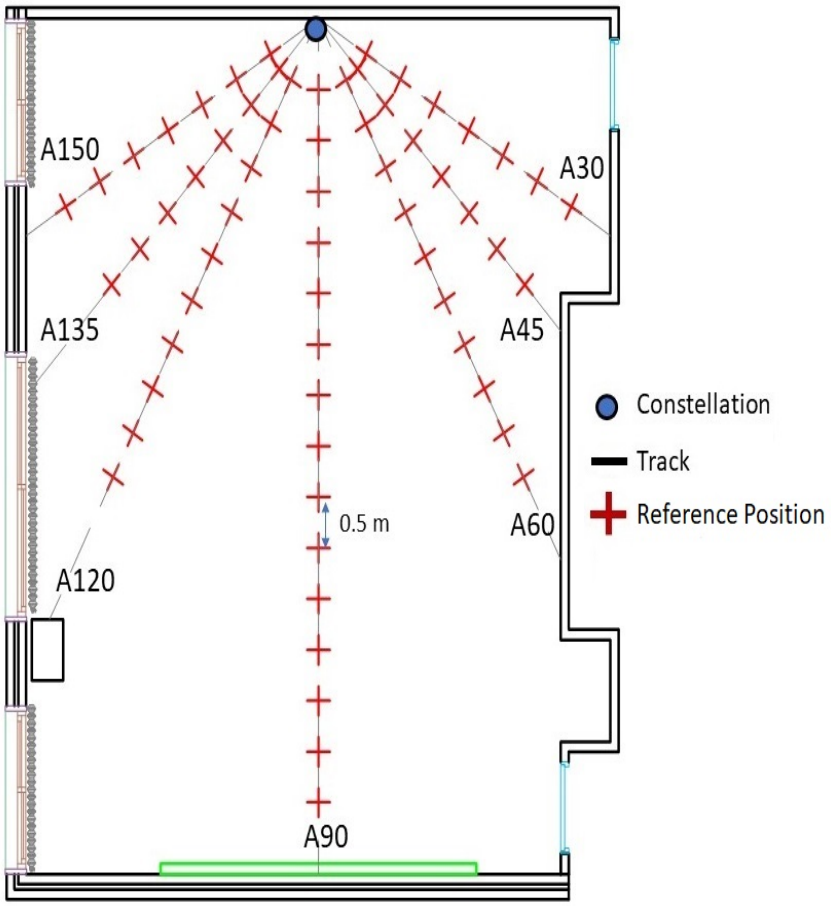

Figure 5.3 Two-dimensional layout of the classroom environment

Signals emitted by the group of tags and captured by the reader antenna were combined by the averaging technique. Furthermore, to determine the optimal radius of the constellation of RFID tags, the estimated tag-reader distances errors' were analyzed for different radii starting from $\lambda/8$ up to $7\lambda/4$ (Figure 5.4). $7\lambda/4$ is the maximum reached radius due to the classroom height. Constellations with radius $\lambda/8$ to λ were studied based on real measurements.

Whereas, constellations with radius 5λ/4, 3λ/2 and 7λ/4, respectively, were evaluated through different simulations due to some practical aspects that prevent real measurements.

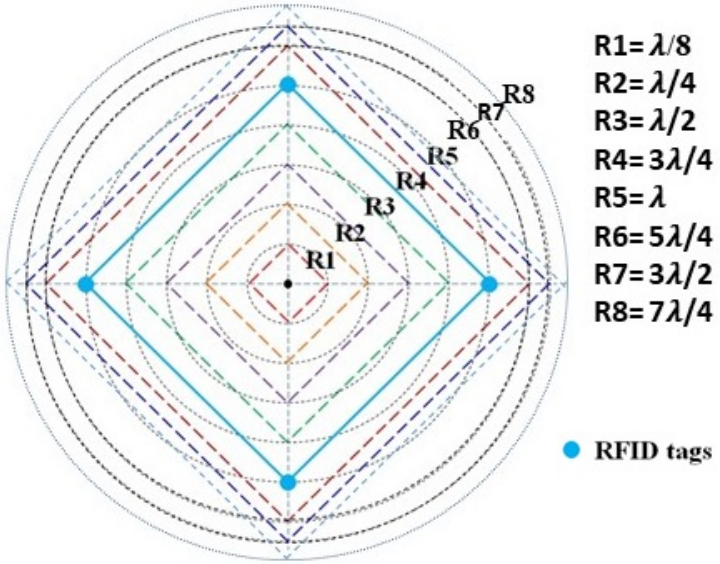

Figure 5.4 Different radii for the constellation of tags

Table 5.1 shows the mean estimated distance errors over the track A90 (Figure 5.3) for the different constellation radii.

Table 5.1 The mean estimated distance errors for different radii of constellations with OSM

Constellation's Radius R [cm]		**λ/8 8.75**	**λ/4 17.5**	**λ/2 35**	**3λ/4 52.5**	**λ 70**	**5λ/4 87.5**	**3λ/2 105**	**7λ/4 122.5**
Track A90	**Mean Distance Error [m]**	2.24	2.09	2.31	2.05	1.94	1.98	2.13	2.2
	Standard deviation	1.58	1.03	1.43	1.31	1.26	1.32	1.36	1.41

Looking on values of Table 5.1, it can be noticed that the mean estimated distance error, obtained over track A90, presents a maximum error for the radius equal to λ/8, which confirms the effect of coupling between tags' antennas. The minimal distance error is reached for the constellation with radius R equal to λ. Moreover, the standard deviation presents low variation with the radius equal to λ. Thus, a constellation of tags with radius λ will be used in the following tests.

5.2.4 Optimal Shape and Number of Tags

In order to determine the best constellation and after the selection of the optimal radius, it is also challenging to determine the best shape and the optimal number of tags that constitute the constellation. Several shapes, with a radius R equal to λ, are studied over the same track A90: a triangle constellation with three tags (Figure 5.5 (a)), diamond shape with four tags (Figure 5.5 (b)), square cross with five tags (Figure 5.5 (c)) and pentagon with five tags (Figure 5.5 (d)).

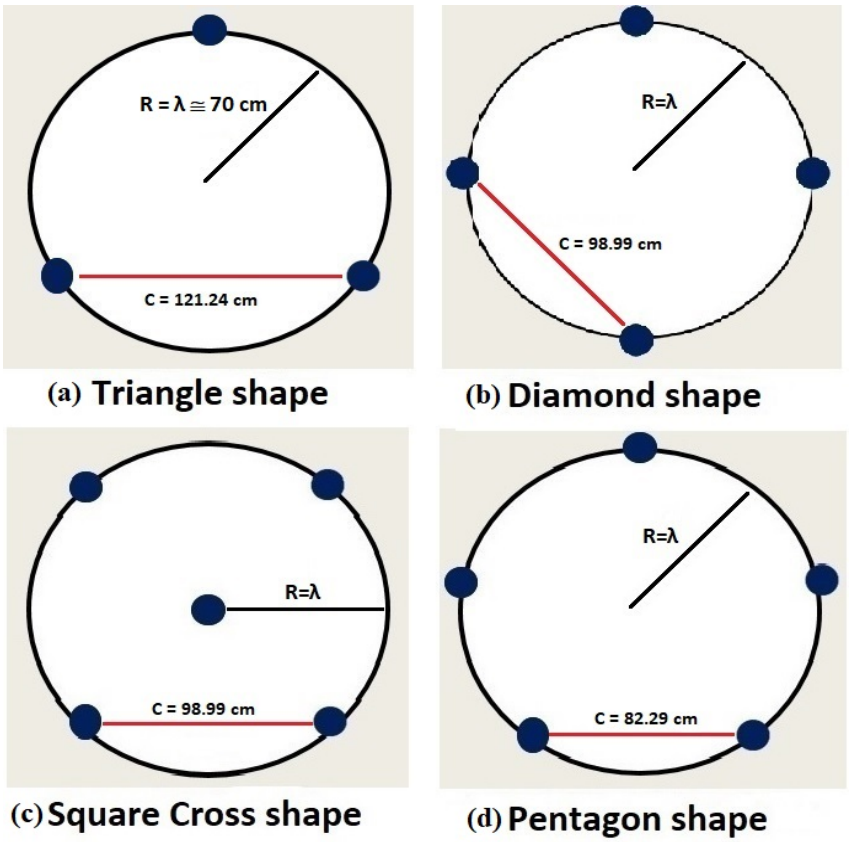

Figure 5.5 Constellation of tags with different shapes and different number of tags

The mean estimated distance errors over track A90 for the different shapes and different numbers of tags in the constellation are shown in Table 5.2.

Table 5.2 The mean estimated distance errors for different constellations with OSM

Constellation Tags' Number		**3 Tags**	**4 Tags**	**5 Tags**	**5 Tags (Penta)**
Track A90	**Mean Distance Error [m]**	2.04	1.94	1.92	1.95
	Standard deviation	1.07	1.26	1.05	1.31

It is worth mentioning that by increasing the number of RFID tags constituting the constellation, with a defined radius, the inter-tags distance "C" decreases and the coupling between tags antennas' increases (Figure 5.5).

In Table 5.2, it is apparent that there are fewer errors in the constellation with five tags where one of them is at the constellation center (Figure 5.5 (c)). However, adding an extra tag to the four-tag constellation, in order to improve the accuracy by just 2 cm, makes the choice of a four-tag constellation (diamond shape) cost effective.

5.3 Constellation versus Single Tag

In this section, performance of the optimal constellation of tags (diamond shape with a radius equal to λ) is compared to those obtained with a single tag under the same conditions.

To validate the constellation approach while avoiding the long durations needed for on-site measurements, a reliable modelling of the classroom environment can be a suitable alternative, as shown in Figure 5.6 .

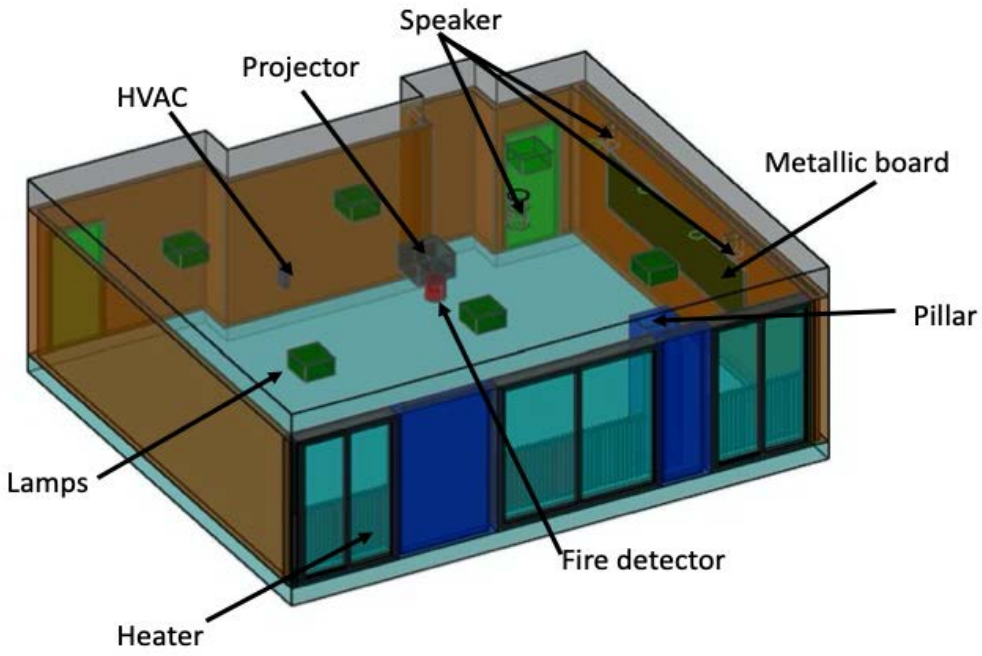

Figure 5.6 Three-dimensional layout of the classroom

It is worth recalling that the experimental and the simulated results already presented in chapter 3 had a similar behavior, with maximum deviation of 0.5 dB. Hence, the behavior of the constellation of tags will be studied in-depth, via the simulated model, over the tracks

A60, A90 and A120 (Figure 5.3) in the subsection 5.3.1.1. As already mentioned in chapter 4, subsection 4.5.3, these three tracks are chosen as they have enough number of positions that may better reflect signals propagation.

5.3.1 (Tags-Reader) Distances Estimation

To evaluate the optimal constellation of tags features in localization, a first comparison with the single tag configuration in terms of estimated distances is essential. The single tag and, alternatively, the center of the constellation was placed at the center of the front wall as shown in Figure 5.3.

Received power values at the various positions were measured to characterize the signal behavior in terms of the tag-reader distance over the tracks A60, A90 and A120 (Figure 5.3).

Over each track, the estimated distances errors were analyzed first while a single tag is used, then with the optimal constellation of tags, and finally for each tag of the optimal constellation independently to see the behavior of each one. Actually, it is important to present behaviors separately in order to show that each tag's signal takes a different path to reach the reader due to multipath in the classroom. Moreover, comparison is realized on distance errors, obtained by the single tag and constellation, following the block diagram illustrated in Figure 5.7.

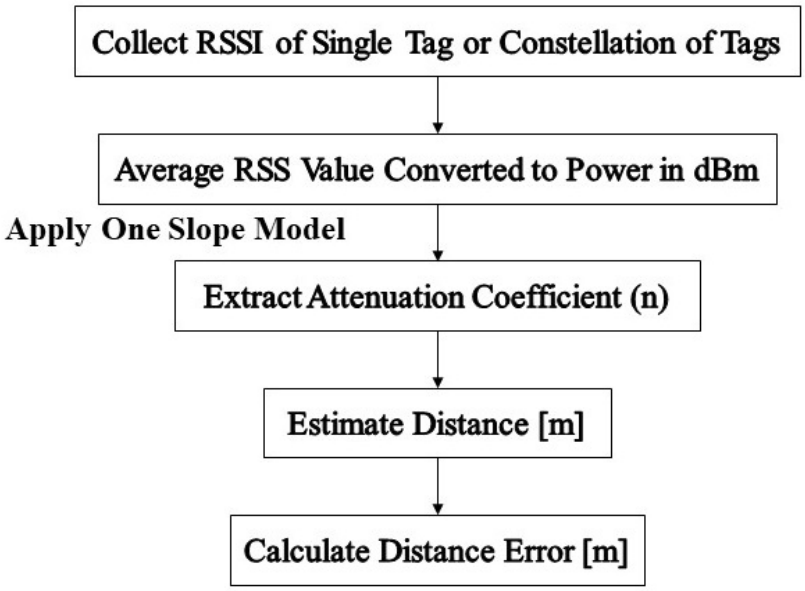

Figure 5.7 Steps for the estimated distance error calculation

5.3.1.1 Measurements Accuracy

Based on real power measurements, estimated distances errors for the single tag and the constellation of tags scenarios are evaluated. Table 5.3 shows MDEs based on real power values collected by the RFID reader.

Table 5.3 Mean estimated distance errors based on real measurements

		Single Tag	**Constellation of Tags**
Track A60	**Mean Distance Error [m]**	0.99	0.82
	Standard deviation	0.59	0.49
Track A90	**Mean Distance Error [m]**	2.45	1.98
	Standard deviation	1.64	1.26
Track A120	**Mean Distance Error [m]**	2.18	0.73
	Standard deviation	1.12	0.46

Based on the MDEs presented in Table 5.3, it can be noticed that the constellation of four tags architecture presents less errors compared to that with a single tag. For instance, the constellation of tags reduces distances errors by 17 centimeters over the track A60, 42 centimeters over A90 and 45 centimeters over A120.

Moreover, the constellation of tags also presents more stability as the standard deviation is smaller than that for the single tag configuration. Thus, the concept of using multiple transmitting antennas, to reduce the effect of multipath fading on distances estimation, is well validated.

Furthermore, Figure 5.8 (a), Figure 5.9 (a) and Figure 5.10 (a) present the estimated distances errors' distribution over the three tracks A60, A90 and A120 for the single tag scenario. Those obtained by the optimal constellation of tags and by each tag of the optimal constellation independently are shown in Figure 5.8 (b), Figure 5.9 (b) and Figure 5.10 (b).

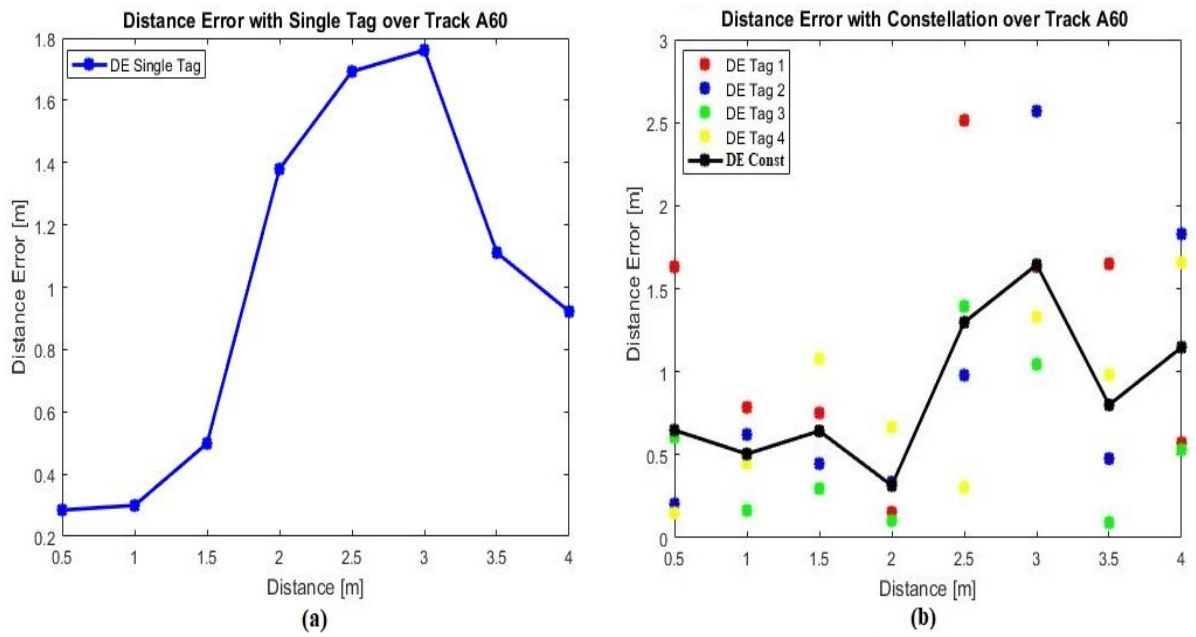

Figure 5.8 Distance errors for single tag and constellation of tags scenarios over track A60

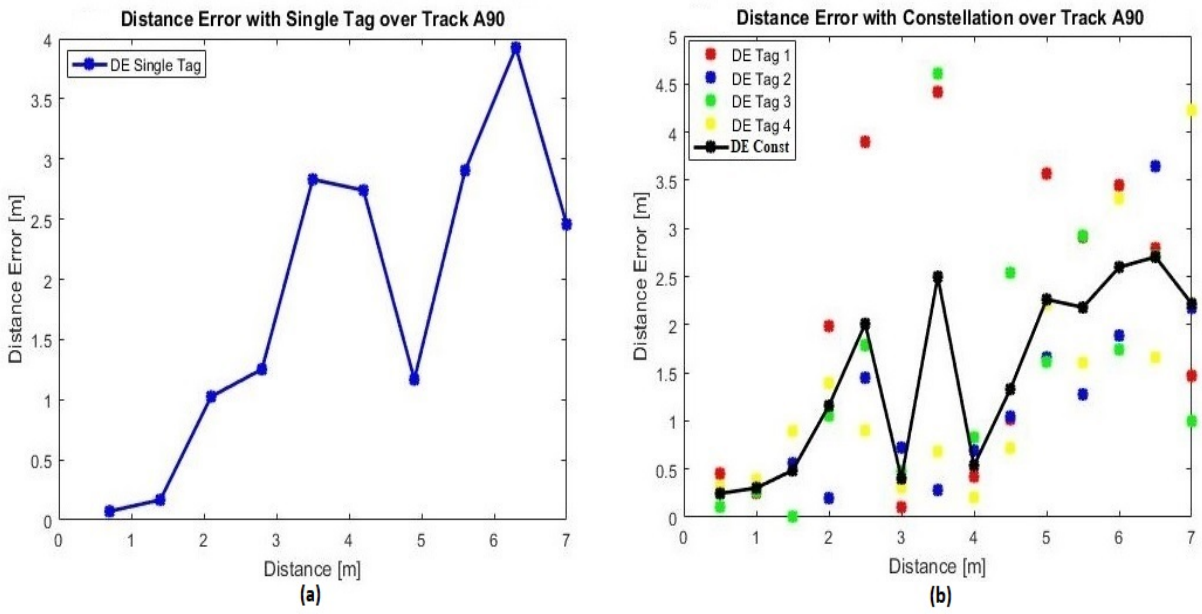

Figure 5.9 Distance errors for single tag and constellation of tags scenarios over track A90

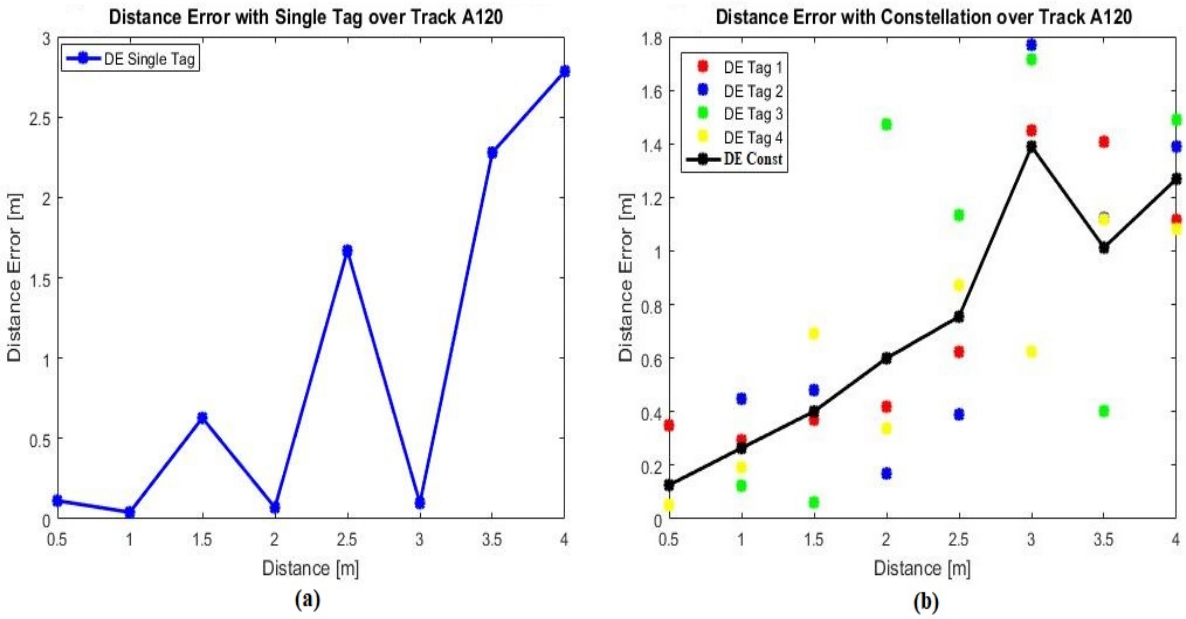

Figure 5.10 Distance errors for single tag and constellation of tags scenarios over track A120

Scales of Figure 5.8 and Figure 5.10 are not uniform with that of Figure 5.9 because, according to Figure 5.3, RSS observations are collected every 50 centimeters to reach 4 meters over tracks A60, A120, and 7 meters over track A90.

Back to the subsection 5.2.1, MISO systems achieve a better performance in terms of reliability through signals diversity [9]. Referring to Figure 5.8 (b), Figure 5.9 (b) and Figure 5.10 (b), the estimated distance error, at each position, differs from one tag to another. Thus, the transmitted signals take different paths to reach the reader due to many effects such as the multipath fading. It is worth mentioning that the constellation of tags assessment versus the single tag is studied via averaging technique. It can be noticed that combining multiple signals emitted by a group of tags performs better than a signal tag.

5.3.1.2 Simulations

Following the simulated setup presented in chapter 3, section 3.4, the whole experiment done in the real environment are reproduced over WinProp (Figure 5.11).

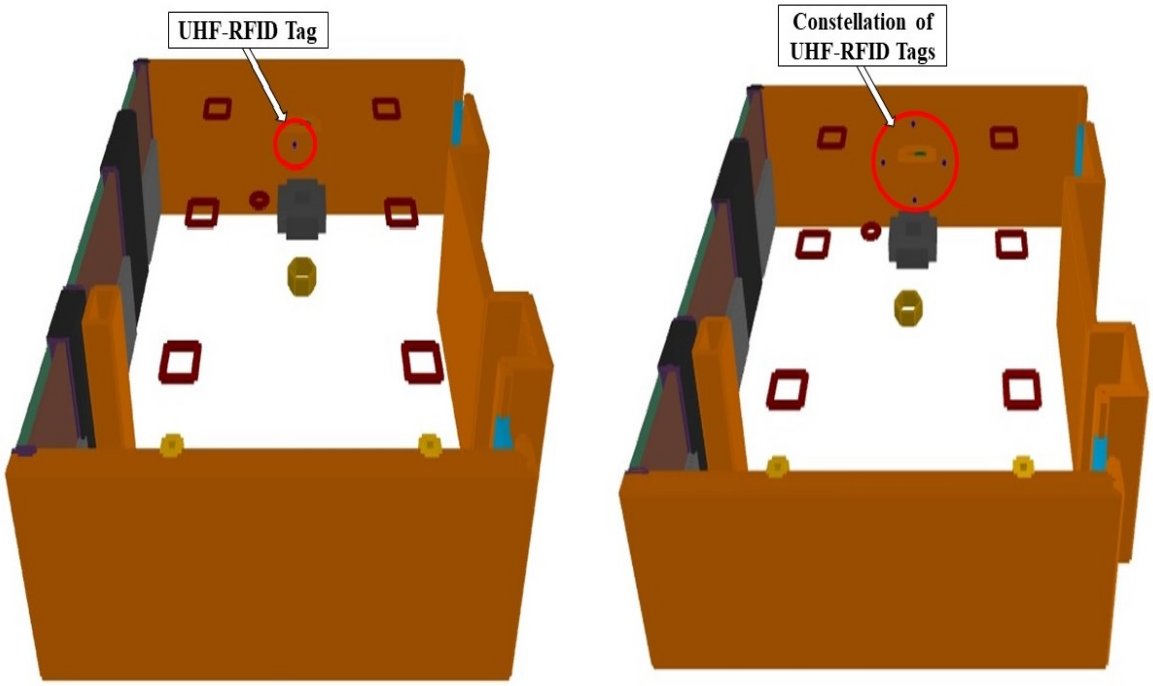

Figure 5.11 single tag and constellation of tags simulated scenarios

Restate that the single tag and alternatively, the center of the constellation was placed on the center of the front wall, as shown in Figure 5.3.

Also, the received power values are collected each 50 centimeters by moving the configured RFID reader forward over the corresponding tracks (Figure 5.3).

Table 5.4 illustrates the MDEs with the single tag and with the constellation of tags configurations.

Table 5.4 The mean estimated distance errors by simulation

		Single Tag	**Constellation of Tags**
Track A60	**Mean Distance Error [m]**	1.02	0.81
	Standard deviation	0.59	0.45
Track A90	**Mean Distance Error [m]**	2.41	1.93
	Standard deviation	1.62	1.21
Track A120	**Mean Distance Error [m]**	1.19	0.71
	Standard deviation	1.04	0.49

According to the MDE values presented in Table 5.4, the constellation performs better than single tags thanks to signals diversity. For instance, within simulations, the constellation of tags decreases the distances errors to 21 centimeters over the track A60, 48 centimeters over A90 and 42 centimeters over A120. In addition, the constellation of tags presents more stability due to the receiving signals' diversity created by the group of RFID tags. In fact, the obtained standard deviation is smaller than that for the single tag system in the indoor environment.

Furthermore, referring to Table 5.3 and Table 5.4, it can be noticed that measurements and simulations present very closed results. More precisely, these tables show that the maximum difference in MDEs obtained between measurements and simulations is only 4 centimeters over A60, and 1 centimeter over tracks A90 and A120 in the single tag scenario. Similarly, this difference reaches only 1 centimeter over A60, 5 centimeters over A90 and 2 centimeters over A120 in the constellation of tags scenario.

5.4 Localization Assessment

This subsection aims to assess the localization performance of the proposed system, comparing it to the conventional system under different aspects. Experiment was performed in the unfurnished classroom environment that has been presented in chapter 3, section 3.2.

Restate also, as described in chapter 2, section 2.4, the signal propagation within the offline stage is characterized over seven paths A30 to A150, using one RFID tag placed on the center of the front wall, as shown in Figure 5.3. Two hundred RSS values were collected every 50 centimeters over the seven trajectories.

First, the RSS samples are combined via the averaging technique. Then, MLE is applied in order to increase the location accuracy and improve the system's reliability. The propagation models DOSM or DOSSOM, with WAAF already introduced in chapter 4, were applied over each track to determine reliable attenuation coefficients, corresponding to the classroom environment.

Within the online stage, the localization phase is performed in a way similar to the process described in chapter 4, section 4.8. Position errors are estimated at thirty-two different positions. Only twenty-four locations are uniformly distributed in the space with a distance of 70 centimeters over the three paths A60, A90 and A120, as illustrated in Figure 4.12. Eight other positions are chosen randomly to evaluate the localization accuracy.

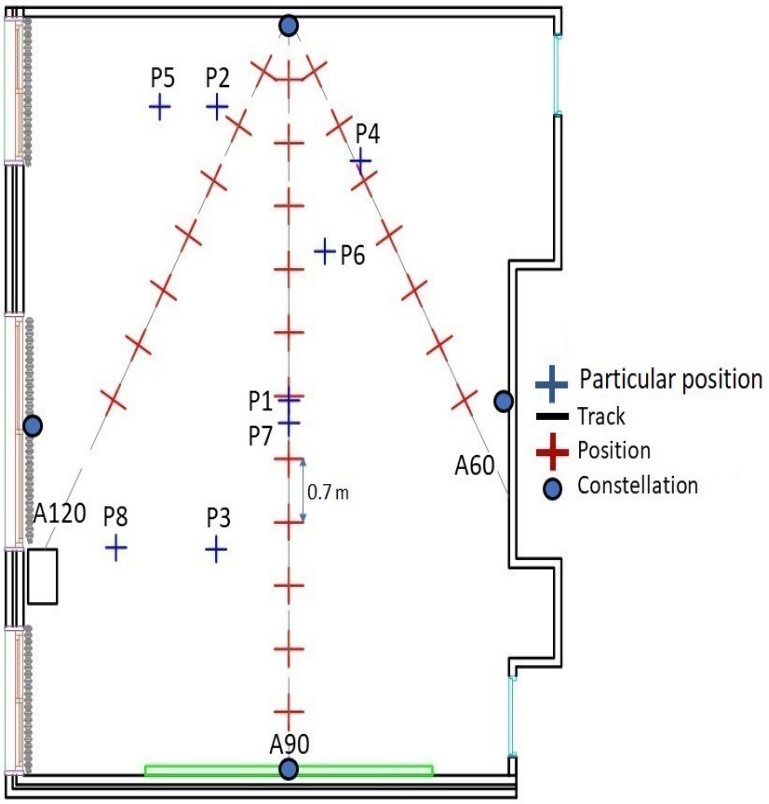

Figure 5.12 Two-dimensional layout of the classroom environment (online stage with constellation)

The localization based on a single tag is performed with four independent RFID tags (Figure 5.13). Each one is fixed on the center of each wall, as shown in Figure 5.12.

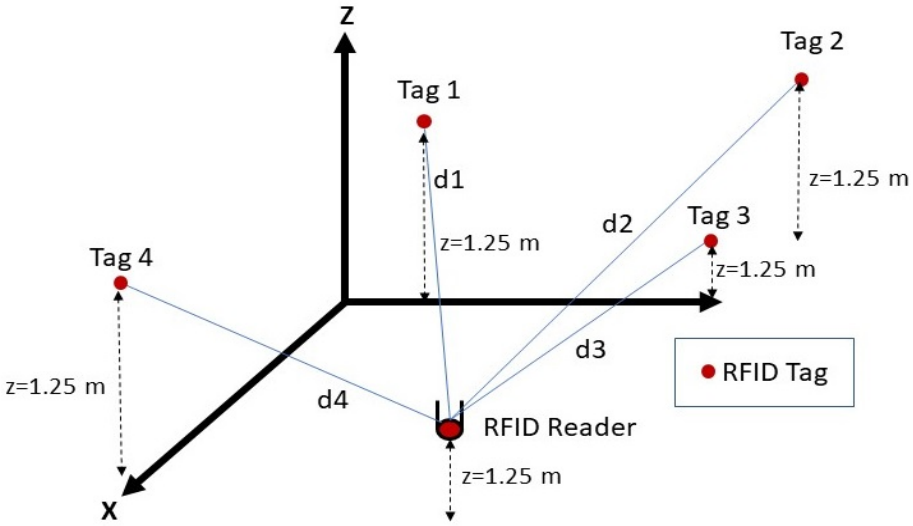

Figure 5.13 Multilateration with the single tags' scenario

Whereas the localization based on the constellation of tags was carried out with four constellations of four RFID tags each (Figure 5.14). The center of each constellation is situated on the center of each wall.

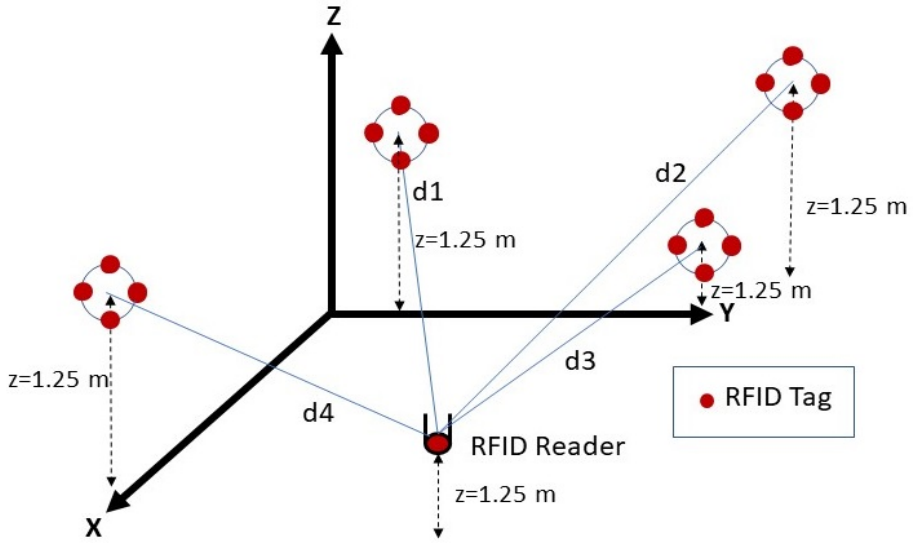

Figure 5.14 Multilateration with the constellation of tags scenario

In this stage, twenty RSS samples are collected at each position.

Then, by applying the multilateration technique, and following the proposed DOSM and DOSSOM indoor propagation models associated with the Weighted Average Attenuation Factors (WAAF), that cover the whole classroom environment, errors were estimated at the thirty-two different positions illustrated in Figure 5.12.

5.4.1 Localization Assessment based on Constellations

In this subsection, location accuracy is analyzed while RSS samples are combined by averaging.

After performing the WAAF calibration procedure that was introduced in the previous chapter, positions errors with the constellation of tags are analyzed and compared with those obtained using single tags. Figure 5.15 presents the Cumulative Density Functions (CDF) of the positions errors' while applying the Dual One Slope propagation Model (DOSM) associated with the WAAF calibration approach.

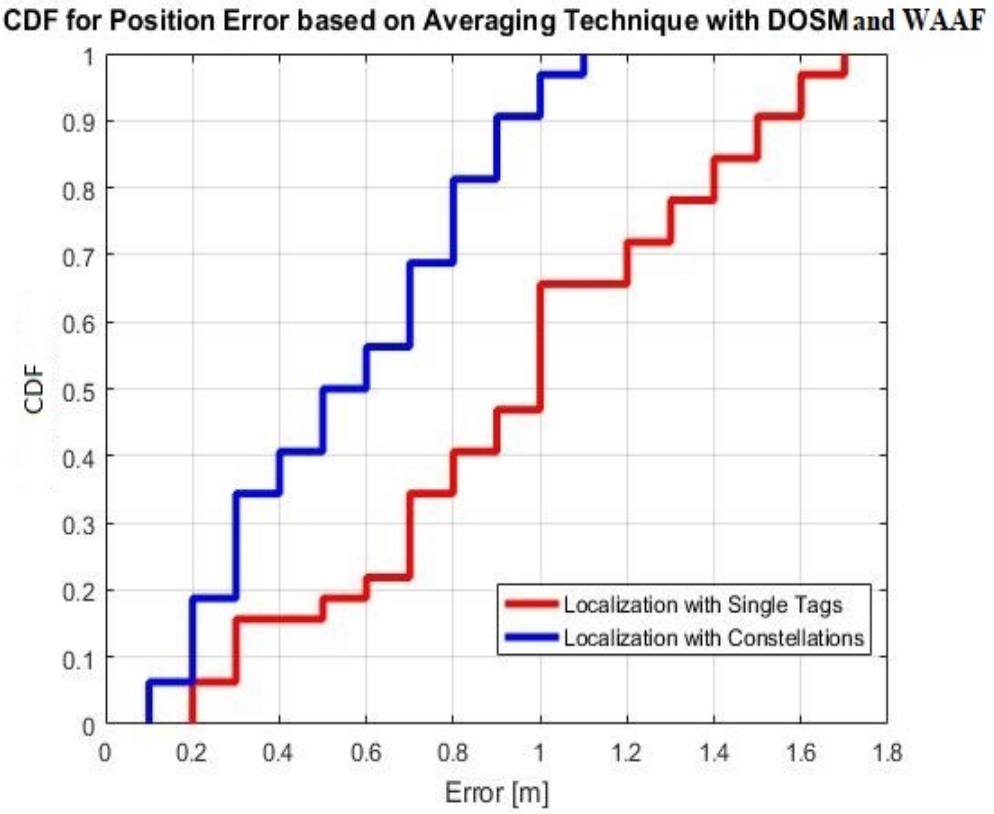

Figure 5.15 CDF for positions errors by RSS Averaging using DOSM and WAAF

According to the CDF illustrated in Figure 5.15, positions errors' achieved, at 90% CDF and applying DOSM associated with WAAF, are 1.5 meters and 90 centimeters with the single tag and the constellation of tags, respectively. In short, the location accuracy is improved by 40 percent while performing the constellation of tags with DOSM and WAAF.

As a following step, the location accuracy was studied with the Dual One Slope with Second-Order Polynomial propagation Model (DOSSOM). Figure 5.16 presents CDF of positions errors' by applying DOSSOM with WAAF.

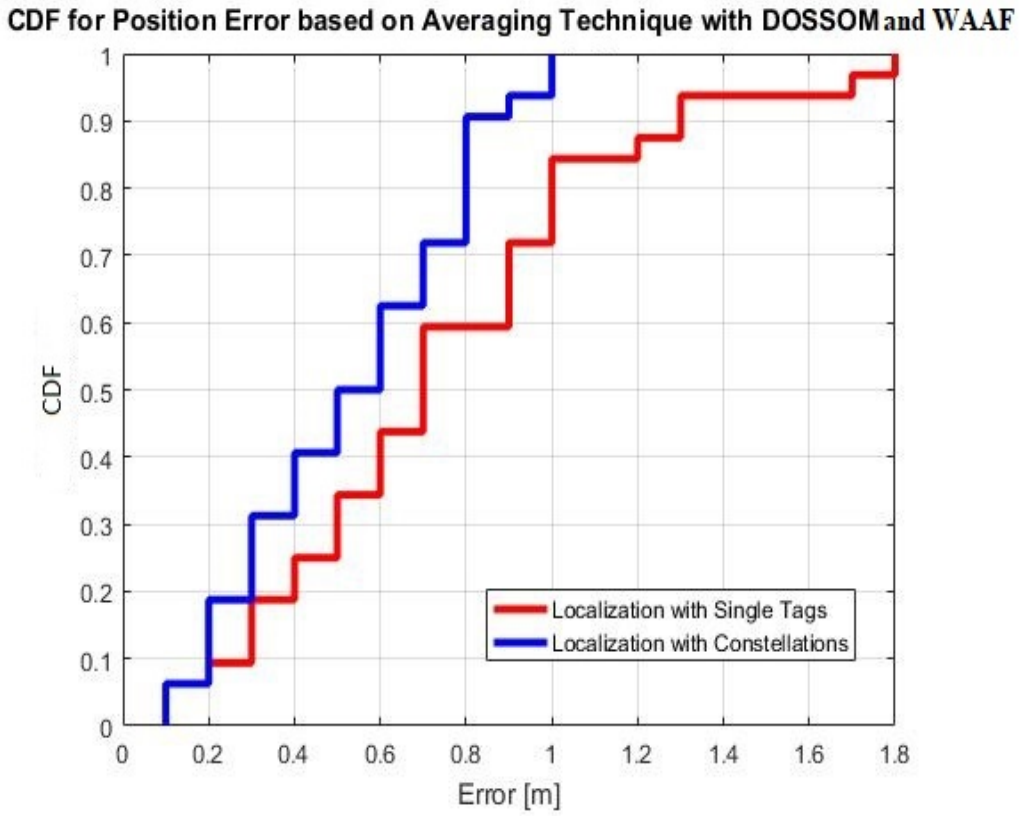

Figure 5.16 CDF for positions errors via RSS Averaging using DOSSOM and WAAF

As shown in Figure 5.16, positions errors' achieved, at 90% CDF while using DOSSOM associated with WAAF, are 1.3 meters and 80 centimeters with the single tag and the constellation of tags, respectively. Thus, the use of the constellation of tags with DOSSOM and WAAF increases the location accuracy by 38.4 percent.

Considering the gathered results, localization based on the constellation approach, while combining RSS samples by averaging, improves location accuracy by 46.7 percent as compared to that obtained with the single tags architecture. Thus, the efficiency of using the constellations of tags for localization purposes in an indoor environment is well proved.

5.4.2 Localization Assessment based on Constellations and RSS Combined by MLE

As already demonstrated in chapter 4, the proposed ILS presents an improvement in the location accuracy while using the MLE as RSSs combining technique in the single tag scenario. Assessment presented in 4.8.2, multilateration along with DOSM, and DOSSOM with WAAF indoor propagation models, are applied to estimate positions errors at the thirty-two different positions appearing in Figure 5.12.

Obtained results by performing the constellation approach are analyzed and compared to those results obtained in the single tag scenario.

Figure 5.17 presents the CDF of positions errors' while applying DOSM associated with WAAF in the classroom environment.

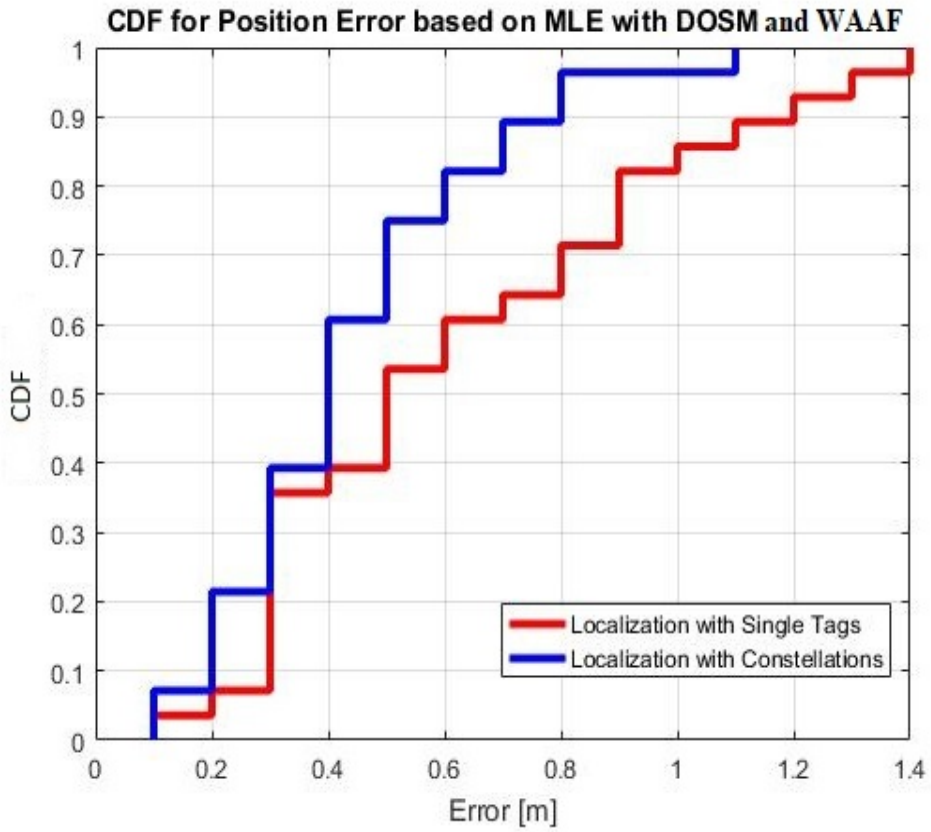

Figure 5.17 CDF for positions errors via MLE using DOSM and WAAF

According to the CDF illustrated in Figure 5.17, positions errors', achieved at 90% CDF and applying DOSM with WAAF, are 1.1 meters and 70 centimeters with the single tag and the constellation of tags, respectively. In short, the location accuracy is improved by 36.4 percent while performing the constellation of tags with DOSM and WAAF.

Finally, location accuracy was studied with the Dual One Slope with Second-Order Polynomial propagation Model (DOSSOM) and WAAF. Figure 5.18 presents the CDF of positions errors' using DOSSOM associated with WAAF.

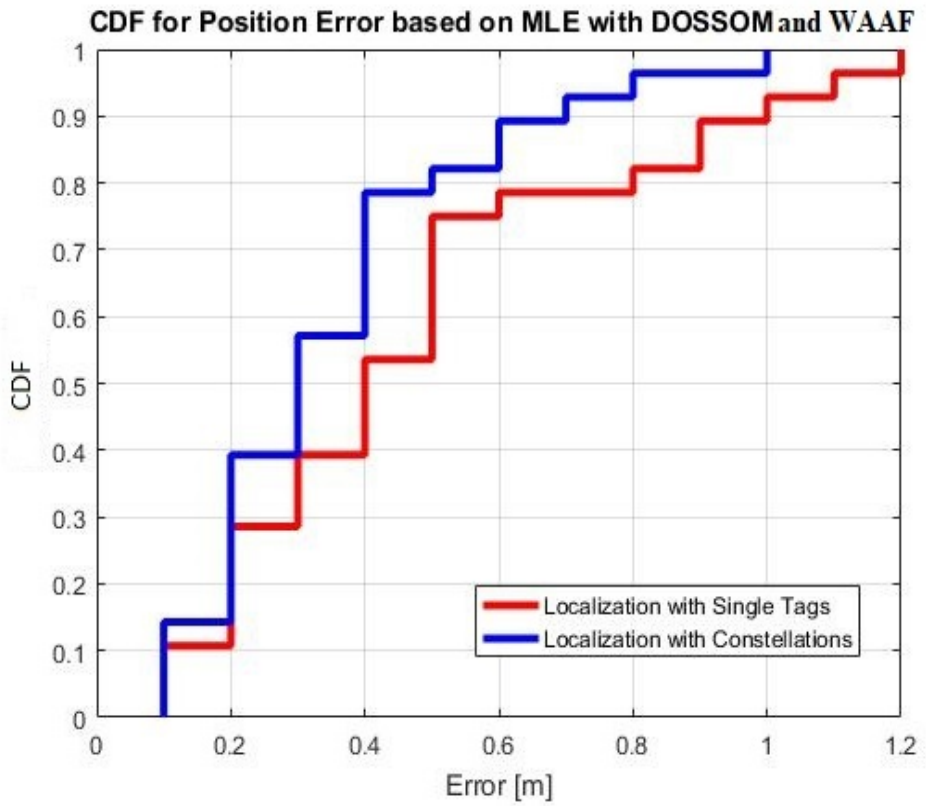

Figure 5.18 CDF for positions errors via MLE using DOSSOM and WAAF

As illustrated in Figure 5.18, positions errors', achieved at 90% CDF while using DOSSOM, are 90 and 60 centimeters with the single tag and the constellation of tags, respectively. Thus, the use of the constellation of tags with DOSSOM associated with WAAF increases location accuracy by 33.33 percent.

Recall that, in the single tag scenario, the proposed RFID based localization achieves optimal accuracy of 1.3 meters and 90 centimeters, while combining RSS samples by applying the averaging technique and the Maximum Likelihood Estimator, respectively. However, the constellation scenario's location accuracy reaches 80 and 60 centimeters, while using the averaging technique and the Maximum Likelihood Estimator, associated with WAAF respectively. Thus, the location accuracy is improved by 60 percent while performing the constellation of tags within the proposed system based on MLE and WAAF.

5.5 Summary

A new approach for a positioning system based on constellations of RFID tags is presented and studied in order to increase the localization accuracy. It consists in replacing the single tag by a group of tags and follows the same concept as that of MISO communication systems.

Various radii and different numbers of tags per constellation are studied in-depth. Moreover, mean estimated distance errors, using the average value of the power received by the RFID reader and emitted by the constellation, are widely elaborated. Based on measurements and simulations, the optimal constellation is constituted of four RFID tags and has a radius equal to the wavelength. In terms of the distance error, the constellation performance is compared to those obtained with the single tag scenario.

Besides, using the Weighted Average Attenuation Factor (WAAF) calibration procedure, a series of localization experiments are completed with both single tag and constellation of tags scenarios by applying the multilateration technique and following the OSM, DOSM, and DOSSOM indoor propagation models. RSSs are combined with two methods i.e. Averaging technique and the Maximum Likelihood Estimator. As a result, the optimal estimated positioning error achieved thanks to the constellation approach, the DOSSOM model and the Maximum Likelihood Estimator combining technique is around 60 centimeters, with the cumulative distribution function at 90% while deploying 0.25 RFID tags per square meter only.

Bibliography

[1] M. Dashti, H. Claussen, “A metric to describe access point significance in location estimation,” in Proc. IEEE 13th Workshop Positioning, Navigation and Communications (WPNC), Bremen, Germany, pp. 1–6, 2016.

[2] Y. Zhu Y, G. Zheng, L. Wang, K. K. Wong, and L. Zhao, “Content placement in cache-enabled sub-6 GHz and millimeter-wave multi-antenna dense small cell networks,” IEEE Transactions on Wireless Communications, vol. 17, no. 5, pp. 2843-2856, 2018.

[3] D. Bala, G. M. Waliullah, M. A. Hena, M. I. Abdullah, and M. A. Hossain, “Study the Performance of Capacity for SISO, SIMO, MISO and MIMO in Wireless Communication,” Journal of Network and Information Security, vol. 8, no. 1 & 2, pp. 1-6, 2020.

[4] O. L. López, H. Alves, R. D. Souza, and S. Montejo-Sánchez, “Statistical analysis of multiple antenna strategies for wireless energy transfer,” IEEE Transactions on Communications, vol. 67, no. 10, pp. 7245-7262, 2019.

[5] M. El-Absi, F. Zheng, A. Abuelhaija, A. H. Abbas, K. Solbach, and T. Kaiser, “Indoor Large-Scale MIMO-Based RSSI Localization with Low-Complexity RFID Infrastructure,” Sensors, vol. 20, no. 14, p. 3933, 2020.

[6] H. Tian, and L. Zhu, “MIMO CSI-based Super-resolution AoA Estimation for Wi-Fi Indoor Localization,” in Proc. IEEE 12th International Conference on Machine Learning and Computing, Shenzhen, China, pp. 457-461, 2020.

[7] H. H. Saleh, and S. T. Hasson, “Improving Communication Reliability in Vehicular Networks Using Diversity Techniques,” Journal of Computational and Theoretical Nanoscience, vol. 16, no. 3, pp. 838-844, 2019.

[8] N. Parveen, R. Islam, K. Abdullah, and R. I. Boby, “Performance of BER with Different Diversity Techniques for Millimeter-Wave Communication System,” Int. J. Innov. Technol. Explor. Eng., vol. 8, no. 6S4, pp. 1149-1152, 2019.

[9] L. Wei, C. Huang, G. C. Alexandropoulos, and C. Yuen, “Parallel Factor Decomposition Channel Estimation in RIS-Assisted Multi-User MISO Communication,” in Proc. IEEE 11th Sensor Array and Multichannel Signal Processing Workshop (SAM), Hangzhou, China, pp. 1-5, 2020.

[10] M. Wang, F. Gao, S. Jin, and H. Lin, “An overview of enhanced massive MIMO with array signal processing techniques,” IEEE Journal of Selected Topics in Signal Processing, vol. 13, no. 5, pp. 886-901, 2019.

[11] S. Hamdoun, A. Rachedi, A. Benslimane, “RSSI-based localization algorithms using spatial diversity in wireless sensor networks,” International Journal of Ad Hoc and Ubiquitous Computing, vol. 19, no. 3-4, pp. 157–167, 2015.

[12] A. Zhu, T. Fan, Z. Gu, Q. Lv, C. Li, and L. Ran, “Indoor localization based on a single-tone SIMO-structured Doppler radar system,” in Proc. IEEE Radio andWireless Symposium (RWS), San Diego, California, USA, pp. 15–18, 2018.

Global Evaluation of Performance and Deployment Density

The main aim of the thesis was to develop and implement an accurate and reliable ILS based on the active UHF-RFID technology. It shall also provide the high locations accuracy with a reduced number of RFID tags deployed.

The concept of our localization system is classified as a moving RFID reader and fixed active tags. It is divided into two stages: offline and online. The offline stage represents the environment calibration and the online one is properly the positioning phase.

Performance of most RFID based indoor localization systems depend mainly on the number of deployed RFID tags or readers and on advanced positioning algorithms. Our attention is drawn to the number of deployed RFID tags and the location accuracy achieved with active UHF RFID positioning systems already presented in chapter 2, section 2.2, as compared to our proposed system features.

Associated to the installed software, different indoor location methods such as LANDMARC, VIRE and others have been introduced [1]-[3]. LANDMARC is the first feasible technique using active RFID tags as anchors, usually placed in the form of a regular grid with limited number of RFID readers. For instance, [1] introduces the LANDMARC concept as a solution while 4 readers and 24 RFID tags operating at 308 MHz, are deployed in an indoor environment of 36 square meters. Recently, [2] establishes an RFID based localization system using 4 readers and 28 reference tags, operating at 433 MHz. The improved LANDMARC approach presents an average estimated positioning error of 75 centimeters in 50 square meters. Therefore, VIRE method is applied to improve the localization performance based on LANDMARC. [3] adapts VIRE solution by adopting an array formed by 8 reference tags and one RFID reader. This approach is validated in 9 square meters through simulations. The achieved average location error is 37 centimeters.

Otherwise, researchers focused also on developing algorithms to improve the localization system performance. For instance, [4] shows a novel hybrid system for indoor localization; both SA-LANDMARC and COCKTAIL algorithms were introduced within a tested area of 36 square meters using 49 RFID deployed tags, operating at 303.82 MHz. The accuracy reached 70 and 45 centimeters respectively. Despite the SA-LANDMARC's

implementation simplicity and COCKTAIL's efficiency, the achieved high precision, using both algorithms, refers to the dense deployment of RFID tags i.e., around one tag per square meter.

In this framework, the different indoor localization architectures were studied and compared to the proposed system based on either single tags or constellation of tags, to evaluate its performance. The following Table C. 1 characterizes the different active UHF RFID-based ILSs found in the literature and ours, in terms of locations accuracy and the number of RFID tags deployed in the considered indoor environment.

Table C. 1 Comparative summary for different RFID-based ILS

RFID based ILS		**Accuracy [meters]**	**Number of Active Tags deployed**	**Technique**	**Tag density [m^2]**
[1] L. M. Ni		2	24	LANDMARC	0.66
[2] D. Cui		0.75	28	LANDMARC	0.56
[3] E. Ferraz		0.37	8	VIRE	0.88
[4] Z. Dian		0.45	49	COCKTAIL	1.36
Proposed System	**Single Tags**	0.9	4	Multilateration	0.062
	Constellations	0.6	16	Multilateration	0.25

According to Table C. 1, the presented localization systems provide several solutions for indoor positioning. Authors focused on the location accuracy while neglecting the complexity and the cost of the number of deployed UHF RFID tags. More precisely, [1], [2] and [3] use around 0.66, 0.56 and 0.88 active RFID tags per square meter while performing LANDMARC and VIRE algorithm. The solution of [4] uses 1.36 active RFID tags per square meter to improve the location accuracy. After providing a fair number of use case examples, we can notice that most systems count on a large number of deployed active RFID tags for better performance.

For this reason, we have suggested reducing the number of tags and improving the stability of the RSS via MLE. The proposed localization system based on either single tags or constellations is able to determine the reader's location with an optimal position error of 90

and 60 centimeters using only four and sixteen active RFID tags, respectively, in a classroom environment of 63.75 square meters.

Bibliography

[1] L. M. Ni, Y. Liu, Y. C. Lau, and A. P. Patil, “LANDMARC: indoor location sensing using active RFID,” in Proc. of the First IEEE International Conference on Pervasive Computing and Communications (PerCom 2003), Fort Worth, TX, USA, pp. 407-415, 2003.

[2] D. Cui and Q. Zhang, “The RFID data clustering algorithm for improving indoor network positioning based on LANDMARC technology,” Cluster Computing, vol. 22, no. 3, pp. 5731-5738, 2019.

[3] E. Ferraz, P. Seixas and C. Carvalho, “Three-dimensional location in RFID systems with mobile reader,” in Proc. International Conference on Artificial Intelligence and Advanced Manufacturing, Dublin, Ireland, pp. 1-6, 2019.

[4] Z. Dian, L. Kezhong, and M. Rui, “A precise RFID indoor localization system with sensor network assistance,” China Communications, vol. 12, no. 4, pp. 13–22, 2015.

Conclusions and Future Works

Conclusions

Most ILSs have some common and critical issues such as the instability of RSS measurements affected by the multipath effects, the human error as well as the thorough cost of manpower/time for data collection.

In addition, none of the indoor propagation models found in the literature and used for calibration have yet successfully provided a reliable radio map covering all indoor environments.

In the same context, ILSs often need an accuracy of the sub-meter level and adaptation to multiple scenarios. Hence, there is no unique solution that can cover all challenges of reliability, simplicity, accuracy, etc.

To this end, our work conclusions are summarized in accordance with four objectives. The first one was to model indoor environments in order to reduce time needed for real measurements. Then, based on empirical studies, the second objective was to suggest two generic and configurable indoor propagation models i.e. the Dual One Slope propagation Model (DOSM) and the Dual One slope with Second Order propagation Model (DOSSOM) followed by a reliable calibration procedure, the Weighted Average Attenuation Factor (WAAF), that covers the whole considered indoor environment. Moreover, in order to improve localization performance, while implementing a simple and low-cost system, two purposes were elaborated: introducing constellations of RFID tags instead of single tags, as well as combining RSS samples collected by the RFID reader via the Maximum Likelihood Estimator (MLE).

Indoor Environment Modeling

Series of experiments were conducted in a classroom to analyze the coverage of propagating signals indoors. These experiments need the collection of a large amount of data, which require manpower and is large time-consuming; all this complicate the creation of a reliable fingerprinting.

For this reason, the indoor environment is modeled, via the WinProp tool, in order to reduce the need for costly measurements.

Empirical losses and Fresnel parameters, corresponding to all materials that constitute the considered medium, were defined.

Signals propagation characteristics are then analyzed using 3D Ray-Tracing. Experimental and simulated results had similar behavior with a maximal distance error difference of 10 centimeters (Figure 3.24), over the classroom environment.

Empirical Indoor Propagation Models and Reliable Calibration Procedure

It is widely recognized that indoor propagation characteristics greatly differ from the outdoor ones, mostly because of the indoor environmental particularities, such as shorter tags-reader distances, power fluctuations, and obstacle effects. In the context of propagation modeling, several empirical indoor propagation models, found in the literature, tend to focus on a particular characteristic including temporal fading or inter-floors losses. However, none of these models have yet successfully created reliable attenuation parameters, totally covering the considered indoor environment.

The importance of the suggested models DOSM and DOSSOM reside in representing signals behavior better, while being generic and configurable.

Associated with the new calibration approach WAAF, DOSM and DOSSOM present higher reliability in characterizing signals attenuation by covering the entire classroom environment and using only one active RFID tag.

Constellation of Tags

In order to even more improve the location accuracy, the concept of constellation was introduced.

The constellation is a group of tags that operate at the same frequency. Using constellations can reduce the multipath effects by benefiting from signals diversity. After investigating performance of the constellation with different radii, shapes and number of tags, the diamond four-tags constellation) with radius equal to the wavelength presents the optimal accuracy.

Localization Performance

Once the attenuation parameters extracted accurately, multilateration is applied to estimate the reader location.

Most conventional ILSs combine RSS samples by averaging; the proposed system performs by applying the Maximum Likelihood Estimator (MLE) as combining technique during both stages.

The effectiveness of using MLE with WAAF is validated by reaching a location accuracy of 90 and 60 centimeters with the single and the constellation of RFID tags, respectively.

Finally, the analysis on the impact of tags density proposes a trade-off challenge between the optimized deployment and the location accuracy. Regarding our system's cost and complexity, only four active RFID tags are used in the single tag and sixteen in the constellation of tags scenario.

Future Works

Based on the aforementioned conclusions, some future research axis can be addressed to further improve the proposed localization system:

- The system resolution varies with the number of RSS samples collected by the RFID reader in both offline and online stages. Hence, the optimal number of power acquisitions should be well investigated.
- A theoretical study regarding the constellation of tags may be useful to confirm the optimal dimensions of the constellation of RFID tags already demonstrated empirically.
- Location accuracy provided by the proposed indoor localization system may be investigated in a three-dimensional plane in the same classroom environment and with the same number of deployed RFID tags.
- Experiments may be conducted in different and more complex indoor environments to fully justify the effectiveness of the empirical and configurable indoor propagation models (DOSM and DOSSOM) and validate the solution with the optimal constellation of RFID tags.

Publications

The work conducted during this thesis has led to the following publications:

Journals

- E. Hatem, S. Abou-Chakra, E. Colin, J.-M. Laheurte, B. El-Hassan, "*Performance, Accuracy and Generalization Capability of RFID Tags' Constellation for Indoor Localization, "* Sensors, special Issue *"Advanced Approaches for Indoor Localization and Navigation"*, vol. 20, no. 15, p. 4100, 2020.

- E. Hatem, S. Fortes, E. Colin, S. Abou-Chakra, J. -M. Laheurte, B. El-Hassan, "Accurate and Low-Complexity Auto-Fingerprinting for Enhanced Reliability of Indoor Localization Systems," Sensors, special Issue *"Intelligent Wireless Networks"*, vol. 21, no. 16, p. 5346, 2021.

- E. Hatem, S. Abou-Chakra, E. Colin, J.-M. Laheurte, B. El-Hassan, *"Optimized and Sub-Metric RFID Indoor Localization System,"* submitted to IEEE Sensors Journal, 2021.

Conferences

- E. Hatem, B. El-Hassan, J.-M. Laheurte, S. Abou-Chakra, E. Colin, C. Marechal,"*Study the Estimated Distance Error in Indoor Localization using UHF-RFID,"* Proceedings of IEEE Middle East & North Africa COMMunications Conference (MENACOMM), Jounieh, Lebanon, pp. 1-5, 18-20 April 2018.

- E. Hatem, E. Colin, S. Abou-Chakra, B. El-Hassan, J.-M. Laheurte,"*Constellations of active UHF-RFID tags for indoor positioning,"* Proceedings of the International Conference on Indoor Positioning and Indoor Navigation (IPIN), Nantes, France, pp. 1–4, 24–27 September 2018.

- E. Hatem, E. Colin, S. Abou-Chakra, B. El-Hassan, J.-M. Laheurte,"*New empirical indoor path loss model using active UHF-RFID tags for localization purposes,"* Proceedings of the IEEE International Conference on RFID Technology & Application (RFID-TA), Macau, China, pp. 1–6, 26-28 September 2018.

- E. Hatem, E. Colin, S. Abou-Chakra, J.-M. Laheurte, B. El-Hassan,"*Caractérisation de la propagation d'un signal UHF-RFID à 433 MHz pour la localisation indoor,"* Proceedings of JNM 2019 (21èmes Journées Nationales Micro-Ondes), Caen, France, 14-17 May 2019.

- E. Hatem, S. Abou-Chakra, E. Colin, J.-M. Laheurte, B. El-Hassan,"*3D Modeling for Propagation of UHF-RFID Tags' Signals in an Indoor Environment,"* Proceedings of the 2nd IEEE Middle East and North Africa COMMunications Conference (MENACOMM), Manama, Bahrain, pp. 1-6, 19-21 November 2019.

Award

- Winner of the 2019 Altair Electromagnetic Student Competition
  - https://web.altair.com/student-competition-2019
  - https://www.altair.com/news/winner-announced-for-the-annual-altair-electromagnetic-student-competition